Contractor Report 270

Transport and Road Research Laboratory

Department of Transport

Geotechnical stress analysis for bridge abutment design

by M D Bolton
(University of Cambridge)

E

Crowthorne Berkshire RG11 6AU Tel: Crowthorne (STD 0344) 773131 Telex: 848272 Fax: 0344 770356

TRANSPORT AND ROAD RESEARCH LABORATORY
Department of Transport

Contractor Report 270

Geotechnical stress analysis for bridge abutment design

by M D Bolton
(University of Cambridge)

Paper to be distributed at Workshop on Limit State Design, TRRL, 25 September, 1991

The work reported herein was carried out under a contract placed on the University of Cambridge by the Transport and Road Research Laboratory. The research customer for this work is Bridges Engineering Division, DTp.

Structural Analysis Unit
Structures Group
Transport and Road Research Laboratory
Old Wokingham Road
Crowthorne, Berkshire RG11 6AU

1991

ISSN 0266-7045

CONTENTS

ABSTRACT

In recent years considerable difficulties have been experienced in the development of limit state codes for geotechnical analysis. Much of the difficulty has been associated with providing clear and unambiguous statements concerning collapse and unserviceability states and with the related problems of stress calculation for these states.

This report presents methods of calculation for the stresses developed in granular fill behind retaining structures for particular application to limit state design. The analysis procedures are complemented by a range of examples

to assist in allowing a clear understanding of these procedures to be obtained.

FOREWORD BY TRRL

This report must be seen in the context of the considerable controversy and uncertainty surrounding the possible adoption of limit state methods of design in ground engineering in the United Kingdom at the present time. Limit state design methods are the basis of BS 5400 which has been adopted by the Department of Transport for the design of bridges on motorways and trunk roads. Thus at the present time, bridge superstructures are designed on the basis of limit state design methods while their foundations are designed using a permissible stress/lumped factor of safety approach.

Because of the uncertainty on how best to apply limit state design methods in ground engineering, the Laboratory has commissioned research on three different approaches to the problem. This report presents one such approach on the use of design values. Another involves the use of fuzzy-sets, and research on this topic has been carried out by Dr D I Blockley at the University of Bristol (Blockley 1980). The third approach utilises the method of reliability analysis and has been carried out by Dr G N Smith (Smith 1986).

The three approaches have provided valuable insights in limit state design. Critical examination of these approaches highlights strengths and weaknesses of the alternative procedures enabling more soundly based decisions to be made on the context and form of proposed limit state design methods in ground engineering.

Dr G P Tilly
Head of Structures Group

INTRODUCTION

This report gives consideration to the stress analysis of earth retaining structures, with particular regard to bridge abutment walls.

The approach adopted throughout relies on equilibrium analyses to determine the mobilised strength in the zones of soil around the wall. The strength to be mobilised can then be compared directly with the maximum strength capable of being mobilised: this deals with safety against collapse. Furthermore, mobilised strength can be used - given the appropriate stress/strain data - to estimate mobilised strains: this leads to a serviceability check. This objective approach facilitates the optimum design of substructures in relation to the performance requirements of bridge superstructures.

Previous design recommendations included arbitrary factors of safety against "overturning about the toe", "sliding", etc, together with nominal values of earth pressure or permissible bearing stresses. Neither real safety margins nor the effects of in-service deformations were previously considered. However, a Limit State approach can be adopted for the evaluation of geotechnical designs by direct evaluations of both safety and serviceability through the Analysis of Critical Events. The circumstances pertaining to these Events need to be detailed, usually by a highway department or other authority, so as to create a sufficiently rigorous approach. Following the designation of load combinations, environmental conditions, etc, to be as hazardous as reason will allow, the rational calculation of effects can then be addressed by the methods set out in this report.

Chapters 1 and 3 each present basic soil mechanics dealing, respectively, with the collapse and deformation of retained soil. In the succeeding chapters, 2 and 4, the basic concepts are applied to particular situations relevant to bridge abutments. Chapters 5 and 6 similarly deal with the collapse and displacement of spread foundations which might be selected for abutment walls on favourable soils.

NOTATION

α | β	angles between major principal stress direction and a plane of stress discontinuity
γ	shear strain, $\epsilon_1 - \epsilon_3$, (Chapter 1 et seq)
γ	soil unit weight (Chapter 2 et seq)
γ_i	initial shear strain, eg due to placement process
γ_{f3}, γ_m	partial factors used in BS 5400 Part 4 to check on load effects
δ	secant angle of shearing developed on a surface, $\tan^{-1}(\tau/\sigma')$
ϵ	direct compressive strain at a point
$\epsilon_1, \epsilon_2, \epsilon_3$	largest, intermediate, smallest principal strains at a point
ϵ_a	axial strain in a triaxial test
ϵ_v	volumetric strain
η	proportional height of action of resultant lateral thrust on a wall (figure 2.15)
θ, $\Delta\theta$	angle, especially of wall rotation, change of angle
θ_i	equivalent initial wall rotation, corresponding to γ_i
λ	non-dimensional soil stiffness (equation 3.8)
$\nu, (\nu_d, \nu_u)$	Poisson's ratio, (drained, undrained)
ρ	soil settlement
$\rho, (\rho_d)$	bulk density, (dry)
σ	total normal stress
σ'	effective normal stress
$\sigma'_1, \sigma'_2, \sigma'_3$	largest, intermediate, smallest effective principal stress
σ'_h, σ'_v	horizontal, vertical effective normal stress
$\sigma_b, \sigma_r, \sigma_n$	normal stresses: beneath a strip load, of required overburden, on a wall
σ_c	compaction-induced lateral earth pressure
σ_f, σ'_f	total, effective, bearing capacity
σ_o	overburden pressure, γD
$\tau, (\tau_b)$	shear stress (on a strip base)
ϕ	effective secant angle of shearing, $\sin^{-1}(t/s')$
ϕ_{crit}	...in a crititcal state of continued shearing
ϕ_{max}	...at peak strength
ϕ_{mob}	...mobilised at equilibrium
ϕ_o	ϕ_{mob} in one dimensional compresion
ϕ_i	ϕ which can be developed at a soil-structure interface
ψ	angle of dilatancy, $-\sin^{-1}(d\epsilon_v/d\gamma)$ in plane strain
ω	angle of tilt of a foundation
Δ, Ω	angles on Mohr circle of stress, figure 2.4
A	dimensionless factor related to G_{max} (equation 3.1)
B	width of a strip load
C_w	distance of wall centre of gravity from the heel (figure 5.1)
D	depth of deformable soil beneath wall base
E	Young's modulus
E_o	modulus in one-dimensional compression
G, G_{max}	soil shear modulus (t/γ), maximum value at small strain
G_{grain}	shear modulus of soil mineral
G_s	specific gravity (density relative to water) of soil mineral
H	height of retained soil
I	second moment of area of a structural section
I_D	relative density
I_R	relative dilatancy index (equation 1.4)
I_v, I_h, I_w	influence factors for foundation movements (vertical, horizontal, tilting)

K	bulk modulus
K	earth pressure coefficient, σ'_h/σ'_v
K_a, K_p, K_o	K on frictionless wall, in active, passive, one-dimensional strain conditions
K_n, K_t	normal and tangential active earth pressure coefficients on wall developing friction
K_i	initial earth pressure coefficient
L	separation of edge of line load from wall (Chapter 2)
L	length of wall base projecting beneath the backfill to the heel
M	bending moment
N	thrust normal to wall
N_c, N_q, N_γ	bearing capacity coefficients
P	lateral thrust
P_a, P_q	active thrust due to selfweight, due to uniform surcharge
Q	logarithmic index of grain crushing (Chapter 1); line load per unit length (Chapter 2 et seq)
R	magnitude of soil reaction
R	ratio of stresses across a discontinuity in soil with limiting ϕ (Chapter 1)
R	overconsolidation ratio (Chapter 4)
S_r	saturation ratio
T	tangential force on wall
U	thrust due to water pressure
W	weight
X	effective base width, reduced due to eccentricity
c'	intercept of envelope of drained effective strength data at $\sigma'=0$
c_u	undrained shear strength
c_{ub}	undrained shear strength developed on concrete base
c_{mob}	shear stress mobilised in equilibrium
g	gravitational acceleration
h	height above the foot of a wall
i_c, i_q, i_γ	reduction factors on N_c, N_q, N_γ due to inclined thrust
n	number of stress discontinuities to be crossed
p'	mean effective stress at a point
p'_c	effective stress index of grain crushing
q	uniform surcharge
s'	mean effective stress in plane considered (dash may be omitted)
t	maximum shear stress at a point, $(\sigma'_1 - \sigma'_3)/2$
u	pore water pressure
u_o	pore pressure in clay beneath foundation excavation, undrained
u_u	pore pressure in clay beneath foundation following backfilling, undrained
z	depth
z_p	depth of maximum lateral earth pressure due to passage of a compactor
z_o	depth of enhanced lateral pressure due to compaction in layers (equation 1.4)

1 PLASTICITY IN GRANULAR SOILS

1.1 Strength

1.1.1 Basic Definitions

It has been shown, Bolton (1986), that the mobilised strength of granular soils is most practically expressed in terms of the secant angle of shearing ϕ_{mob} defined in figure 1.1 . For this purpose only the major and minor effective principal stresses σ_1' and σ_3' are involved: the effect of the intermediate principal stress σ_2' is dealt with empirically.

Typical rates of development of shear strain $\gamma(= \epsilon_1 - \epsilon_3)$ for axisymmetric (triaxial) and plane compression on a dense sand are contrasted in figure 1.2. Also shown is the dilatancy rate, defined as $(-d\epsilon_v/d\epsilon_1)$, for both types of test. The angle of dilatancy ψ for a plane test is defined with respect both to a simple shear test and a Mohr circle of strain increments in figure 1.3. The value of ψ is also shown in figure 1.2 for the plane strain test.

It will be seen that the maximum angle of shearing ϕ_{max} is mobilised at the same instant as the maximum rate of dilation. After this point of peak strength there is usually strain softening followed by localisation of strains in shear bands which are only of the order of 10 particle diameters in thickness. Even small relative displacements across the band then cause extremely large shear strains within it, which are effectively impossible to measure. However, in terms of boundary displacements, the soil usually appears to soften swiftly to its critical state, at which shear can continue at an angle of shearing ϕ_{crit} without further change of volume.

1.1.2 Empirical Correlations

A simple idealisation of the effects of dilation is presented in figure 1.4, showing the relative displacement of interlocked saw-blades. The angle of the blades to the slip surface is ψ, and a coefficient of friction ϕ_{crit} is invoked on the teeth. It will be seen that for slip to take place between interlocked blades, the angle of shearing ϕ measured with respect to the serrated edge is given simply by

$$\phi = \phi_{crit} + \psi \qquad (1.1)$$

Of course, soil particles have many more degrees of freedom and will actually move in three dimensions. Rowe (1962) and Horne (1965, 1969) outlined a stress-dilatancy theory for aggregates of rigid rotund particles, which took account of some of these extra considerations. The outcome was expressed in terms of principal effective stress ratio

$$\frac{\sigma'_1}{\sigma'_3} = \left(\frac{\sigma'_1}{\sigma'_{3crit}}\right) \cdot \left(1 - \frac{d\epsilon_v}{d\epsilon_1}\right) \qquad (1.2a)$$

taking compression positive. This can equally be written

$$\frac{(1 + \sin\phi)}{(1 - \sin\phi)} = \frac{(1 + \sin\phi_{crit})}{(1 - \sin\phi_{crit})} \cdot \frac{(1 + \sin\psi)}{(1 - \sin\psi)} \qquad (1.2b)$$

or

$$\tan(45+\phi/2) = \tan(45+\phi_{crit}/2).\tan(45+\psi/2) \qquad (1.2c)$$

Figure 1.5 shows that equation 1.2 can be approximated in the fashion of equation 1.1 :

$$\phi = \phi_{crit} + 0.8\psi \qquad (1.3)$$

There is an enormous amount of corroborative evidence of the applicability of equation 1.2, and therefore of the approximation 1.3, to the shear and dilatancy of all manner of particulate aggregates. Of equal interest, however, is the prediction of either ϕ or ψ in a particular case.

A study of the data of 17 sands, which had been tested by different research workers and reported in the literature, offered empirical correlations based on the initial relative density

$$I_D = (e_{max}-e)/(e_{max}-e_{min})$$

and the current mean effective stress

$$p' = (\sigma'_1+\sigma'_2+\sigma'_3)/3$$

First a relative dilatancy index I_R was defined which combined the influences on dilatancy of soil density and the crushing of asperities caused at high stress:

$$I_R = I_D \ln(p'_c/p') - 1 \qquad (1.4a)$$

where p'_c is a constant for a particular soil, related to the crushing strength of its grains. This can alternatively be written

$$I_R = I_D(Q - \ln p') - 1 \qquad \text{(specifying } p' \text{ in kPa)} \qquad (1.4b)$$

It was found that the strength and dilatancy of quartz or feldspar sands at different densities and stresses could best be linked using the value p'_c = 22000kPa, or Q=10. Data from Billam (1972) indicated that for more crushable materials the value of p'_c or Q was smaller: for limestone particles a fit was achieved with p'_c=3000kPa or Q=8. Data from Lau (1988) show that for finely ground silica flour the residual crushing strength of the grains is rather greater, with p'_c=100000kPa or Q=11.5 .

Having established a value for I_R it was then demonstrated that the following empirical relations were observed.

For plane strain

$$\phi_{max}-\phi_{crit} = 0.8\psi_{max} = 5I_R \quad \text{degrees} \qquad (1.5)$$

For axisymmetric (triaxial) strain

$$\phi_{max}-\phi_{crit} = 3I_R \quad \text{degrees} \qquad (1.6)$$

And for both types of test

$$(-d\epsilon_v/d\epsilon_1)_{max} = 0.3I_R \qquad (1.7)$$

The degree of correlation achieved may be appreciated by taking as typical examples the triaxial data of De Beer (1965) on Berlin sand and Ladanyi (1960) on Mol sand. They are compared in figure 1.6 with relations 1.6 and 1.4 using a value p'_c= 22000kPa appropriate to these quartz sands,together with ϕ_{crit}= 33° for Berlin sand and 32.5° for Mol sand.

Norris (1977) correlated ϕ_{crit} positively with the angularity of the soil grains. There is also circumstantial evidence that feldspar grains tend to have larger values of ϕ_{crit} than quartz grains, but this may equally be due to their coincidentally higher angularity. In any event, the lowest value for 17 sands from around the world was 30° for rounded uniformly graded Ottawa sand: other values ranged from 32° for Mersey River sand to 37° for a glacial outwash sand. It is preferable if ϕ_{crit} is found either from testing loose soil samples, or from an extrapolation of a set of results of ϕ_{max} versus peak dilation rate to deduce the intercept at zero dilation rate. However, Cornforth (1973) has suggested that ϕ_{crit} can also be equated to the angle of repose of a loosely tipped heap of dry material, within an accuracy of about 1°. Indeed, there is hardly much more error in simply assuming that ϕ_{crit} for a typical sub-rounded uniform quartz sand is 33°.

Clearly, ϕ_{crit} offers an easily measured, reliable, and safe lower bound to the strength of granular soils. From the previous discussion it should be obvious that predicting ϕ_{max} requires extra knowledge of placement density and failure stress level, in addition to some knowledge about the relative crushing resistance of the grains. According to Iwasaki et al (1987) anisotropy also reduces ϕ_{max} for shearing parallel to the bedding, to the extent that the simple shear strength of their Toyoura sand fell towards the triaxial strength for samples deposited vertically in the usual way. They also found for Toyoura sand that there was relatively little gain in ϕ_{max} below p'=150kPa. Using p'_c=22000kPa, for example, this would set an upper limit to I_R of

$$I_R = 5I_D - 1 \qquad (1.8)$$

applicable where p'< 150kPa. This conservative limit would, for example, underestimate the triaxial angle ϕ_{max} of dense Berlin sand compressed normal to the bedding with p' = 50kPa by about 3° : see figure 1.6 .

Finally, if there is the possibility of progressive failure, or if it is required that soil constructions are to be robust in the face of unforseeable loading incidents, then it will be necessary to assume in design that shear localisation will be capable of reducing ϕ_{max} to ϕ_{crit} as shown in figure 1.2. Since localisation is invariably observed in the retained soil when an active wedge causes outward sliding of a retaining wall, it will be necessary to ignore the dilatant component of strength of the backfill when this mode of collapse is under consideration.

1.1.3 Example: derivation of values for ϕ

Let us find design values of the angle of shearing resistance of a quartz sand, appropriate to its use as fill behind a 7m high retaining wall, compacted to a specification of 95% maximum dry density.

First, set a design value of 93% maximum dry density to give a margin for compaction control. Then translate this into a relative density. Taking typical values G_s=2.65 , e_{max}=0.8 , e_{min}=0.5 , we get $\rho_{d,max}$=1767kg/m^3 so for design ρ_d= 0.93 x 1767= 1643kg/m^3 giving e= 0.613 and I_D= 0.62 .

Now calculate the largest mean effective stress applicable to the problem. Taking a typical moisture content as 10% , the field bulk density will be, nominally and approximately, 0.95 x 1767 x 1.1 = 1847 kg/m^3. The greatest vertical stress, taking pore pressure to be zero , will then be 1.847 x 9.81 x 7 = 127 kPa at the wall base. In the case of active wall failure an earth pressure coefficient of 0.25 may be applicable. The mean stress will then be approximately

$$p' = \sigma'_v (1+K)/2 = 0.625\ \sigma'_v = 79 \text{ kPa}$$

This is less than 125 kPa (as will usually be the case in active retaining wall calculations) so no further accuracy is required and we will use equation 1.8 to derive a design value of

$$I_R = 5 \times 0.62 - 1 = 2.1$$

Taking the axisymmetric rather than the plane strain correlation, to account conservatively for the possible effects of anisotropy, we use equation (1.6) to get

$$\phi_{max} - \phi_{crit} = 3 \times 2.1 = 6.3°$$

A conservative value for ϕ_{crit} is 32°, so a design value for ϕ_{max} will be 38°. In collapse calculations we should use ϕ = 32° to allow for localisation in shear bands. In serviceability calculations we should consider the stress-strain curve of a compacted granular soil with I_D = 0.62, p' = 79 kPa which we predict would have ϕ_{max} no less than 38°. For example, if we accept an earth pressure coefficent in one-dimensional compression $K_o = 1 - \sin\phi_{max}$ we would obtain K_o = 0.38 .

1.2 Safe States

If all soil elements can be shown simultaneously to possess safe states, in which they are seen to be in equilibrium under external actions whilst mobilizing no greater than their critical effective angle of shearing resistance ϕ_{crit} then the soil construction will not collapse under those actions. Any equilibrium stress distribution will serve for the purpose of demonstrating safety, if

(i) an effective stress analysis demonstrates that ϕ_{crit} will nowhere be exceeded in the soil.

(ii) The stresses on strain-controlled boundaries cannot be less favourable than those assumed. For example, all boundary friction is to be neglected unless the existence of relative sliding in a known direction is inevitable during collapse, in which case a pessimistic angle of interfacial friction is to be assumed.

If it is accepted that neither localisation of shear strain nor progressive failure will affect the collapse of a soil construction, then a larger value

of ϕ may be used. It will then be essential to select the lowest possible peak strength using equations 1.5 or 1.6 . This will involve selecting the loosest possible soil element under the largest possible effective stress to obtain a worst credible value for I_R from equation 1.4 .It may also be necessary to make some deduction for inherent anisotropy due to particle orientation, but only where sliding is possible on planes of bedding.

1.3 Superposition of Limiting Effective Stress Fields

Where it is required to carry boundary stresses in addition to self-weight stresses, whilst maintaining proof of safety, it is possible for fully drained soils to adopt a principle of plastic stress superposition. If two independent plastic stress distributions are known to equilibrate, separately, the actions A and B respectively, then the simple superposition of those stress distributions will create a stress distribution in equilibrium which is itself safe with respect to the combination of the actions A and B, provided that the plastic strength criterion is a constant angle of shearing.

This superposition principle is easily demonstrated with regard to the stresses (σ_1^A, σ_3^A) and (σ_1^B, σ_3^B) where the directions of σ_1^B and σ_1^A may differ by some arbitrary angle θ, as shown in figure 1.7. Only when $\theta = 0$ will the superposed stress state reach the previous limiting ϕ line, as shown in figure 1.8a. For any finite relative rotation of the individual stress components, the maximum compounded angle will comprise non-limiting components and will itself lie within the previous limiting ϕ-line as shown in figure 1.8b . It can be shown, for example, that when $\phi^A = \phi^B = 30$ and the relative rotation $\theta = 30°$, the maximum angle mobilized after superposition is always greater than $\phi^C = 25.7°$ recorded when the two separate stress components are equal in magnitude. If $s^A >> s^B$ or $s^B >> s^A$ then $\phi^C \rightarrow \phi^A$ or ϕ^B, and the potential for overconservatism reduces. If $s^A = s^B$ and $\theta > 30$ the combined maximum mobilized angle of shearing resistance reduces quite rapidly through 21° when $\theta = 45°$ and towards zero at $\theta = 90$ when the two shear stress components annihilate each other.

1.4 The Effective Stress Discontinuity

In assembling equilibrium stress fields it is useful to consider the conditions which would permit two differently stressed zones to be in contact. Figure 1.9 depicts two such zones A and B, each mobilizing a limiting friction angle ϕ, and in equilibrium across the stress discontinuity DD which mobilizes a smaller angle δ. The stresses are characterised by the magnitudes of the major principal components σ_1^A, σ_1^B and their directions α and β relative to the discontinuity. The mean plane stresses s^A and s^B are used in the derivation.

In the Mohr circles,

$$\text{angle } DA\sigma^A_1 = 2 \times (\pi/2 - \alpha) = \pi - 2\alpha$$

$$\text{angle } DB\sigma^B_1 = 2 \times (\pi/2 - \beta) = \pi - 2\alpha$$

Now let us find auxilliary angle Ω.

$$AM = OA\sin\phi = s^A\sin\phi$$

But $AD = AM$

$$\therefore \quad AD = s^A \sin\phi$$

Likewise $DB = BN = s^B \sin\phi$

So considering triangle OAD for example,

$$\frac{AD}{\sin\delta} = \frac{OA}{\sin\Omega}$$

$$\therefore \quad \sin\Omega = \frac{\sin\delta}{\sin\phi} \cdot \frac{s^A}{s^A}$$

$$\therefore \quad \Omega = \sin^{-1}(\sin\delta/\sin\phi) \tag{1.9}$$

We can now determine α and β in terms of Ω using the angles of triangles OAD and OBD respectively.

$$\pi - 2\alpha = \Omega + \delta$$

$$\therefore \alpha = \frac{\pi}{2} - \frac{\Omega}{2} - \frac{\delta}{2}$$

and $$2\beta = \Omega - \delta$$

$$\therefore \beta = \frac{\Omega}{2} - \frac{\delta}{2} \tag{1.11}$$

The rotation θ in the major principal direction is simply

$$\theta = \alpha - \beta = \pi/2 - \Omega \tag{1.12}$$

Lastly, the stress increase from A to B can be determined using the sine rule on triangle ADB.

$$\frac{s^A \sin\phi}{\sin 2\beta} = \frac{s^B \sin\phi}{\sin(\pi - 2\alpha)}$$

$$\therefore \quad \frac{s^B}{s^A} = \frac{\sin(\pi - 2\alpha)}{\sin 2\beta} = \frac{\sin(\Omega + \delta)}{\sin(\Omega - \delta)} \tag{1.13}$$

It follows, by similar triangles, that each corresponding stress is increased by the same factor R so that, for example,

$$R = \frac{s^B}{s^A} = \frac{\sigma_1^B}{\sigma_1^A} = \frac{\sin(\Omega + \delta)}{\sin(\Omega - \delta)} \tag{1.14}$$

Different combinations of δ and ϕ provide different stress increments. For example,

$$\phi = 35.3°, \quad \delta = 30°$$

gives

$$\Omega = 60°, \quad \theta = 30°$$

$$\alpha = 45° \quad \beta = 15°$$

and $R = 2$

so that when the major stress is "refracted" away from the normal, its magnitude increases. These conditions are set out in figure 1.10 .

In the absence of self-weight, discontinuities such as these can be assembled so as to enclose elements of uniform stress which are in equilibrium at their boundaries. Particularly useful patterns are the fan and the kite, shown in figure 1.11 .

The fan comprises discontinuities radiating at intervals of θ (equal to the directional jump) so that each is correctly inclined to provide a similar jump in stress magnitude. Sufficient discontinuities can be chosen to rotate the major principal direction by any chosen amount.

The kite is a figure enclosed by α and β discontinuities. A succession of coaxial kites has the effect of producing a quasi-radial stress field, with no net rotations along the axis but with stress magnitudes altering in geometrical progression.

In particular problems, the magnitude of the rotation of major stress direction from one place to another will often be clear. For example, a 90° rotation will occur from the active zone beneath a smooth footing to the passive soil zone just outside its edge. For this reason, the most useful particular stress discontinuities are those which mobilize particular values in the various soil zones, and which rotate the stress direction by some sub-multiple of 90°, such as 30°, 15°, 7½° etc; see table 1. It will be seen that 30° stress jumps mobilize $\delta = 0.85\phi$ on the discontinuities, whereas 15° jumps mobilize $\delta = 0.96\phi$ and 7½° jumps mobilize $\delta = 0.99\phi$. The proportion δ/ϕ may be used as an indicator of the degree to which strength is being sacrificed on the boundaries of elements, and therefore of the degree of underprediction of strength which might ensue.

1.5 Effective Stress Characteristics

Plastic stress characteristics can be thought of as infinitesimal stress discontinuities, $\theta \rightarrow d\theta$. Then, from equation 1.12,

$$\Omega = \pi/2 - d\theta \qquad (1.15)$$

and from equation 1.9

$$\sin\Omega = \cos d\theta = \sin\delta/\sin\phi$$

so that $\delta = \phi$ (1.16)

Then equations 1.10 and 1.11 give

$$\alpha = \pi/2 - (\pi/2 - d\theta)/2 - \phi/2$$

or $\alpha = \pi/4 - \phi/2 + d\theta/2 \rightarrow \pi/4 - \phi/2$ (1.17)

and $\beta = (\pi/2 - d\theta)/2 - \phi/2$

or $\beta = \pi/4 - \phi/2 - d\theta/2 \rightarrow \pi/4 - \phi/2$ (1.18)

Furthermore, equation 1.13 yields

$$\frac{s' + ds'}{s'} = \frac{\sin(\pi/2 + \phi - d\theta)}{\sin(\pi/2 - \phi - d\theta)}$$

$$= \frac{\cos(\phi - d\theta)}{\cos(\phi + d\theta)}$$

$$= \frac{\cos\phi + \sin\phi d\theta}{\cos\phi - \sin\phi\, d\theta}$$

$$= 1 + 2\tan\phi\, d\theta$$

$$\therefore \frac{ds'}{s'} = 2\tan\phi\, d\theta \qquad (1.19)$$

These conditions represent the familiar α and β stress characteristics depicted in figure 1.12, along which

$$\left.\frac{ds'}{s'} = \pm 2\tan\phi\, d\theta\right\}_{\alpha}^{\beta} \qquad (1.20)$$

In moving along the α - direction, the path is jumping over a sequence of infinitesimal β - discontinuities, and vice versa. The + and - signs for α and β lines in equation 1.20 are easily derived from the necessity to hold to a consistent definition for rotation θ - anticlockwise positive - irrespective of whether stress is increasing or reducing. It may be perceived from table 1 that 7½° stress jumps conform quite closely to stress characteristics. A solution in terms of 7½° jumps will therefore be almost "exact" in the sense of mobilizing the full plastic strength everywhere, and achieving failure geometries and loads similar to an ideal characteristic solution of the type of Sokolovski (1960) though in the absence of self-weight. An additional advantage, however, will accrue from the constancy of stress within any element, and the regular geometric stress factors: these will greatly facilitate ad-hoc stress analyses using finite stress jumps.

2. ACTIVE EARTH PRESSURES IN GRANULAR BACKFILL

2.1 Rankine's Active Stress Field

The simplest example of a safe stress field is Rankine's active earth pressure condition, in which any possible friction on vertical surfaces is ignored. This generates a simple system of vertical principal stresses so that, following the limiting Mohr circle of effective stress in figure 2.1

$$\sin\phi = \frac{ST}{OS} = \frac{(\sigma'_v - \sigma'_h)/2}{(\sigma'_v + \sigma'_h)/2} = \frac{\sigma'_v - \sigma'_h}{\sigma'_v + \sigma'_h} \qquad (2.1)$$

Therefore

$$\frac{\sigma'_h}{\sigma'_v} = K_a = \frac{(1 - \sin\phi)}{(1 + \sin\phi)} \qquad (2.2)$$

where K_a is referred to as the active earth pressure coefficient. To show conclusively that collapse cannot occur the value ϕ_{crit} should be used for ϕ. The vertical effective stress is simply determined by resolving vertically for self weight γ and uniformly distributed surcharge q, taking possible pore water pressures u into account :

$$\sigma_v' = \gamma z + q - u \qquad (2.3)$$

2.2 Wall Friction Effects

The effect of wall friction is most easily demonstrated for the case of a vertical wall mobilising a friction angle δ as it supports an "active" rectangular mass of weightless granular material subject to a uniform surcharge q as shown in figure 2.2. A valid net of stress characteristics is shown in figure 2.3 , with corresponding Mohr circles of stress in figure 2.4. There are three regions : a uniform stress zone W near the wall, a fan zone F, and the usual active Rankine zone A.

Taking the earth pressure coefficient to be K_n normal to the wall, the resultant inclined stress is $K_n \sec\delta . q$ .Figure 2.4 then shows that in zone W the mean stress is given by

$$\frac{s'_w}{K_n \sec\delta\ q} = \frac{\sin\Omega}{\sin\Delta} \qquad (2.4)$$

where $$\Omega = \sin^{-1}(\sin\delta/\sin\phi) \qquad (2.5)$$

and $$\Delta = \Omega - \delta \qquad (2.6)$$

Also, the major stress in zone W is rotated through an angle from the vertical

$$\theta_W = \Delta/2$$

It follows from equation 1.20 that for a rotation θ_W through the fan zone F,

$$s'_A/s'_W = \exp(2\theta_W \tan\phi) \qquad (2.7)$$

where $q/s'_A = (1 + \sin\phi)$ (2.8)

Finally, by combining 2.4, 2.5, 2.6, 2.7 and 2.8 we obtain

$$K_n = \frac{\cos\delta \sin\Delta \exp(-\Delta\tan\phi)}{\sin\Omega\ (1 + \sin\phi)} \quad (2.9)$$

Some values for K_n are arranged in table 2.1. Since superposition can be applied safely to a constant-ϕ soil, K_n can be used in figure 2.5 to solve the influence of a heavy layer of thickness dz at height z above a point A in dry granular soil on the point of collapse,

$$d\sigma_n = K_n\gamma dz$$

Integrating these effects for every layer

$$\sigma_n = \int_0^h K_n\gamma dz = K_n\gamma h$$

It is therefore proved that K_n from equation 2.9 can safely be used as the earth pressure coefficient for any similar problem of surcharge or self-weight. The difference between the safe expression in 2.9 and the well known numerical solutions for self weight published by Caquot and Kerisel (1949) approaches a maximum of 2% at full wall friction.

It is also obvious that the beneficial effect of full wall friction is only equivalent to the extra provision of 5° to ϕ. Furthermore, the degree of relative sliding necessary to create full wall friction is not necessarily present behind a cantilever L-wall. For these reasons alone, Rankine's simple stress distributions may be preferred as the basis for safe state calculations of granular backfill. Moreover figure 2.4 shows that the source of lateral stress reduction with wall friction is the reduction in vertical stress in the soil near the wall. Since the design of the wall structure will require the production of an equilibrium stress diagram which includes the effect of the weight of the backfill acting on the wall base, there are also some practical advantages in adopting the safe strategy of ignoring wall friction.

2.3 Effect of Surface Loads on Fully-Drained Granular Soil

2.3.1 Weightless Soil

Consider a uniform weightless soil half-space capable of mobilizing some effective angle of shearing resistance ϕ. Figure 2.6 demonstrates the essential steps in generating a limiting stress field in equilibrium under a long strip load which applies a normal stress σ_b to the surface. The major principal stress under the centreline of the load must remain vertical, by symmetry, and to be consistent with "active" conditions. The major principal stress on the horizontal plane outside the load must remain horizontal, since no shear stress is permitted on that surface, and the limiting state will be "passive" under the required overburden σ_b/N_q. Between the active and passive surface zones there must be a plastic fan which rotates the stresses through 90°. Beneath the fan, a succession of close-packed kites will permit the stress to spread and reduce roughly in inverse proportion to the radius.

Figures 2.7, 2.8 and 2.9 show nets of stress discontinuities each for

ϕ' = 32°, drawn with stress deviations of 30°, 15° and 7½° respectively. The major principal stress in any element can be found by dividing the applied stress σ_b by a factor R^n where n is the total number of the stress jumps required from beneath the load to reach the element - counting positive clockwise across the β lines and anticlockwise across the α lines. The stress ratio R is 1.8324 for 30° deviations, 1.3800 for 15° and 1.1770 for 7½°. It is therefore possible to deduce the required overburden σ_r by the side of the load, using each of the nets in turn. Since σ_r is the minor principal stress

$$\sigma_r = K_a \frac{\sigma_b}{R^n} \qquad (2.10)$$

where $K_a = (1 - \sin 32°)/(1 + \sin 32°) = 0.307$

We thereby obtain for σ_r: $\sigma_b/20.0$ for the 30° net, $\sigma_b/22.5$ for the 15° net and $\sigma_b/23.0$ for the 7½° net. We know that the "correct" solution is σ_b/N_q where

$$N_q = \frac{\exp(\pi \tan\phi)}{K_a} \qquad (2.11)$$

giving $\sigma_b/23.2$. We therefore know that in this region of the nets the degree of over-conservatism (in the sense of requiring more overburden than strictly necessary) is 14% for the 30° net, 3% for the 15° net and 1% for the 7½° net. Of course the stress changes by the factor n^2 in an artificial fashion around an internal intersection of stress discontinuities. Such errors are highly localised, and tend to even out when the stress is integrated in order to find the thrust on a surface. This can be seen in figure 2.10 in which is plotted the horizontal stress on the centreline as a function of depth, for each of the nets of figures 2.7, 2.8 and 2.9 . The largest lateral stresses exerted on any vertical plane in the soil are precisely those on the centreline. It can easily be shown that the popular alternative calculation, using an elastic half- space solution to obtain σ_v and deriving σ_h by multiplying by K_a, underestimates the lateral stress by a factor of about 0.6 at all depths $z > B$.

Nets of 7.5° discontinuities are drawn in figures 2.11, 2.12, 2.13, and 2.14 for soils with ϕ = 30°, 35°, 40°, and 45° respectively. These solutions depend on the co-existence of a line load with sufficient surcharge σ_r immediately around it just to hold it in equilibrium. The actual overburden pressure σ_o, due to the weight of the pavement, must equal or exceed the required surcharge σ_r ,and any excess must be accounted for.

The simplest way of achieving this is to deduct from the lateral stress implied by the plastic stress fields, shown in figures 2.9, and 2.11 to 2.14, the uniformly distributed active stress $K_a\sigma_r$ which would have been created by the required surcharge. What then remains may be taken (for superposition purposes) to be solely the effect of the line load. The full overburden pressure σ_o corresponding to the weight of the pavement must then, of course, be treated as additional uniform surcharge in the usual way, with a check performed to test that it at least provides the required overburden. We know that

$$(\sigma_r + Q/B) \;/\; \sigma_r = N_q$$

so that

$$\sigma_r = \frac{Q}{B(N_q-1)} \qquad (2.12)$$

Figure 2.15a shows a weightless granular fill subject to a uniformly distributed surcharge σ_r over its entire surface, and an additional strip load Q per unit length distributed on the surface of the fill over a width B , and with its centreline a distance L from a vertical wall. It is required to analyse the wall at a depth H beneath the surface. Figure 2.15b shows a 15° plastic net for this case, and the resulting wall stresses σ_w , γ_w due to Q and σ_r are plotted in 2.15c. In d the active lateral stresses which would be due to σ_r alone are plotted, and in e the difference between c and d, which may be taken as the net effect of Q alone. Recall, however, that further superposition of at least stresses d will later be necessary.

Figure 2.15f then defines net thrust coefficients K_n and K_t, and a height of action $h = \eta H$, all of which may be found numerically by integrating the net stresses in figure 2.15e .The Q-component of bending moment at depth H may then be expressed as $M = \eta K_n Q H$.

Values of K_n, K_t and η are drawn out as functions of H/B for a range of values of L/B, for each separate value of ϕ (30°, 32°, 35°, 40°, 45°) , in figures 2.16 to 2.20 respectively.

Since many loading cases will involve the imposition of a strip load on the fill immediately adjacent to the wall, this particular case (L/B = 0.5) is picked out from the preceding figures and re-presented in a compact form in figure 2.21 . It is then apparent that both K_t and η are rather insensitive to values of ϕ in the range 30° to 45° while K_n remains roughly proportional to K_a. This permits the use of the following approximate curve-fitting expressions.

For L/B = 0.5 :

$$K_t = 0.16 + 0.19 \ln H/B \qquad 1 < H/B < 6$$
$$K_t = 0.5 \qquad 6 < H/B < 32 \qquad (2.13)$$

$$\eta = 0.5 \qquad H/B < 1.7$$
$$\eta = 0.43 + 0.13 \ln H/B \qquad 1.7 < H/B < 32 \qquad (2.14)$$

$$K_n = K_a (0.9 + \ln H/B) \qquad 1 < H/B < 6$$
$$K_n = 2.7K_a + 0.15\ln[\, H/(6B)\,] \qquad 6 < H/B < 32 \qquad (2.15)$$

For relatively wide superimposed loads (H/B < 1) it will be necessary to treat the load as a uniformly distributed surcharge, and to use section 2.2 (equation 2.9 and table 2.1) for earth pressure coefficients with wall friction. A simpler alternative is to neglect wall friction in these circumstances, when a uniform active zone would offer:

$$K_n = K_a \, H/B$$

$K_t = 0$ (2.16)

$\eta = 0.5$

The adoption of different degrees of wall friction for the various load components is not illogical. It is convenient to select lateral stresses due to strip loads on the basis that the wall has the same friction as any other plane through the soil, so that the foregoing stress analyses may be made independent of the wall interface. It is, however, essential when all the various components of stress have been superimposed, that the mobilised wall friction δ does not exceed its permissible value. This can generally be assured by discounting wall friction with regard to the components due to uniformly distributed surcharge and the self-weight of the fill.

Certain features of figures 2.16 to 2.21 may initially seem counter-intuitive.

(i) For relatively narrow strip loads (H/B large) the thrust coefficient K_n can exceed K_a by a factor of three. In the past, many analysts have ignored the stress concentrations beneath strip loads and have underestimated their effects.

(ii) It will be noted that for combinations of moderate L/B and large H/B the coefficient K_t exceeds 0.5. Now the shear force transmitted to each side by the strip carrying Q is only 0.5Q. The explanation for the anomaly is that the surcharge σ_r required around the foundation "arches" or spreads its effect sideways, just as the strip load does. This creates extra shear force on vertical planes remote from the strip, which is included in the coefficient K_t. The quoted values are safe.

(iii) The position of the resultant thrust can be lower than 0.5H, even though the effect of a strip load should be to tend to create "pressure-bulbs" at higher elevations close to the load. This occurs most noticeably at L/H = 1, H/B = 1 so that a gap of H/2 exists between the edge of the wall and the strip load. In this geometry, relatively little extra stress is created on the top half of the wall.

2.3.2 Example: superposing load and self-weight effects

Figure 2.22 shows the three-dimensional problem of a 45 unit HB bogey on the pavement adjacent to a 10 m long abutment wall unit. The total nominal load of 900 kN on the two axles is to be factored by 1.3 for ULS design according to BS 5400 Part 2. In plan view, the load is spread over an area C = 3.5 m along the wall by B = 2 m normal to its face. In this example, as an arithmetical simplification, HA loading equivalent to 1.3x10=13 kN/m^2 surcharge is to be carried in a 6 m wide strip in the remaining part of the carriageway. No pore water pressures are anticipated. The objective of the calculation is to estimate the bending moment at the base of the wall stem, appropriate to a plastic hinge analysis.

The first step is to demarcate a strip of wall to carry the effects of the HB vehicle. Elastic diffusion of load through the asphalt pavement corresponds approximately to a 1:2 angle of spread over a 0.5 m depth of bound material. The equivalent bearing area on the fill is therefore C' = 3.5 + 2 x 0.5 x 0.5 = 4 m, B' = 2 + 0.5 x 0.5 = 2.25 m: this is shown in figure 2.23 . For convenience of analysis, lateral spreading of load in the fill will be restricted to the direction normal to the face of the wall. Conservatively,

frictionless planes 4 m apart will be considered to divide the wall into two sections, 'a' influenced and 'b' uninfluenced by the HB vehicle.

The second step is to select a soil ϕ value: taking $\phi_{crit} = 32°$ in this case will certainly be conservative. If a more angular crushed rock were available, ϕ_{crit} would be greater. Furthermore, the design scenario is one of wall rotation about a hinge at the base and this will tend to cause uniform soil strains, so that dilatant peak values of ϕ_{max} would be likely to be retained up to significant wall movements, before the soil strain began to localise permitting softening to a critical state. Nevertheless, if a robust design is required which is insensitive to fill type or wall movement, an assumed value of $\phi = 32°$ will be necessary.

It follows that $K_a = 0.31$. We can now read off values from figure 2.17 using $L/B = 0.5$ since the load is adjacent to the wall, and $H/B = 7.5/2.25 = 3.33$. Taking into account the logarithmic scale for H/B on figure 2.17, we find that 3.33 is at (log3.33 - log3)/(log4 - log3) = 37% of the interval between 3 and 4. Then we find:

$$K_n = 0.61,\ K_t = 0.38,\ \eta = 0.60$$

In the HB loaded section, figure 2.23a, we obtain

$$Q = 1.3 \times 900 / 4 = 293 \text{ kN/m}$$

so that the bending moment due to the load,

$$M_Q = K_n Q \eta H$$

$$= 0.61 \times 293 \times 0.60 \times 7.5 \quad = 804 \text{ kNm/m}$$

In addition, the effect of the pavement taken as an equivalent surcharge $q_a = 11$ kPa , will be

$$M_{qa} = 0.5 K_a q H^2$$

$$= 0.5 \times 0.31 \times 11 \times 7.5^2 \quad = 96 \text{ kNm/m}$$

And the self-weight term will be

$$M_\gamma = 0.167 K_a \gamma H^3 = 0.167 \times 0.31 \times 18 \times 7.5^3 = 392 \text{ kNm/m}$$

In section 'a' therefore,

$$M_a = M_Q + M_{qa} + M_\gamma \quad = 1292 \text{ kNm/m}$$

In section 'b' however,

$$M_b = M_{qb} + M_\gamma \quad = 601 \text{ kNm/m}$$

Taking into account that there are 4 m of 'a' and 6 m of 'b' , the average design bending moment to be resisted at the base connection is

$$M = (4 \times 1292 + 6 \times 575) / 10 = \underline{878 \text{ kNm/m}}$$

Certain formal checks are now necessary.

(i) Check required surcharge in section 'a' .

From equation 2.12 and table 2.10 ,

$$\sigma_r = \frac{293}{2.25\ (23 - 1)} = 5.9\ kN/m^2$$

Since $q = 11\ kN/m^2 > 5.9\ kN/m^2$ this is admissible.

(ii) Check required on wall friction in section 'a' .

The total normal thrust

$$N = K_n Q + K_a q H + 0.5 K_a \gamma H^2$$

$$= 0.61 \times 293 + 0.31 \times 11 \times 7.5 + 0.5 \times 0.31 \times 18 \times 7.5^2$$

$$= 361\ kN/m$$

The total tangential force

$$T = K_t Q = 0.38 \times 293 = 111\ kN/m$$

Therefore, the mobilised angle of wall friction

$$\delta = \tan^{-1}(111/361) = 17°$$

The permissible angle will be at least 25°, so this is acceptable.

(iii) Check of local load effects in structure.

Only the average bending moment was calculated, whereas the loading on the structure, being different in sections 'a' and 'b' is asymmetric. Further calculations of local bending and twisting moments may be necessary. These load effects are then multiplied by partial factor $\gamma_{F3} = 1.1$ and compared with ultimate resistances based on strengths factored down by appropriate values γ_m, according to BS 5400 Part 4

2.4 Water Pressure

The use of granular backfill will usually ensure that no significant ponding of pore water will occur above the level of the weepholes in the wall stem. In these circumstances it will be sufficient to consider that the long term piezometric levels in the backfill, and beneath the wall base, will be hydrostatic with an elevation equal to that of the weepholes. Figure 2.24 indicates the typical water elevations which should be used to calculate water pressures u for substitution in equation 2.3 to calculate the vertical effective stresses due to selfweight and uniform surcharge.

Where the base of the wall can be provided with drain holes at intervals, and the bottom surface can be drained without ponding, even these small water pressures can be reduced to negligible levels. The base drain may consist of

a) a longitudinal drainage trench laid to a fall
b) lateral trench drains at sufficient intervals

c) a well compacted or stabilised drainage blanket.

Since the safety and serviceability of the completed structure will depend completely on the ability of the drainage system to prevent the build-up of water, it will be necessary to take suitable precautions where particular water hazards may occur. These additional evasive measures may include:

a) a permeable filter,such as an appropriate geotextile, to prevent the ingress of fine grained soil fractions into material which is intended to remain more permeable.

b) a blanket drain of selected drainage material placed either above or below the wall base, and possibly extending beneath the backfill interface.

c) an impermeable barrier such as asphalt, concrete, or plastic sheet, to prevent the infiltration of surface water on the retained hinterland, coupled with corresponding surface drainage measures.

Where, for any reason, anticipated water pressures larger than those indicated in figure 2.24 can not be forestalled,it will be necessary to construct a flow net consistent with the hydrogeological conditions. Figure 2.25 shows a situation in which continuous infiltration and downward percolation cannot be prevented in the hinterland of natural ground, although the rectangle of granular fill is acting as a drain.

It will be clear that, in this case, water pressures in excess of those of figure 2.24 occur in the "active" zone of natural soil against the granular backfill. They cause the selfweight thrust on the wall/backfill monolith to be increased.

Stress analysis is difficult in cases such as this, but it is possible to make straightforward calculations using Coulomb's trial wedge method, as shown in figure 2.26. The use of Coulomb's technique gives answers to active thrust problems which are acknowledged to be close enough to the truth, and close enough to the results of more detailed stress analyses, to require no further correction. Reasonable assumptions do additionally have to be made regarding the distribution of stresses corresponding to the calculated thrusts. It will be as important that the eccentricity of the foundation reaction is correctly estimated as it is that the magnitude is properly calculated.

It can easily be verified that the mean water pressure on a plane inclined at θ radians within a height H in figure 2.25 is approximately $0.2\gamma_w H\theta$. The effect can be shown to be to increase the horizontal component of the thrust on the retaining wall by between $0.05\gamma_w H^2$ and $0.075\gamma_w H^2$ approximately. The lower value applies where one of the two required slip surfaces is free to form at any desired angle within the drained fill: the higher value applies where the rectangle of fill is either relatively narrow or relatively strong so that slip surfaces within it are constrained or eliminated. These thrusts may, with sufficient accuracy, be taken to act uniformly on a vertical plane through the heel of the wall. They may be assumed to be transmitted ultimately down to the base, except where this is so short that an active wedge behind the stem would project beyond the heel.The corresponding change in the vertical component of thrust from the backfill onto the retaining wall can generally be safely neglected.

Superposition of isolated loads can be treated as before, so long as the soil

response to the loading is fully drained. Where excess pore pressures may be created in clayey fills it will usually be necessary to undertake both drained and undrained analyses so as to examine the possible range of soil behaviour.

3 STRAINS IN GRANULAR BACKFILL

3.1 Shear and Volumetric Components

Many types of apparatus are available for testing the response of soils to imposed stresses or strains. Samples may be cubical or cylindrical, may deform with rigid or flexible boundaries, in axisymmetric or plane strain, plane stress, or indeed in an arbitrary stress or strain path through the use of computer control. However, the standard test remains the triaxial compression test on a solid cylindrical sample.

Soil responds in quite distinct ways to increases in mean effective stress and shear stress. All soils tend to reduce in volume and increase in strength and stiffness when their mean effective stress is increased. On the other hand, an increase in shear stress will provoke a progressively reducing shear stiffness leading eventually to a shear failure.

For this reason, the data of soil tests are often interpreted solely in terms of shear stress and strain. Volumetric stiffness, when required, is usually measured indirectly through the one-dimensional compression modulus $E_o = 1/m_v$ measured in an oedometer. The measurement of volume changes in a triaxial test could suffer from membrane penetration errors. Direct strain measurement between internal markers fixed to or beneath the latex membrane can, however, give reliable data: Symes and Burland (1984).

For an elastic material, the ratio of oedometer modulus E_o to bulk modulus K is exactly 2 at a typical Poisson's ratio υ of 0.2, and tends to 1 as υ tends to 0.5 .

The most readily applied interpretation of shear tests remains the Mohr circle analysis of stresses and strains in the deviatoric plane containing the major and minor principal stresses. Figure 1.1 shows the definition of the greatest shear stress t, and the average effective stress s′ in the deviatoric plane, mobilised in a triaxial test at a particular shear strain

$$\gamma = \epsilon_1 - \epsilon_3$$

and a volumetric strain,

$$\epsilon_v = \epsilon_1 + \epsilon_2 + \epsilon_3$$

which would be negative in the case of dilation.

These conventional definitions do not involve the intermediate principal stresses. The habitual observation that strength and stiffness is greater in plane than in axisymmetric strain is, therefore, either conservatively ignored or dealt with empirically. The mean effective stress p′ in plane strain is usually taken to be equal to mean stress s′ in the deviatoric plane.

3.2 Cycles of Shearing

Figure 3.1 shows a typical shear stress-strain curve for a previously unsheared sample of granular soil. The virgin response OA involves a relatively large amount of irrecoverable plastic strain, chiefly associated with sliding at particle contacts as the grain structure accommodates to new stress states. The rebound - reloading stiffness AB,BC is evidently rather

larger than the virgin loading stiffness. It is also seen that the initial rebound-reloading stiffness is not simply elastic, or even simply hysteretic, since $\gamma_C > \gamma_A$. Only after a few load cycles does the behaviour shake down into a stable hysteresis loop DE. The number of cycles necessary to achieve cyclic stability increases as the shear stress amplitude approaches the static shear stress limit t_{max}, and is always greater for loose soils than for dense.

Since soil backfill will have been subjected to many cycles of loading and unloading during its compaction, it will be sensible to treat its condition as stably hysteretic - at least for stress excursions upto the magnitudes of those induced during compaction. It has been found, Hardin and Drnevitch (1972), that the relation between cyclic amplitudes of shear stress and strain for a wide range of quartz and feldspar sands can be represented with reasonable accuracy by a hyperbolic relation, fitted to the soil state as shown in figure 3.2 .

Strain cycles with amplitudes below about 10^{-5} (or one thousandth of one percent) receive an approximately linear response with a maximum shear modulus, which is a function only of void ratio e and mean effective stress s', and which can be written for quartz or feldspar sands

$$G_{max} = A(G_{grain}\ s')^{½}/(1 + e)^3 \qquad (3.1)$$

where A is a dimensionless factor depending on the nature of the asperities at points of grain contact and the organisation of contact forces, the function $1/(1 + e)^3$ accounts for the usual 2-fold reduction in G_{max} over the range e_{min} to e_{max}, and $(G_{grain}\ s')^{½}$ is a dimensionally correct function of intrinsic grain stiffness and the mean soil stress in the plane of shearing. For typical quartz and feldspar sands this can be simplified to

$$G_{max} = 50000(s')^{½}/(1 + e)^3 \qquad (3.2)$$

where G and s' are both measured in kPa.

For many purposes it is sufficient to describe the large strain response in terms of a limiting shear stress $t_{max} = s'\sin\phi_{max}$, achieved asymptotically. In fact, of course, t_{max} is reached at a finite shear strain of between 10^{-2} and 10^{-1}. In the development of that peak strength, volumetric dilation will have been increasingly evident, reaching a maximum rate at the same instant that the shear strength reaches a maximum, as was shown in figure 1.2 . At this juncture the soil may rupture, with subsequent deformations intensified in localised shear bands. These large post-peak strains permit the void ratio of the soil to increase (in the case of an initialy dense soil) to its critical state value e_{crit} at which the dilation capacity will be exhausted. The shear strength will then have fallen to $t_{crit} = s'\sin\phi_{crit}$. The selection of appropriate values for ϕ_{max} and ϕ_{crit} was dealt with in section 1.1 .

Equations 1.5 or 1.6 for ϕ_{max} together with 3.2 for G_{max} allow the hyperbolic approximation in figure 3.2 to be written

$$t = \frac{G_{max}\ \gamma}{(1 + G_{max}\ \gamma/t_{max})} \qquad (3.3)$$

The correct datum for shear stress and strain is the instant of the last load reversal. If the shear stress at that instant was t_i then a modification to equation 3.3 is necessary for subsequent strains γ

$$(t - t_i) = \frac{G_{max}\,\gamma}{[1 + G_{max}\gamma/\,(t_{max} - t_i)]} \qquad (3.4)$$

It should be recalled that equation 3.2 for G_{max} will only hold (approximately) for the stable hysteretic response of soil which has been repeatedly cycled. The initial stiffness G_{max} relevant to virgin loading may be lower by a factor between about 2 for dense soils and 5 for loose soils; Duncan and Chang (1970).

3.3 Effects of Wall Rotation : a Simplified Approach

Equation 3.4 can be converted into a relation between earth pressure coefficient and the rotation of a wall about its base, using the simple displacement field of Bransby and Milligan (1975), shown in figure 3.3 . They showed that the implied shear strain in the assumed zone of uniform deformation OAZ is related to the rotation θ about the toe of the wall by the expression

$$\gamma = 2\ \sec\psi\ \theta \qquad (3.5)$$

where ψ is the soil's angle of dilation, introduced in figure 1.3 . Although this involved the neglect of wall friction, it was also shown that the same displacement field could be observed with rough walls. Also, the relation between γ and θ was found to be valid for flexible walls, where zero-extension lines parallel to OZ could be drawn at $(45 - \psi/2)$ to the vertical to derive a curved ground surface ZA' compatible with a curved wall surface OA'.

It is now possible to derive the K,θ relation for a smooth rigid wall rotating about its toe. In this particular case there is no rotation of principal stress, so the alternative "elastic" and "plastic" approaches to earth pressure prediction discussed by Wroth (1972) are almost exactly equivalent if the same stress-strain data are used to derive the parameters. If the vertical effective stress at depth z remains constant at γz , then when the lateral earth pressure coefficient is K, from figure 1.1,

$$t = \gamma z(1 - K)/2 \qquad (3.6)$$

Substitution in equation 3.4 gives

$$(K_i - K)\gamma z = \frac{4\ \sec\psi\ G_{max}\,\theta}{1 + \dfrac{4\ \sec\psi\ G_{max}\,\theta}{(K_i - K_{limit})\gamma z}}$$

where the initial earth pressure coefficient is K_i.

This can be written

$$K = K_i - \frac{(K_i - K_{limit})}{1 + \dfrac{(K_i - K_{limit})\cos\psi}{\lambda\theta}} \qquad (3.7)$$

where

$$\lambda = 4\ G_{max}\ /(\gamma z) \qquad (3.8)$$

$$K_{limit} = K_a = (1 - \sin\phi_{max})/(1 + \sin\phi_{max}) \qquad \text{for} \qquad \theta > 0$$

$$K_{limit} = K_p = (1 + \sin\phi_{max})/(1 - \sin\phi_{max}) \qquad \text{for} \qquad \theta < 0$$

Equation 3.2 for the G_{max} of cyclically pre-strained sand can be inserted into 3.8 to give

$$\lambda = \frac{140000(1 + K)^{\frac{1}{2}}}{(1 + e)^3 (\gamma z)^{\frac{1}{2}}} \qquad (3.9)$$

It is now clear that equations 3.7 and 3.9 represent a highly non-linear expression for the earth pressure coefficient K as a function of θ, and one which properly should be solved incrementally.

The degree of non-linearity can, however, be reduced by recognising the following simplifications.

1) The effect of variations of K on G_{max} is through the term $(1+K)^{\frac{1}{2}}$ relating to the current mean stress. This term is able to vary only from about 1.2 to 1.1 during outward rotation from an initial state with a typical $K_o = 0.45$ to a fully active state with $K_a = 0.2$. Even if inward rotation upto $K_p = 5$ were being considered, $(1+K)^{\frac{1}{2}}$ would only vary from 1.2 to 2.4 . The more serious problem with passive rotation would be the likelihood that the soil would regain a virgin plastic state, so that G would have to be significantly reduced in any event, perhaps by a factor of 10. It follows that the value for λ in 3.9 might simply be calculated on the basis of a current value for K, and used directly in the non-incremental expression 3.7 for K. This simplification is tantamount to assuming that the earth pressure coefficient in a particular case is dependent on the total wall rotation and the current stress level, and not on the precise path they took. Indeed, for the purposes of a rough hand calculation it will be acceptable to base the value for λ on a moderate value for K, say 0.5, and then to iterate once, deriving a first value for K from 3.7 and inserting it again in 3.9 for λ, then deriving a better value for K from 3.7 .

2) Although dilation varies with shear strain in the general fashion of figure 1.2, the angle of dilation ψ is found to be confined within the range $\pm 25°$ for all granular soils at all stages of test. This restricts $\cos\psi$ to the range 0.9 to 1.0. In these circumstances $\cos\psi$ may be taken to remain unity with negligible error, once again eliminating strain path difficulties.

It follows that a sufficiently accurate representation of wall rotation effects is given by

$$K = K_i - \frac{(K_i - K_{limit})}{1 + \frac{(K_i - K_{limit})}{\lambda\ \theta}} \qquad (3.10)$$

where the non-dimensional soil stiffness λ is given by equation 3.9 .

This relation is sketched in figure 3.4a for outward wall rotation from a sequence of initial values K_i between 0.4 and 3.2, and for relative densities of 20%, 60%, and 100%, relevant to a point at 4 m depth in a soil with the

following properties :

$G_s = 2.65$ $S_r = 0$ (dry)
$e_{max} = 0.85$ $e_{min} = 0.55$
$\phi_{crit} = 32°$

and using the larger plane strain ϕ value given by equation 1.5 .

The relevant values of λ involved in the production of these curves are listed in table 3.1 . In a typical bridge abutment of 8 m height, the soil at 1 m depth should behave about three times stiffer than the soil at 8 m. The $z^{\frac{1}{2}}$ term in the shear modulus means that the abscissae of figure 3.4 can be construed as $\theta(4/z)^{\frac{1}{2}}$ except where stress level effects might affect the maximum shear strength (e.g. for large passive rotations of a wall against dense sand).

Figure 3.4a shows that there is relatively little reduction in earth pressure at an outward rotation of 10^{-5} radians. Fully active conditions are mobilised at a rotation of about 10^{-2} radians, after which the soil would be vulnerable to rupture along a slip surface with a consequent increase of earth pressure towards critical state conditions. The rotation necessary to halve the difference between K_i and $K_a(min)$ is in the range 10^{-4} to 4×10^{-4}.

An estimate of the effect of inward rotation producing passive pressure is shown in figure 3.4b . There is negligible increase in earth pressure at a rotation of 10^{-5} radians. At 10^{-4} the absolute changes in K are commensurate with the active case, but they now appear negligible in relation to the eventual attainment of K_p. Fully passive conditions are only mobilised at an inward rotation of about 10^{-2}. The rotation necessary to halve the difference between K_i and K_p is approximately 6×10^{-4}. It is essential to recognise that these predictions are for pre-cycled soils with no tendency to progressive failure. Three effects would tend to soften the rate of passive mobilisation compared with figure 3.4b.

1) On the first passive cycle, the soil would soon escape beyond its compaction pre-loading and behave more like a virgin material with extra irrecoverable strains upto 5 times greater than those indicated.

2) Volumetric compression was neglected in the present formulation, but this could be significant for loose soils.

3) Progressive failure would tend to interupt the progress towards $K_p(max)$ for dense soils and lead to lower critical state pressures.

3.4 Initial Strain

Equation 3.10 expressed the change of earth pressure coefficient against the shear strain (or equivalent wall rotation) occuring since the last strain reversal. Stiffness then reduces as strain increases, although this is partly disguised in figure 3.4 by the choice of a logarithmic strain axis. It is clear, however, that the analyst must have regard to whether some process - such as wall rotation - will continue a previous strain path referred to some previous strain datum, or will reverse the path and set the strain datum back to zero.

If soil is lightly dumped behind a rigid retaining wall, there will be vertical compression due to the self-weight of the overlying fill. This vertical compression includes shear strains which will act as the datum for any future outward wall rotation (which also tends to cause vertical compression), whereas inward wall rotation will imply a reversal of strain path with the datum reset to zero.

The strains due to one-dimensional compression under self-weight alone can be estimated. Figure 3.5 shows a layer of soil of depth dz being placed. The effect at depth z is of an increment of shear stress

$$dt = (d\sigma_v - d\sigma_h)/2 = (1 - K_o)\rho g\, dz/2 \qquad (3.11)$$

If the soil responds with its maximum shear modulus then there will be a corresponding increment of shear strain

$$d\gamma = \frac{dt}{G_{max}} = \frac{(1 - K_o)\rho g\, dz}{2\, G_{max}}$$

On substitution of equation 3.2 for G_{max} and using

$$s' = (1 + K_o)\rho g z/2$$

and $$\rho = G_s / (1 + e)$$

we obtain

$$d\gamma = \frac{4.43 \times 10^{-5}(1 - K_o)\, G_s^{0.5}(1 + e)^{2.5}\, dz}{(1 + K_o)^{0.5}\, z^{0.5}}$$

On integration to find the magnitude of initial shear strain due to one-dimensional compression following placement of height z of fill

$$\gamma_i = \frac{8.86 \times 10^{-5}(1 - K_o) G_s^{0.5}(1 + e)^{2.4}\, z^{0.5}}{(1 + K_o)^{0.5}} \qquad (3.12)$$

Remarkably, it is found that using

$$K_o = 1 - \sin\phi_{max}$$

together with equation 1.6 for ϕ_{max} , and using typical values $e_{min} = 0.5$ and $e_{max} = 0.8$ for the calculation of relative density I_D, the functional dependence of γ_i on e completely disappears, and 3.12 reduces to

$$\gamma_i = 2.5 \times 10^{-4} \sqrt{z} \qquad (3.13)$$

The initial shear strain following compaction is much harder to estimate, since it will depend on the precise stress history of an element of soil that will have suffered continuous cycles of compaction stress, reducing in intensity as its burial causes the mean stress to rise. At relatively shallow depths the cyclic component may be dominant, and the strain datum might be set to zero. As elements are buried, the tendency for compression under self-weight will tend to overwhelm the cyclic component, and the strain datum might approach the value calculated in equation 3.13 . If there is any doubt,

the conservative step is to invoke initial strains since their effect is to reduce soil stiffness quite considerably. It will usually be necessary, therefore, to assume that there has been initial shear strain due to placement, which will affect subsequent outward deflections, and that this will be approximately as given in equation 3.13 leading to the introduction of an equivalent initial wall rotation of $\theta_i = 1.25 \times 10^{-4} \sqrt{z}$. This is marked on figure 3.4a as the datum following placement. The accompanying scale for subsequent soil strain is distorted, being the original logarithmic scale decremented throughout by γ_i .

3.5 Predictions of wall rotation effects.

The accuracy of equation 3.10 and figure 3.4, optionally modified by 3.13, may be demonstrated through comparisons with published tests. Figure 3.6 shows some of the data of Terzaghi (1934) in which a dry, uniform, angular sand was subjected to outward rotation about the base of a stiff retaining wall, over a height of 1.5 m. In test 2 the sand was reported as being compacted in 150 mm layers to 71% relative density using concrete tampers. In test 3 the sand was simply dumped in place and reported to be at 0% relative density, though this seems to be unlikely. Each of the test curves of K against θ are compared with two predictions, based on an effective depth of 1 m and on initial shear strains of either zero or 2.5×10^{-4}, and fitted to the observed initial pressure coefficient.

It will be seen, firstly, that both pairs of predictions overestimate earth pressure coefficients at wall rotations of 10^{-3}. This can be attributed to some or all of the following factors :

- the neglect of wall friction in our prediction.
- the probable underestimation by Terzaghi of relative density, following an underestimation of the maximum void ratio of the sand; 0.85 would be uncharacteristically low for angular, uniform, sands.
- the probable underestimation $\phi_{crit} = 34°$ based on Terzaghi's observation that this was the angle of repose; at least 37° would be expected for an angular sand.

Ultimately, at rotations of about 10^{-2}, the dense soil dilated towards a critical state and its earth pressure coefficient began to increase again. This is one of the problems to be faced in designing for collapse limit states.

None of these factors should seriously have affected the initial K,θ behaviour relevant for serviceability, however, and it may be seen that the initial gradients in the two tests conform quite well to expectation. The uncompacted fill in test 3 behaves as though it had an initial shear strain $\gamma_i = 2.5 \times 10^{-4}$. The compacted fill in test 2 fits the prediction based on zero initial strain.

The divergence between predictions for $\gamma_i = 0$ and for $\gamma_i = 2.5\sqrt{z} \times 10^{-4}$ is evidently significant. If there is any doubt about the strain history of a soil bed it will be necessary, in design, to assume the worst case. Figure 3.7 shows data of three model studies in which outward wall rotation was imposed on uncompacted sand. Although the relative densities of these sands covered a wide range, the heights of the models were only in the range 1 to 2m.

In each case, the simple theory adopted here fits quite well, once the initial

strain γ_i has been accounted for according to equation 3.13 .

Similar data of Rehnman and Broms (1973) for gravelly sand which had been compacted in five 400 mm layers with a 400 kg vibratory plate are shown in figure 3.8, and compared with predictions based on both $\gamma_i = 0$ and $\gamma_i = 2.5/z \times 10^{-4}$ at an effective depth of 1.33 m. It will be seen that the initial variation of earth pressure coefficient K is intermediate between the two predictions, and that K eventually falls lower than either. The presence of capillary suction due to moisture in the soil may have affected these results, in addition to wall friction developed at larger rotations.

An omission in all these comparisons has been that the variation of earth pressures over a realistic depth appropriate to bridge abutments has not yet been included. However, Broms and Ingleson (1971) have presented data of the lateral pressure changes during the construction and early life of a stiff 4m high abutment wall, forced to rotate about its base as the expansion and contraction of the bridge deck was communicated directly to its crest. Two particular episodes of outward rotation, stages B to C and E to F, are presented using profiles of pressure coefficient versus depth in figure 3.9a. In each case the initial distribution of coefficient K was idealised, and a prediction made of the effects of the observed rotations, which were both of the order of 10^{-3} radians.

Since the fill had been subjected to cyclic strain both during compaction and in service, and since clear points of strain reversal had been chosen for the starting states B and E, the shear strains were based directly on wall rotations, with $\gamma_i = 0$. Having the benefit of the highest possible soil stiffness, a large reduction of earth pressure coefficient was seen in each case, well predicted by the chart in figure 3.4a . In particular, it is confirmed that the significant precompression in the upper part of the backfill requires a significant rotation before it can be eliminated.

For inward rotation, the data of stage D to E in the same study is compared in figure 3.9b with the predictions of figure 3.4b. Once again, the general trend is reasonably predicted : scatter in the data makes exact comparison difficult, however. Since situation E is the instant of maximum lateral earth pressure it could have been expected that the soil would be approaching a virgin loading curve with perhaps half the stiffness assumed in equation 3.9. In the event, there is some over- prediction of earth pressures in figure 3.9b at 2 and 3.5 m depths, but quite a good correlation at 2.5 and 3 m. There must be no doubt that figure 3.4b would generally over-estimate soil stiffness on the first approach to passive pressure, perhaps by an order of magnitude.

The implications for the stress profile of a more typical 8m high abutment wall subject to rotation following compaction can now be deduced. It will be supposed that the initial process of compaction has led to lateral pressures of $25kN/m^2$ between 0.5 m and 3.7 m depth, with a passive type of zone above, and a zone with $K_o = 0.38$ beneath. The relative density of the fill is taken to be 60%.Figure 3.10a depicts the reduction of earth pressures with outward wall rotation, assuming zero initial shear strain. Figure 3.10b includes $\gamma_i = 2.5/z \times 10^{-4}$ leading to a much more gradual attainment of fully active earth pressure conditions. Even under these pessimistic conditions, a wall rotation of 10^{-3} is sufficient to eliminate two thirds of the excess lateral prestress due to compaction, and to reduce the overall thrust of the compacted fill below that of loose fill, for example.

4 PRECOMPRESSION IN GRANULAR BACKFILL

4.1 Significance

The lateral stresses which could be found to be acting in the backfill behind a retaining wall are difficult to predict with any accuracy. They will depend not only on the soil properties (ϕ, etc) but also on its stress history including the condition of the soil prior to compaction, the type of compaction plant and the manner in which it is used, and the cycles of soil loading which have been experienced. Wall movements will have had an equally significant effect, whether due to flexibility, temperature cycling, or foundation compliance. In any event, the presence of lateral stresses in service which are in excess of the "active " value simply indicates that the wall is not at the point of collapse. If some subsequent live load were to endanger the wall so that either a sliding, bearing or bending failure were to begin, it may be assumed that the compaction prestress would be lost as the relevant soil elements mobilized their available strength against the new load. This approach is analogous to the treatment of rolling stresses in steel sections, and is generally valid for ductile materials and structures.

Furthermore, it should be appreciated that precompression can safely be eliminated from soil serviceability considerations such as in foundation displacement calculations. Figure 3.10 showed that an outward wall rotation about the base of 10^{-2} could be relied upon to eliminate typical built-in stress states entirely. Such a rotation would be typical of the serviceability limit to be imposed on the design of spread footings.

Other modes of movement are possible of course. Wall translation tends to result in localisation of strains in shear bands, which enhances the erasure of stress history. The possibility of such localisation will cause the designer to use critical state strengths in collapse analyses, perhaps ϕ_{crit} = 32° rather than ϕ_{max} = 38° for a sub-rounded sand fill guaranteed to be at least at 60% relative density. In proceeding this way, the designer may assume that he will be successful in eliminating shear bands. It would then be logical to assume uniformly well-compacted soil for the purposes of a serviceability calculation, while taking fully softened soil in a collapse scenario.

The practical significance of a strenuous critical state collapse condition is made apparent in figure 4.1 .The response of medium dense soil to outward wall rotation, shown in figure 3.10b for the pessimistic case of pre-existing strain due to compression following placement, is superimposed onto a simple Rankine stress profile for fully softened soil with ϕ_{crit} = 32°. If the wall were to rotate outwards, the initial construction stresses would have fallen below the critical state collapse condition at a rotation of only 10^{-3}, and would then remain below unless shear rupture occurred and the soil softened.

There is also concern about the effects of inward wall rotation where soil consolidation might lead to differential settlements as shown in figure 4.2, for example. Here, the possible passive reaction would tend to counter-balance the tendency for rotation, so that soil serviceability calculations will tend to be conservative if they ignore this soil- structure interaction effect.

Precompression due to stress history is therefore of concern principally in structural serviceability calculations. It will be essential to check that

compaction stresses will not cause impermissible cracks or deflections in the reinforced concrete. Subsequent highway loads will also have to be considered. Finally, an estimate will also have to be made of the effects of any forseeable long-term ground movements, especially if inward rotation of the abutment is possible. Wall flexibility will have an important influence in all these matters, but good estimates of the effects of wall rotation can be made using the analysis of section 3.3 if suitable allowances are made for possible deviations in soil stiffness, as discussed in sections 3.4 and 3.5 .

4.2 Stresses Beneath a Compaction Machine

The designer will inevitably be uncertain about the type of compaction plant which will be used to construct the backfill, and the orientation it might have with respect to the wall. The best that can be achieved will be an understanding of the mechanisms involved in the induction of lateral soil stresses, and the creation of an upper bound estimate which can be verified through field measurements. This should lead to the adoption of a rational criterion for excluding excessively heavy construction plant from the vicinity of the wall.

For the purposes of creating a safe bound, it will be sufficient to analyse the lateral stresses beneath a roller in a plane transverse to its axis, as shown in figure 4.3 . It will be assumed that these stresses come to act equally at every location and in every orientation, while the machine is overhead. Spread of stress along the wall will conservatively be ignored.

Broms (1971), Ingold (1979), Duncan and Seed (1986), and others have gone on to use Boussinesq's elastic solutions. Although Forssblad (1965) shows some data in support of this approach, it is well known that the mobilised angle of shearing deduced beneath the edges of a surface load in an elastic analysis will, in practice, exceed the soil's capacity. There are also difficulties in making elastic predictions close to retaining walls since the classical solutions refer to loads on the surface of an elastic half-space. If it is required to prevent any lateral movement of a rigid wall, it is necessary to invoke reflected images of the load on the surface of the "imaginary" soil on the other side of the wall which, by superposition, annul deflections on the plane of symmetry and double the lateral stresses on the wall compared with the free field. A wall which was more flexible than the elastic quarter-space it replaced would attract, correspondingly, lateral stresses smaller than those of the free field.

Advantage will therefore be taken of the alternative plastic stress distributions created in section 2.3 and selected to mobilise some desired angle of shearing.

Consider, for example, a vibrating steel roller. Let the total maximum force per unit length of roll applied by the joint action of gravity and imposed cyclic acceleration be Q. Assume that the bearing stress distribution can be identified with that in an N_γ bearing capacity solution with some mobilised angle of shearing ϕ. Here, the penetration of the roller is assumed to be negligible in comparison to its width of contact B.

Then,

$$Q = \tfrac{1}{2}B^2\gamma N_\gamma \qquad (4.1)$$

so that

$$B = \sqrt{(2/N_\gamma)}\sqrt{(Q/\gamma)} \qquad (4.2)$$

and the bearing stress

$$\sigma_b = Q/B = \sqrt{(N_\gamma/2)}\sqrt{(Q\gamma)} \qquad (4.3)$$

Now assume, following section 2.3, that the stress distribution beneath the roller can safely be considered to be the sum of Rankine's active self-weight stresses and the plastic stress distribution appropriate to the N_q bearing capacity solution.

Figure 4.4 depicts the lateral stress distribution beneath the centre line of a strip load, as a function of the mobilised angle of shearing, compared with the elastic half-space solution. The plastic stresses were taken from figures such as 2.11 to 2.14 modified to comprise a larger number of very small stress jumps, so that smooth curves were obtained. Four features of figure 4.4 may be noted:

(i) A cut-off at $\sigma_h = K_a\sigma_b$ applies within an active wedge of depth $z_o = (B/2).\tan(45 + \phi/2)$

(ii) The curves for given values of ϕ remain roughly in proportion at all depths.

(iii) The curves are roughly hyperbolic.

(iv) Lateral stress increments predicted in an elastic half-space reduce extremely rapidly with depth in comparison with the plastic solutions.

Further insight may be gained by plotting equivalent solutions for vertical stress increments, against the <u>inverse</u> of the depth ratio: see figure 4.5 .It will be seen that with negligible variation the extra vertical stress induced on the centreline can be characterised, irrespective of ϕ in the range 30° to 45°, as

$$\sigma_v = \sigma_b \qquad \text{for } B/z > 1$$

$$\sigma_v = \sigma_b\, B/z \qquad \text{for } B/z < 1 \qquad (4.4)$$

The corresponding extra lateral stress will be $K_a\sigma_v$ which will accordingly be reduced the higher is the mobilization of ϕ. Combining equations 4.2, 4.3 and 4.4 and superimposing self-weight, we obtain the approximate result

$$\sigma_h = K_a\gamma z + K_a\sqrt{(N_\gamma/2)}\sqrt{(Q\gamma)} \qquad \text{for } z < \sqrt{(2/N_\gamma)}\sqrt{(Q/\gamma)}$$

$$\sigma_h = K_a\gamma z + K_aQ/z \qquad \text{for } z > \sqrt{(2/N\gamma)}\sqrt{(Q/\gamma)} \qquad (4.5)$$

4.3 Stresses Following Compaction of a Layer

The original lateral stresses will tend to reduce when the roller passes away. However, this reduction may be quite small in proportion if, as is usually the case, the bending stiffness of the wall is small in comparison to the shear stiffness of the retained fill. In effect, the wall is unable to rebound into the stiffer soil and therefore tends to retain the bending moments it possessed while the compaction plant was working against it. The lateral compaction stresses are, as it were, locked in.

However, some lateral stress reduction is inevitable in the most superficial soil zone where the lateral stress would otherwise exceed the "passive" limit. This was the simplification introduced by Broms (1971) in the first rational assessment of post-compaction stresses: see figure 4.6. Let us assume that this possible "passive" zone will extend to a depth z_p, and that $z_p > \sqrt{(2/N_\gamma)}\ \sqrt{(Q/\gamma)}$. Then, using equations 4.5

$$K_p \gamma z_p = K_a \gamma z_p + K_a\, Q/z_p$$

i.e.
$$z_p^2 = \frac{K_a Q}{(K_p - K_a)\gamma} \qquad (4.6)$$

Since $K_p = 1/K_A > 3$ it is possible to write

$$z_p \simeq K_a\, (Q/\gamma) \qquad (4.7)$$

It is now possible to see that the assumption $z_p > \sqrt{(2/N_\gamma)}\ \sqrt{(Q/\gamma)}$ was justified since $K_a \geq \sqrt{(2/N_\gamma)}$ for $\phi \geq 30°$. On back substitution for z_p we obtain

$$\sigma_{h\,max} = K_p \gamma z_p = \sqrt{(Q\gamma)} \qquad (4.8)$$

a value which would hold when the roller has passed away, irrespective of the mobilized angle of shearing resistance in the usual range.

A similar result was obtained by Ingold (1979) except that Q in equations 4.7 and 4.8 is replaced by $2Q/\pi$. The effect after finding the square root is that Ingold's formulae are smaller by the factor 0.8. The foregoing approach makes consistent use of plastic stress distributions in contrast to the mixture of elastic and plastic assumptions used by Ingold. The similarity between the two results demonstrates once again that vertical stress distributions beneath surface loads are dictated chiefly by the conditions of geometry and equilibrium, rather than the constitutive relation assumed for the material. Ingold reported that such field data as existed seemed to fit the theory quite well.

A revised estimate can be made if the elastic rebound of the neighbouring wall will not tend to lock stress into the soil being unloaded. The earth pressure coefficient after one-dimensional unloading from effective stress σ_{vi} to σ_v can be written, following Schmidt (1965)

$$K = K_i\, R^\alpha \qquad (4.9)$$

where the overconsolidation ratio

$$R = \sigma_{vi} / \sigma_v$$

and where the parameter α can be equated approximately to the angle of shearing of the soil, ϕ in radians. The initial vertical stress, derived from the superposition of self-weight onto equation 4.4 is, as before:

$$\sigma_{vi} = \gamma z + \sqrt{(N_\gamma/2)}\sqrt{(Q/\gamma)} \qquad \text{for } z < B$$

$$\sigma_{vi} = \gamma z + Q/z \qquad \text{for } z > B \qquad (4.10)$$

The final vertical stress is simply

$$\sigma_v = \gamma z$$

so that the overconsolidation ratio is

$$R = 1 + \sqrt{(N_\gamma/2)}\sqrt{(Q/(\gamma z^2))} \qquad \text{for } z < B$$

$$R = 1 + Q/(\gamma z^2) \qquad \text{for } z > B \qquad (4.11)$$

Then from 4.9, for unloading one-dimensionally from an active state,

$$\sigma_h = K_a \gamma z [1 + \sqrt{(N_\gamma/2)}\sqrt{(Q/(\gamma z^2))}]^\phi \qquad \text{for } z < B$$

$$\sigma_h = K_a \gamma z [1 + Q/(\gamma z^2)]^\phi \qquad \text{for } z > B \qquad (4.12)$$

The maximum value of lateral stress after relief can then be shown, for typical conditions, to occur at $z = B$ so that

$$\sigma_{h\,max} = K_a \gamma \sqrt{(2/N_\gamma)}\sqrt{(Q/\gamma)}\ [1 + N\gamma/2]^\phi$$

or

$$\sigma_{h\,max} = K_a \sqrt{(2/N\gamma)}\ [1 + N\gamma/2]^\phi \sqrt{(Q\gamma)} \qquad (4.13)$$

Typical values are

ϕ :	30	35	40	45
$\sigma_{h\,max}/\sqrt{(Q\gamma)}$:	0.37	0.39	0.48	0.70

Duncan and Seed (1986) went on to study the effect of soil hysteresis on successive load/unload cycles, but the additional changes are not particularly significant since they tend to fall between the extremes already established in equations 4.8 and 4.13 . Taking into account all the uncertainties regarding the precise use of compaction plant, it may be considered that sufficient has been done to establish the significant parameters and the possible range of values of the peak lateral stresses induced by compacting a single layer.

4.4 Compaction of Many Layers

Consider the compaction of a perfectly drained well graded granular fill, up to a unit weight γ = 20 kN/m^3 , and strength ϕ = 40°, using a vibrating roller applying a gross cyclic force of 40 kN/m to layers of 150 mm depth. The following dimensions are pertinent: from equation 4.2, B = 0.144m; from equation 4.7, z_p = 0.217 m. Figure 4.7 displays the calculated stress distribution in relation to the thicknesses of the layers. It may be surmised that the effect of compaction over the suface of layer C is

(i) to thoroughly disturb that layer by the initiation of repeated large-strain bearing failures

(ii) to compact layer B by repeated small-strain stress cycles, leaving an average lateral compaction stress σ_c locked into that layer of between $0.9\sqrt{(Q\gamma)}$ and $0.45\sqrt{(Q\gamma)}$.

(iii) to affect the stresses in layer A relatively little, since the stress cycles during the rolling of layer C would be smaller than those which would previously have been caused in A by the rolling of layer B.

This sequence is consistent with the observations of Youd (1972). It is also interesting to note that the maximum thickness D,of compacted layer recommended in Table 6/4 of the Department of Transport Specification for Road and Bridge Works (1987) is almost exactly in proportion to the square root of the mass per metre of the roller, $D \simeq 0.16\sqrt{(Q/\gamma)}$. It follows that the proportions $D:B:z_p$ which are so significant a feature of figure 4.7 would remain unchanged whatever weight of machine were selected, if the specification were adhered to. In each case the mean stress locked into the next-buried layer, such as B in figure 4.7, will be in the range $0.45\sqrt{(Q\gamma)}$ to $0.9\sqrt{(Q\gamma)}$. A middle range vibrating roller could have a mass of 2000 kg/m so that with a dynamic force factor of 2 it will deliver Q = 40 kN/m and generate lateral compaction stresses in the range 12 to 25 kN/m^2.

As the layers are successively buried, consideration needs to be given to possible further increases in lateral stress. Figure 4.8 shows a simplified but acceptable stress path from the compaction point C for a soil near a rigid wall, or in the free field. Point C is identified as having a lateral stress σ_c derived from equation 4.12 and a vertical stress related to the thickness of a compacted layer. The soil will react with little extra lateral stress until point D is reached at which the earth pressure coefficient is K_o. This will be, referring to figure 4.9, at a depth

$$z_o = \sigma_c \; / \; (K_o\gamma) \qquad (4.14)$$

Subsequent compression will take place along the K_o line if there is no wall deflection. The resulting stress profile in figure 4.9 is identical to that first proposed by Broms.

4.5 Effect of Wall Movement

If a wall flexes as soil is compacted against it, two effects may be noticed. In the layer most recently placed, the wall will tend to spring back into the soil thus tending to preserve the lateral stress when the machine moves away.

The compaction stress σ_c should initially tend towards its upper limit of $0.9/(Q\gamma)$. Deeper soil layers will, however, relax due to the continued outward movement of the wall as fresh layers press against it.

Figures 3.10 and 4.1 demonstrated that a rigid wall rotation of the order of 10^{-3} could be successful in reducing typical compaction stresses to a Rankine profile equivalent to the mobilization of $\phi = 32°$ or less. This result could be generalised for a range of initial states using figure 3.4 .

If the designer of a flexible wall is to make use of this concept, the required rotation must be available subsequent to the placing of material at a particular level. Consider, for example, a layer at height h in a fill of total height H, supported by a cantilever wall of flexural stiffness EI, as shown in figure 4.10. We will calculate the flexibility conditions necessary to ensure the mobilisation of some particular earth pressure coefficient K.

The local wall slope as the layer is placed at height h is initially

$$\theta_i = \frac{K\gamma H^4}{24\ EI}$$

The final slope at h as the fill is completed is

$$\theta_f = \frac{K\gamma[H^4 - (H-h)^4]}{24\ EI}$$

Then the wall rotation effective in creating supportive soil shear strains will be

$$\Delta\theta = \theta_f - \theta_i = \frac{K\gamma[H^4 - (H-h)^4 - h^4]}{24\ EI} \qquad (4.15)$$

and this symmetrical function is plotted in figure 4.11 . It will be seen that the local wall rotation exceeds

$$\Delta\theta = 0.02\ \frac{K\gamma H^4}{EI} \qquad (4.16)$$

for the middle 70% of the wall. The upper 15% will, in any event, be subject to overstress due to traffic loads. The lower 15% is not in any position materially to affect bending moments. A criterion therefore emerges for the flexibility of the wall necessary to reduce the main body of compaction and K_o stresses to some smaller desired earth pressure coefficient. Following figure 4.1, for example, and allowing at least 10^{-3} rotation to reduce K to 0.31 :

$$\Delta\theta > 10^{-3}$$

So, substituting in 4.16

$$EI < 20\ K\gamma H^4 \qquad (4.17)$$

Taking K = 0.31 and ρ = 2000 kg/m , γ = 19.6 kN/m , we get :

$$EI < 120\ H^4 \qquad (4.18)$$

This shows that an 8 m wall with granular backfill compacted to at least 60% relative density will be sufficiently flexible to shed part of its compaction stresses, and mobilise $\phi = 32°$, if its flexural stiffness EI is less than about 0.5×10^6 kNm^2/m, commensurate with typical reinforced concrete design to a wall thickness of about 700 mm.

Similar criteria could be set so as to achieve more or less earth pressure following completion of construction. However, two points should be borne in mind. First, there is little point in reducing seviceability earth pressures below collapse values based on ϕ_{crit}. Secondly, there will be no possibility of relieving traffic or compaction stresses in the top of the fill : the proper design condition will include appropriate live loads on the surface.

The possibility of slippage on the base might equally be used to limit the possible build-up of compaction stresses through the whole depth of backfill. There must, however, be no tendency to slip under the effects of superimposed loads : all that can be achieved is the erasure of historic lateral stresses greater than presently required to resist current loads.

There may be some advantage in designating a 2m zone near the wall in which a smaller compactive force Q' is to be used. The compaction stresses should not then exceed the larger of $0.45\sqrt{(Q\gamma)}$ for the free field and $0.9\sqrt{(Q'\gamma)}$ for the zone near the wall. It should be recalled that friction on the base of the fill is the only agency preventing larger lateral pressures in the hinterland from bearing on the wall itself.

4.6 Effect of superimposed loads

The effect of superimposing a uniformly distributed surcharge q over the surface of the compacted fill is demonstrated in figure 4.12 . In principle, the mobilized earth pressure coefficient for on-going plastic deformation will change from K_1 to $K_2 < K_1$ as the wall rotates outwards under the extra stress, and the compaction stresses in the upper region of the fill will similarly be reduced as shown in figure 4.12a . In practice, the extra wall rotation may be negligible, or can conservatively be neglected, and the previous value of K can be retained for those elements responding to the extra vertical stress. Between depths z_1 and z_2, however, we have elements which are still over-compressed, and these stresses can remain unaltered for the purposes of a simple, conservative calculation. If more accuracy is required, iteration can be used to derive a new wall rotation from the simple pressure distribution in figure 4.12b, leading to the derivation of modified pressures, and so on.

A similar approach can be taken for concentrated loads, but there can be an allowance for the vertical stress increment reducing with depth beneath the surface. Since some soil elements will respond quasi-elastically where they have been pre-compressed, while other elements will be mobilizing quasi-plastic earth pressure coefficients, the exact stress distribution could be disputed and either elastic or plastic distributions might be used with equal justification. If elasticity is used, however, consideration needs to be given to the possible influence of the wall. Figure 4.13 demonstrates the use of an "image" load Q* to create a plane of symmetry in the desired location of a rigid wall. Their superposition in the free field eliminates lateral movement at the wall, but has the effect of doubling all the normal

stress increments near the wall. The more flexible the wall, the smaller the stress it attracts. If the wall were to be as flexible as the soil it replaces, the free field solution would apply unaltered, and if the wall were even more flexible the stress increment it would receive would be smaller than the simple elastic half- space solution.

It would be equally satisfactory to use the plastic distributions of stress beneath a strip load which were sketched in figures 2.9 to 2.14, or the simplified version in figure 4.5 . Figures 2.16 to 2.20 showed that there is little difference between the lateral thrust factors K_n appropriate to L/B = 0 and 0.5, and loads are usually required to act in their most damaging location, closest to the wall.

Consider, as an example, the wall of section 2.3.2 assuming that it has been shown to be flexible enough to partially relieve compaction pressures and to mobilise an average earth pressure coefficient of 0.31, commensurate with $\phi = 32°$: see figure 4.1 . Assume that a similar ϕ value can be uniformly mobilised in bearing, beneath a superimposed load. This exactly recreates the scenario of figure 2.22 and the succeeding analysis, but relevant in this case to a serviceability check rather than to collapse. Given the same loads, the same load effects would obviously emerge. However, BS 5400 requires no load factor on the HB load for a serviceability check, so the calculated load effects would be corresondingly smaller. In the HB-loaded section 'a' M_Q reduces to 618 kNm/m, M_a to 1106 kNm/m and the average bending moment to 787 kNm/m.

It is, of course, possible that calculated load effects at a serviceability limit state actually exceed calculated effects at collapse. Suppose, for example, that in the previous case the wall had been effectively rigid prior to yield of the reinforcement, so that there was no reduction of compaction stress. Also suppose that the designer wished to permit compaction everywhere with a 2000 kg/m vibratory roller. Taking a dynamic amplification of 2, this would apply 39 kN/m so that an upper estimate of compaction stress could be $\sigma_c = 0.9\sqrt{(Q\gamma)} = 25$ kN/m^2. Figure 3.10 indicates that, for no relief of stress to be allowable, the wall rotation θ must be less than 10^{-4} radian, implying an extremely stiff integral box abutment.

Now consider the possible stress distribution for a section of wall carrying an HB bogey, shown in figure 2.22 and 2.23a. Discarding the previous load factor, we have Q = 900/4 = 225 kN/m spread over a width of 2.25 m adjacent to the wall, applying a corresponding vertical stress of 100 kN/m^2. It is now necessary to select an appropriate value for ϕ, recognising that the decision will not very greatly affect the vertical stress profile which emerges. An approach is therefore to select a value which would offer an appropriate lateral stress directly beneath the load. Vertical compression in a soil which is not free to expand laterally is recognised to generate an earth pressure coefficient

$$K_o = 1-\sin\phi_{max} \qquad (4.19)$$

where ϕ_{max} is the peak triaxial angle of shearing. The earth pressure coefficient related to the currently mobilised angle of shearing is

$$K_{a\,mob} = \frac{(1 - \sin\phi_{mob})}{(1 + \sin\phi_{mob})} \qquad (4.20)$$

It is therefore easy to equate K_o to a mobilized K_a to find a particular value of ϕ_{mob} , ϕ_o say, which applies during one-dimensional virgin compression. It is easy to check that

$$\phi_o = \phi_{max} - 11.5° \qquad (4.21)$$

satisfies 4.19 within $\pm 4\%$ for ϕ_{max} in the range 30° to 45°. For a soil compacted, according to specification, to a 95% optimum dry density, the relative density $I_D \simeq 0.73$. Collapse calculations would certainly require a further margin for error, but with regard to serviceability it might be decided to use $I_D = 0.73$ in equation 1.8 to get $I_R = 2.67$ which in equation 1.6 would offer triaxial $\phi_{max} = \phi_{crit} + 8°$. A sub-rounded sand might then give $\phi_{max} = 40°$ and an angular crushed rock perhaps 5° more. It follows from 4.21 that $\phi_o \simeq 30°$ should suffice for an estimate of lateral stress due to the load.

Figure 4.14a shows the lateral stress deduced for the HB-loaded section using the plastic distribution of stress with $\phi = 30°$, figure 2.11, and overlaying a wall of the correct H/B ratio, 7.5/2.25 = 3.33. Having obtained the increments of stress due to the strip load, it is necessary to calculate the required surcharge using equation 2.12 :

$$\sigma_r = 100/17 = 5.9 \text{ kN/m}^2$$

Since this is already incorporated in figure 2.11 it is only necessary to add 5.1 kN/m^2 to re-create the pavement surcharge of 11 kN/m^2. The components of figure 4.14a can then be assembled. Only then can it be seen that the precompression of 25 kN/m^2 is everywhere exceeded. This having been ascertained, figure 2.16 can be used to derive :

$$K_n = 0.65 \ , \ K_t = 0.39 \ , \ \eta = 0.64$$

We can then calculate

$$M_Q = 0.65 \times 225 \times 0.64 \times 7.5 = 702 \text{ kNm/m}$$

$$M_{qa} = 0.5 \times 0.33 \times 11 \times 7.5^2 = 103 \text{ kNm/m}$$

$$M_\gamma = 0.167 \times 0.33 \times 18 \times 7.5^3 = 422 \text{ kNm/m}$$

so that

$$M_a = 1227 \text{ kNm/m}$$

which is only 5% less than the previous collapse estimate including the load factor.

Figure 4.14b shows the lateral stress deduced for section 'b' with a uniformly distributed traffic load to add to the pavement surcharge. Here, the sum of the current lateral stress generators does not exceed the precompression at depths between 0.2 and 3.0 m. We therefore must consider three components of bending moment at the base :

$$M_\gamma = 422 \text{ kNm/m}$$

M_{qb} = 0.5 x 0.33 x 21 x 7.5^2 = 197 kNm/m

together with the precompression component taken directly from figure 4.14b,

M_c = 0.5 x 0.3 x 15 x 7.1 + 0.5 x 2.5 x 15 x 6.17

= 132 kNm/m

Summing, we obtain

M_b = 751 kNm/m

which is 25% greater than the previous value calculated for collapse.

The weighted average bending moment calculated for this serviceability check is then

M = (4 x 1227 + 6 x 751)/10 = 941 kNm/m

which is 7% greater than the collapse value, even in the absence of the collapse load factor.

Just as with compaction effects, it must be expected that 50% to 100% of the load-induced stresses will remain locked in when the heavy load has passed. If it is possible that repeated, abnormally heavy loads could travel in any arbitrary traffic lane, the precompression assumed for neighbouring sections should not be less than half the live load increment in the currently loaded section.

5 COLLAPSE INDUCED BY SOIL FAILURE

5.1 Free Body Diagram

Figure 5.1 shows a possible free body diagram for an L - wall in limiting global equilibrium. The self weights W_w of the wall and W_s of the soil lying directly above the wall base, together with the superimposed dead load q_d and live loads q_l and Q acting via the pavement on this rectangle of fill, represent the actions which must be supported by soil boundary stresses acting on the base. Passive support has been ignored.

The lateral stresses on the vertical plane through the heel should be limiting stresses. Since foundation collapse would entail substantial movements on slip surfaces through the fill, earth pressures should be consistent with the mobilisation of the critical state strength of the soil: they can be calculated in accordance with chapter 2. It is necessary to know both the magnitude and line of action of the lateral thrusts. The horizontal Rankine self-weight thrust ignoring water pressures in the soil and the possibility of friction on the plane, is

$$P_a = \tfrac{1}{2}K_a\gamma H^2$$

and acts at H/3 above the base. The Rankine surcharge thrust is

$$P_q = K_a(q_d + q_l)H$$

and acts at H/2.

The presence of any line load Q transmitted through the pavement onto the surface of the fill will also generate normal and tangential thrusts which can be superimposed on the vertical plane following the method of section 2.3.2 and taking appropriate coefficients from tables 2.2 to 2.9, or figures 2.16 to 2.20. The critical location of loads will be such as to generate thrust on the vertical plane through the heel without contributing to the weight of the sliding block which would enhance base friction. Accordingly, the critical position for a line load would be with its effective edge (allowing for spread through the pavement) above the heel. Following figure 2.15, therefore, the appropriate case for calculating thrust on that plane will be L/B=0.5 . Thrust coefficients K_n and K_t and height ratio η=h/H can then be read from figure 2.21 or equations 2.13 to 2.15 .

The foundation stresses may be idealised as uniform (τ_b, σ_b) over a reduced width X on the base so that for horizontal equilibrium of the rectangular monolith

$$\tau_b X = P_a + P_q + K_n Q \qquad (5.1)$$

and for vertical equilibrium

$$\sigma_b X = W_w + W_s + q_d L + K_t Q \qquad (5.2)$$

and for moment equilibrium about the heel

$$\sigma_b X(B - X/2) = W_w.C_w + W_s L/2 + q_d L^2/2 + P_a H/3 + P_q H/2 + K_n Q h \qquad (5.3)$$

Equations 5.2 and 5.3 can be merged to find X, which can then be substituted in 5.1 and 5.2 to find τ_b and σ_b.

5.2 Undrained Bearing Capacity Calculations

Values of base stresses τ_b and σ_b can then be inserted into a bearing capacity analysis which takes account of load inclination, in order to find what soil strength would need to be mobilised. It is known, for example, that for undrained bearing failure on soil with shear strength c_u, there exists a set of stresses in plastic equilibrium such that

$$\sigma_f = \sigma_o + c_u[1 + \pi - \beta + \cos\beta] \qquad (5.4)$$

where $\beta = \sin^{-1} (\tau_f/c_u)$

and $\sigma_o = \gamma D$

for a long footing at depth D in soil of unit weight γ. Iteration would then show what value of c_u, c_{mob} say, must be mobilised to prevent failure under bearing stresses(τ_b, σ_b). This could be compared with the worst undrained shear strength which might in fact be experienced, consistent with the site investigation and the level of inspection or testing to be demanded during construction. Where a softer clay layer lies at some depth beneath the base, equivalent bearing stresses on that layer can be found by extending the rectangular block in figure 5.1 downwards, and allowing for the extra active and passive thrusts on its sides.

Undrained base sliding in the absence of vertical bearing failure must also be prevented: the direct application of equation 5.1 should show that $\tau_b < c_{ub}$.The undrained shear strength on the base will be

$$c_{ub} = \sigma'_{ub}\tan\sigma_i \qquad (5.5)$$

where ϕ_i is the effective angle of shearing resistance of the interface and σ'_{ub} is the undrained normal stress. Also,

$$\sigma'_{ub} = \sigma_b - u_u$$

where u_u, the undrained pore pressure immediately beneath the base can be written, following Terzaghi's conventional assumption,

$$u_u \simeq u_o + \sigma_b \qquad (5.6)$$

where u_o is the initial pore pressure after excavation (presumably negative). Then

$$c_{ub} = (-u_o)\tan\phi_i \qquad (5.7)$$

This expression neglects the tendency of the horizontal shear stress on the base to create excess pore pressures, which would be supportively negative in the case of heavily overconsolidated clays for which $\sigma_b \ll \sigma'_{v\,max}$. However, shear stresses can not alter pore pressures in elastic materials, and since the base will be designed so as to minimise soil yield it remains possible that an L - wall with a flat base could "aquaplane" on the high pressure water released by the consolidation of an underlying clay which was itself

undisturbed.

Since the initial suction ($-u_o$) after base excavation might be rather modest,it is unlikely that equation 5.7 will offer sufficient short-term shear strength to support the lateral thrust of the retained soil. One of two defensive measures may be taken:

a) Insert a blanket drain beneath the base, and ensure that it is operative at all stages of contruction and consolidation in service. The shear strength of the interface will then be the smaller of $\sigma_b \tan\phi_i$ where ϕ_i is the angle of friction between concrete and drainage zone, and the minimum shear strength c_u of a plane of unconsolidated clay some distance beneath the drainage zone.

(b) Design some form of shear key, such as that shown beneath the heel in figure 5.2, so that base sliding cannot take place without the supporting clay being sheared. The interface then has an undrained shear strength c_u over the whole length from the front of the key to the toe of the wall, which can be inserted into equation 5.1 . Any form of surface indentation sufficient to force the clay matrix to deform would have the same effect.

5.3 Bearing Capacity Calculations using Effective Stresses

Every soil should be checked against drained bearing failures. Equilibrium water pressures, where they might exist, should be taken into account, both on the vertical plane through the heel, and on the whole length of the base. The superimposed block of effective stresses (τ_b, σ'_b) acting on reduced width X of the base can then be deduced by adding the effects of these two hydraulic thrusts into the equilibrium equations 5.1, 5.2 and 5.3. The effective angle of base shearing

$$\delta = \tan^{-1} (\tau_b/\sigma'_b)$$

can then be made to be smaller than the estimated effective angle of shearing of the interface ϕ_i, so that sliding can be prevented.

The drained bearing capacity of a rough strip foundation of effective width X is usually written, adapting Hansen (1966),

$$\sigma'_f = i_q N_q \sigma'_o + \tfrac{1}{2} i_\gamma N_\gamma X \gamma' \qquad (5.8)$$

where σ'_o is the minimum anticipated magnitude of soil effective stress on the interfacial plane just beside the base, and γ' is the effective unit weight (allowing for buoyancy effects) of the soil beneath the base. The values for bearing capacity factors N_q and N_γ can be derived using:

$$N_q = \tan^2 (45 + \phi/2)\exp(\pi\tan\phi) \qquad (5.9)$$

$$N_\gamma = 1.8 (N_q - 1)\tan\phi \qquad (5.10)$$

The values of the reduction factors for load inclination can be taken from:

$$i_q = (1 - \tan\delta)^2 \qquad (5.11)$$

$$i_\gamma = (1 - \tan\delta)^4 \qquad (5.12)$$

Hansen(1970) offers further semi-empirical factors to cover depth, shape, and slope, effects.

An iteration can be performed to determine what value of ϕ, ϕ_{mob} say, must be mobilized to prevent failure under σ'_b and δ. This can be compared with the value which can safely be relied upon in the foundation zone, considering the possible variations of both density and stress.

Meyerhof (1950) showed that the mean operative value of the effective stress as it varies around a failing footing was approximately one tenth of its bearing capacity,

$$p'_{op} = 0.1\ \sigma'_f \qquad (5.13)$$

This can be used to select an equivalent constant value of ϕ_{max} through equation 1.6, which was shown to correlate for triaxial compression tests on typical hard-grained sands. The conservative step of using triaxial rather than plane strain strengths should more than compensate for the lower shear resistance of bedding planes which has sometimes been observed.

The hypothesis that the designer must refute is that failure takes place under collapse load conditions, i.e. that $\sigma_f' = \sigma_b'$. This value can therefore be inserted via equation 5.13 into 1.6 to derive avalue of ϕ_{max}, which must not be less than the value ϕ_{mob} derived by exactly satisfying the equilibrium condition in equation 5.8 .

This demonstration will have relied upon the correct or conservative estimation of soil relative density for insertion into the calculation of the relative dilatancy index in equation 1.4, so that this could be used in equation 1.6 . However, in the event that that the back-analysis of equation 5.8 with collapse loads happens to give $\phi_{mob} < \phi_{crit}$ it clearly follows that complete bearing failure is impossible, whatever the density of the bearing medium. The value of ϕ_{crit} for granular materials can reliably be taken to lie between 32° for rounded particles and 37° for angular particles, though at sufficiently high confining pressures to cause general particle crushing the extra interlocking due to angularity is no longer effective and ϕ_{crit} appears to reduce towards 32°. A safe strategy is therefore available for granular materials irrespective of their density. Note, however, that severe distortions and settlements would still occur in loose deposits if an attempt were made to mobilise ϕ_{crit}: serviceability will be discussed in the next chapter.

For clayey soils, or aggregates which might be more crushable than quartz sands, it will be necessary to perform triaxial tests which establish ϕ_{max} under the appropriate conditions, replacing the empirical correlation in equation 1.6 . It may be preferred simply to derive a conservative value by finding ϕ_{crit} from a test on reconstituted virgin (loose) soil.The back-analysis of long-term retaining wall and slope failures in stiff fissured plastic clays, for example, has shown that critical state (fully softened) strengths were all that could be mobilized, notwithstanding that greater strengths could be observed in monotonic triaxial compression tests on in-tact material.

Figure 5.3 compares the "secant" strength approach used throughout this report with the more usual "tangent" method. It will be seen that both sands and clays can mobilise strengths above their critical state frictional strengths.

These higher strengths are, in both cases, associated with dilatancy. Highly over-consolidated clays are strongly dilatant, and therefore very susceptible to localised softening in rupture bands. The conventional description of the strength of these clays is in terms of the "true cohesion" c' exhibited by the best tangent to their strength envelope, and of its unreliable nature. These are simply contrasting descriptions of the same phenomenon.

It seems likely that the loss of the brittle strength component, however described, is associated with the cyclic strains induced by seasonal groundwater variations, permitting degradation of the stiff clay skeleton through the growth of slickensided ruptures from the seat of pre-exisiting fissures. Watson (1956) described just such a failure zone behind a retaining wall at Uxbridge, which failed 17 years after construction. We can deduce from Henkel's (1956) back-analysis of the collapse that whereas the critical state strength was mobilised in the active zone, a proportion of peak strength was apparently available in the foundation zone. It is not clear whether a further lapse of time would have permitted the softening of the more highly stressed foundation zones, had the wall not collapsed when it did. Skempton (1977) does show, however, that cuttings in Brown London Clay fail in critical state conditions (ϕ_{crit} = 20°) in the long term.

Less plastic sandy or silty clays are apparently less susceptible to this form of progressive failure: Skempton (1961). If the designer wishes to employ an element of the brittle peak component of strength, he can perform triaxial tests around the mean effective stress given by equation 5.13, and deduce an appropriate operational secant ϕ value for comparison with ϕ_{mob} derived from footing analysis, just as he would for granular soils. This should offer sufficient guidance regarding the possible vulnerability of the foundation, though the more usual c',ϕ' approach would obviously give a more accurate prediction of failure loads if these soil parameters were known to give a reliable strength envelope over the required range of effective stress. It would then be appropriate to add a term $i_c N_c c'$ to the bearing capacity equation 5.8, where $i_c = i_q$ and $N_c = (N_q - 1)\cot\phi$. The strong disadvantage of this latter approach is that it entails two parameters, whose mutual variation may not be easy to stipulate in cases where the appropriate strength envelope was not so clearly defined.

6 UNSERVICEABILITY THROUGH FOUNDATION DISPLACEMENT

6.1 Displacement Criteria

The U.S. Federal Highway Administration (Moulton et al, 1985) reported on "Tolerable movement criteria for highway bridges". Their widely circulated questionnaire to highway authorities in North America elucidated that only a small proportion of bridge decks had moved, but this group never-the-less included 314 examples which furnished data on the movement of 439 abutments. Of these, 58 were full-height abutments, 307 perched, and 16 spill-through. Regarding the full-height abutments, two-thirds suffered less movement than 100mm vertically and 50mm horizontally. Perched abutments, by comparison, moved somewhat greater horizontally. Spill- through abutments were more frequently reported to suffer large vertical movements. The larger abutment movements tended to involve both vertical and horizontal components, and were correlated with the presence of fine- grained soils. In terms of foundation type, the average movement of abutments on piles was similar to that of spread footings: it should, of course, be recalled that piled foundations would have been selected more frequently in poor ground conditions.

Regarding the influence of foundation movement on the bridges, FHWA reported that of the 155 bridges with maximum differential vertical movement of less than 100mm, 79 experienced no damage whatsoever and the remaining 76 tended to experience only minor cracking in the abutments. Vertical movements in excess of 100mm increasingly led to distress in the superstructure. Bridge superstructures in both steel and concrete were much more susceptible to horizontal movements: two-thirds of superstructures and one third of bearings were already damaged by movements in the range 25 to 50mm, beyond which abutment damage also began to be reported. By far the most frequent sequence of events involved the inward horizontal movement of abutments, jamming the deck against the back wall of the abutments, closing the expansion joints, and causing serious damage to the bearings. Riding quality was invariably impaired only after deformations which had already compromised the integrity of the structure.

In assessing whether deformations were tolerable, FHWA investigated whether any damage which did occur could be ignored, or economically repaired. Damage was defined as intolerable where whole-life-costs of construction, repair and maintenance will substantially exceed the costs of a hypothetical, more robust, alternative. Differential vertical settlements less than 100mm, and horizontal translations less than 50mm, were found to be tolerable in 90% of cases where these movements were not coupled. Thereafter, movements were increasingly found to be intolerable: only 23% of differential vertical settlements between 100mm and 200mm were thought tolerable, and only 10% of horizontal movements between 50mm and 100mm. When coupled with vertical movements, the horizontal movement tolerance seemed to reduce somewhat, though a translation less than 25mm was almost never found to be intolerable.

The more frequent incidence of damage to concrete rather than steel decks was more than counterbalanced by their greater reported tolerance of damage, implying that minor cracking could readily be observed and ignored. In terms of differential vertical movement expressed as a proportion of span length, it was found that 97% of the distortions less than 0.005 were found to be tolerable. Even simply supported spans could be damaged beyond 0.005 distortion. Analytical predictions should take into account: the rate of soil consolidation, the sequence and timing of construction of embankment, abutment

and deck, and creep in the concrete.

The bridge designer should generate his own list of deformation limits governing the permitted differential movements of abutments and piers. These limits should be selected by reference to the tolerance to movement of the deck and its joints and bearings, the piers and abutments themselves, the ancillary works such as drains and parapets, and the functional requirements of the bridge including headroom and riding quality. The FHWA report suggests that abutments which are to settle more than 0.005 of the span, or to translate inwards more than 50mm, will require special detailing.

6.2 Control of Foundation Movements

The U.S. Federal Highway Authority have also reported on the performance of spread footings for highway bridges (DiMillio 1982, Gifford et al 1987). It was found that footings over inorganic cohesionless materials (defined as those with a plasticity index less than 5%) never settled more than 40mm and only settled in excess of 25mm when the soil was very loose. The actual magnitude of movement was, however, shown to be unpredictable within about 10mm by any of the recognised approaches, of which D'Appolonia (1968) proved the most reliable. This also has the advantage of being based on the theory of elasticity: the only step requiring empirical judgement is the selection of an equivalent soil modulus using available correlations with SPT data, or CPT data using the analogous method of Schmertmann (1970).

Since no abutments on sand moved further than could be tolerated, however, it might be concluded that the existing practice of providing a load factor of three against bearing capacity failure precludes the development of excessive settlements and renders the calculation of such settlements redundant for this class of construction. This conclusion may be fortified by the recognition that the only component of foundation movement capable of damaging the bridge deck is that occuring after it has been erected. Since granular soils respond as soon as they are loaded, only the dead and superimposed loads due to the deck need normally be included in the analysis of deck deformations. Further considerations are, however, necessary when large cyclic loads, such as those generated by earthquakes, must be transmitted to loose granular soils: soil stabilization techniques such as dynamic compaction may then be preferred.

It is interesting to reflect that a reduction of bearing capacity by a factor of 3 is equivalent, over the likely range of angle of shearing, to a rather precise reduction in ϕ of $7.5° \pm 0.5°$. The existing design routine is therefore almost exactly equivalent to designing foundations to mobilise $\phi_{mob} = \phi_{max} - 7.5°$ in a plastic bearing calculation. The derivation of a safe value for ϕ_{max} was covered in section 1.1.3 . The perusal of triaxial tests results on sands at major effective stress levels upto 1000 kN/m^2 will confirm that the mobilisation of $\phi_{max} - 7.5°$ generally requires no more than an axial strain of 0.25% for typical sub- rounded pre-loaded quartz sands: the same figure can be derived from equation 3.10. This required strain may be seen to rise to 0.5% to 1% for virgin-loaded sands, depending on their density. These figures may be further increased if the soil particles are more crushable (e.g. more angular quartz and feldspar, weaker calcareous particles or rockfills subject to weathering). Since the stress induced under a foundation will significantly affect only a zone about twice as deep as the base is wide, these figures are consistent with base distortion ratios (movement/width) in the range 0.5% to 2%, similar to the observations, and broadly acceptable.

Fine-grained soils, and especially clays, are capable of creating much larger foundation displacements, with a significant delayed component due to consolidation which can lead to damaging structural distortions.

The logical relationship between mobilised stress and strain as experienced in triaxial tests and beneath footings was first explored by Skempton (1951) in discussing the immediate, undrained, settlement of isolated foundations on clay. Skempton showed that for a given mobilised strength c_{mob}, derived directly from the plastic bearing capacity equation as described in section 5.2 above, the foundation settlement ratio ρ/B could be expected to be double the axial strain required to mobilise the same strength in a triaxial test. He also showed that for $c_{mob}/c_u = 0.5$ the axial strain in triaxial tests on London clay was about 1%, and that corresponding settlement ratios of footings were accordingly about 2%. Later work has demonstrated the higher stiffness of London clay at smaller strain magnitudes (Jardine et al, 1984), and the rather greater stiffnesses of low plasticity clays. The compression data of an undisturbed,triaxially consolidated, sample of London Clay are shown in figure 6.1 in terms of the mobilized undrained strength ratio versus axial strain plotted on a logarithmic scale.

The use of a strength reduction factor of 2 also prevents local plastic yielding beneath the edges of a footing: it is known that first yield of an ideal elasto-plastic soil subject to a strip of uniform pressure would occur at a bearing stress of $3.14c_u$ prior to collapse at $5.14c_u$. In general practice, a reduction factor of 3 on collapse loads has been used to confer notional serviceability on foundations where stress-strain data have not been available.

It must, however, be recalled that the spread footing of a bridge abutment is not isolated: the influence of the embankment fill must always be taken into account. Figure 6.2 shows an undrained shear strain mechanism for a semi-infinite uniform surcharge being placed on a limited bed of uniform clay of depth D. The clay remote from the edge of the surcharge will initially suffer no strain, but will generate an excess pore pressure equal to the surcharge σ_v. Undrained shear strains will occur beneath the edges of the loaded area however, and they will be idealised as occuring uniformly in two triangular zones, an active zone OFE and a passive zone OFG, for the purposes of this demonstration. The clay below GO and EO will be taken to be immobile: the resulting undrained deformation pattern is shown in figure 6.2 . For simplicity, friction along OF and EF will be ignored for the purposes of stress-analysis.

Let the edge of the loaded area rotate by angle θ : conservation of volume dictates that both OF and GF rotate by the same amount. By analogy with figure 3.3 we know that the shear strain in both OFE and OFG will be 2θ. Let the shear strength mobilised at this shear strain be c, and the increment of horizontal stress σ_h. Then:

$$\sigma_v - \sigma_h = 2c$$

$$\sigma_h = 2c$$

We therefore derive

$$\sigma_v = 4c$$

This offers $4c_u$ as the ultimate bearing capacity, a 22% underestimate due to the neglect of friction on the plane OF. If this underestimation can be dealt with simply by scaling all the mobilised bearing pressures by a factor 1.22, we are left with the result that

$$c_{mob} = \sigma_v/5.14$$

associated with a shear strain beneath the edge of the load of 2θ where the edge rotates through angle θ. Now if c_{mob} is mobilised in a triaxial test at axial strain ϵ_a, say, then the shear strain will be 1.5 ϵ_a. It should therefore follow that $2\theta \simeq 1.5\epsilon_a$, or

$$\theta = 0.75\ \epsilon_a \qquad (6.1)$$

Although this simplified analysis fails to take account of shear stress beneath the wall base , it is already clear that the tendency for outward movement of the soil at edge A is likely to cause the wall to translate by the same order of magnitude as it settles.

It is suggested, for design purposes, that local base rotations be linked through equation 6.1 with axial strains observed or inferred in representative samples forced to mobilise corresponding strengths in triaxial undrained tests. It may be necessary to identify two zones of deformation, 'b' directly beneath the wall base and a deeper zone 'e' influenced by the embankment as shown in figure 6.3. The component of base rotation $\theta_{b,v}$ due to the vertical stress component σ_v would be estimated from the axial strain ϵ_b observed or inferred for a triaxial sample recovered from depth B/2 and forced to mobilise the appropriate shear strength $\sigma_v/5.14$. Zone 'e' would extend for a distance equal to the depth D of deformable material. The tilt θ_e of ground adjoining the wall would be estimated from ϵ_e in a triaxial sample from depth D/2, and therefore presumably stronger, forced to mobilise the same shear strength. The wall would then be expected to move downwards and outwards at its toe by roughly equal amounts

$$\rho \simeq \delta \simeq 0.75[\ B\epsilon_b + (D-B)\epsilon_e\ ] \qquad (6.2)$$

To these displacements and rotations must be added the effects of the horizontal base shear force and the net moment about the centre of the base. These additional effects can best be approximated using elasticity theory, as indicated in the next section. An appropriate elastic modulus may be obtained from the tangent to the triaxial stress-strain curve leading upto the point of strength mobilisation deduced from the bearing capacity equation 5.4 . Suppose, for example, that a wall is to retain 8m of fill which applies 152 kPa to London clay for which figure 6.1 is taken to be relevant. The mobilized strength due to vertical surcharge alone is 152/5.14 = 30 kPa. If a wall base has been designed for shear and moment in the usual way then the local mobilised strength beneath the base might be 45 kPa. If the clay beneath the base had c_u = 100 kPa then these two degrees of strength mobilization would require 0.18% and 0.61% axial strains respectively. The increment of deviatoric stress between these points is 2 x (45 - 30) = 30 kPa, and the increment of axial strain is 0.43%. The equivalent modulus for this increment is therefore 3000/0.43 = 7000 kPa or 70 times the shear strength, which is often taken as a typical tangent modulus around the working bearing stress of overconsolidated plastic clays.

The consolidation component of settlement can be estimated in two ways: from

a consideration of the excess pore water pressures which are to be dissipated (Skempton and Bjerrum, 1957), or indirectly by estimating the total settlement using elastic stress distributions together with a drained soil modulus (or the oedometer modulus coupled with the assumption of one-dimensional strain) and then deducting the previously calculated immediate component. In either approach, the final vertical effective stress will not have to exceed the pre-compression of the clay if large plastic compressions are to be avoided. The likely output of the consolidation calculation will be that the delayed settlement of the heel of the wall will exceed that of the toe, due to the influence of the embankment surcharge. The expected result will be a tendency for reversal of tilting, causing lateral earth pressures to rise as the wall stem pushes into the fill. Once the amount of tilting has been estimated, chapter 3 of this report will enable an estimate to be made of the possible increase in earth pressure. However, the interaction between lateral earth pressures and foundation movements is complex: work on both physical and numerical models is in hand at Cambridge University.

6.3 Foundation Displacement Calculations

Soils which have been prevented from gross plastic yielding may be analysed for deformations using carefully measured values of soil stiffness. Two types of calcualtion are widely used, both based on an assumed elastic stress distribution

(a) neglecting lateral strain, so that a numerical integration of strains can take place using oedometer data.

(b)adopting either a closed-form, finite element, or boundary element solution for displacements, using Young's modulus data from triaxial tests. The one dimensional modulus E_o (or the coefficient of volume compressibility $m_v = 1/E_o$) can be related to the drained elastic parameters Young's modulus E_d and Poisson's ratio υ_d, thus

$$E_o = \frac{E_d(1 - \upsilon_d)}{(1 + \upsilon_d)(1 - 2\upsilon_d)} \qquad (6.3)$$

For a typical value $\upsilon_d = 0.25$, $E_o/E_d = 1.2$

Method (a) is applicable only to total displacements, whereas (b) can be applied separately to immediate or total settlements depending whether undrained stiffness E_u or drained stiffness E_d is used. The settlement ρ due to a load Q acting on a footing of width B on an elastic half-space b is of the form

$$\rho = \frac{I_v Q}{B} \cdot \frac{(1 - \upsilon^2)}{E} \qquad (6.4)$$

where I_v is an influence factor which depends on the geometry of the footing. Using the fact that the shear modulus of an elastic material is unique irrespective of the degree of drainage,

$$G_u = G_d$$

It follows that

$$\frac{E_u}{2(1 + \upsilon_u)} = \frac{E_d}{2(1 + \upsilon_d)} \qquad (6.5)$$

Then the ratio of immediate to long-term settlement

$$\frac{\rho_u}{\rho_d} = \frac{(1 - \upsilon^2_u)}{E_u} \cdot \frac{E_d}{(1 - \upsilon^2_d)}$$

$$= \frac{(1 - \upsilon_u)}{(1 - \upsilon_d)} \qquad (6.6)$$

Using $\upsilon_u = 0.5$, we find that ρ_u/ρ_d for a footing on a half-space takes the narrow range 0.5 to 1, with a typical value of 2/3 when $\upsilon' = 0.25$. This proportion falls towards zero as the bed depth to footing width ratio reduces towards zero and the mode of deformation becomes one-dimensional compression.

With sufficient accuracy, the influence factor I_v in equation 6.4 for a rigid rectangular foundation BxL on the surface of a homogeneous elastic half space can be taken as:

$$I_v \simeq \frac{\sqrt{(B/L)}}{(1 + 0.05L/B)} \qquad (6.7)$$

The horizontal displacement δ due to a horizontal force F acting along the side B of a rigid rectangular footing BxL on a homogeneous elastic half- space can be written

$$\delta = \frac{I_h F}{B\ E} \qquad (6.8)$$

where

$$I_h \simeq \frac{\sqrt{(B/L)}}{(1 + 0.015L/B)} \qquad (6.9)$$

The rotation ω of a rigid rectangle of width B carrying a moment M about the L axis, standing on an elastic half-space, can be written

$$\omega = \frac{I_\omega\ M(1 - \upsilon^2)}{B^2\ LE} \qquad (6.10)$$

where

$$I_\omega \simeq 2(1 + \tan^{-1} L/B) \qquad (6.11)$$

If the depth of the deforming layer is of the same order of size as the footing, or the stiffness varies linearly or stepwise with depth, reference can be made to appropriate tabulations in Poulos and Davis (1974), for example. More generally, Newmark's charts can be used with elastic stress distributions assumed below flexible loaded areas. The settlement of a rigid uniformly loaded rectangular footing may then be approximated as

$$\rho_{rigid} = \tfrac{1}{2}[2\rho_{centre} + \rho_{corner}]_{flexible} \qquad (6.12)$$

There is a particular difficulty in selecting an appropriate modulus for soil, due partly to the non-linear and path-dependent nature of its stress-strain relations, and partly to the difficulty of preventing significant disturbance

of the soil prior to testing. Since stiffness reduces at larger strains, and the largest strains occur immediately beneath a foundation, it will be conservative to determine a stiffness modulus appropriate to that zone. Dividing design displacements by the foundation's width leads to an estimate of the maximum equivalent axial strain in an undrained triaxial test, for example. Some of the implications of the non-linearity of soils for soil-structure interaction analyses are discussed in Jardine et al (1986).

Figure 6.4 shows the pattern of hysteresis typically observed in an undrained triaxial compression test in which care has been taken to minimise the initial bedding error due to inaccurate trimming. The effects of prior stress path can readily be appreciated by considering the possible range of stiffnesses exhibited at points X_1, X_2, X_3 each of which are at a unique deviatoric stress σ_o and each of which are in a phase of stress increase. It should be appreciated that the taking and trimming of a clay sample will inevitably result in a stress cycle which will, in general, affect the future measurement of soil stiffness.

The effects of sample disturbance can be accounted for in part by recognising that the strain-increments occuring after any stress reversal are approximately independent of previous stress history, offering a unique curve of secant modulus E_u against strain ϵ. Figure 6.5 illustrates the method of updating the origin for strain, and the definition of secant modulus.

Figure 6.6 shows the superposition of the data for overconsolidated kaolin (OCR = 8) taken from successive cycles of stress reversal, using a plot of E_u/c_u against axial strain on a logarithmic axis.The figure also shows additional data of more plastic London clay and a less plastic silty clay from the North Sea, in which strains were monitored internally for maximum accuracy (Jardine et al,1984). To use graphs of this sort it is necessary to estimate the strain increment after the last stress reversal in the field. The permitted strain following construction will form part of this, but it may be necessary to make an allowance for strains which have taken place prior to construction. Often, however, the foundation will cause recompression of overconsolidated soils immediately beneath it. In this case this most significant zone will suffer a stress reversal, so the strain magnitude for figure 6.6 could be taken directly from a consideration of projected deflections after construction.

7. CONCLUSIONS

This report describes methods of evaluating the stresses in the granular backfill to retaining structures for purposes of limit state design. The methods presented consider the influence on the stresses of compaction, self-weight and superimposed loads, as well as the effects induced by various modes of wall movement. The conditions pertaining to both collapse and unserviceability of the retaining wall are also considered to enable the methods to be understood and readily adopted. A number of examples are fully described and non-dimensional charts presented.

8. ACKNOWLEDGEMENTS

The work described in this report forms part of the research programme of the Structural Analysis Unit (Head, Dr R T Murray) and Ground Engineering Division (Head, Dr J Temporal) of the Structures Group of TRRL, and is published by permission of the Director.

9. REFERENCES

Billam J.(1972) Some aspects of the behaviour of granular materials at high pressures, Stress-strain Behaviour of Soils, R.H.G. Parry Ed., G.T.Foulis & Co., London, 69-80.

Blockley D I. (1980). The nature of structural design and safety. Ellis Horwood Ltd, Chichester, England.

Bolton M.D. (1986) The strength and dilatancy of sands, Geotechnique, 36, No.1, 65-78.

Bransby P.L. and Milligan G.W.E. (1975) Soil deformations near cantilever sheet-pile walls, Geotechnique, 25, No.2, 175-195.

Broms B.B.(1971) Lateral pressures due to compaction of cohesionless soils, Proc. 4th Conf. on Soil Mech.,Budapest, 373-384, in S.G.I. Reprints No.52, Stockholm.

Broms B.B. and Ingelson I.(1971) Earth pressure against the abutments of a rigid frame bridge, Geotechnique, 21, No.1, 15-28.

Caquot A. and Kerisel J.(1948) Tables for the calculation of passive pressure, active pressure, and bearing capacity of foundations, Gauthiers-Villars, Paris.

Cornforth D.H.(1973) Prediction of drained strength of sands from relative density measurements, Evaluation of Relative Density and its Role in Geotechnical Projects Involving Cohesionless Soils, A.S.T.M., S.T.P. 523, 281-303.

D'Appolonia D.J., D'Appolonia E. and Brissette R.F. (1968) Settlement of spread footings on sand, Jnl.Soil Mech.and Found.Div., Proc.A.S.C.E., 94, SM3, 735-760.

De Beer E.E.(1965) Influence of the mean normal stress on the shearing strength of sand, Proc. 6th Int. Conf. Soil Mech. and Found. Eng., Montreal, I, 165-169.

Department of Transport (1987) Specification for Road and Bridge Works, H.M.S.O., London.

DiMillio A.F. (1982) Performance of highway bridge abutments, U.S. Federal Highway Administration, FHWA/RD-81/184, Washington D.C.

Duncan J.M. and Chang C.Y.(1970) Non-linear analysis of stress and strain in soils , Jnl. Soil Mech. and Found. Div., Proc. A.S.C.E , 96 , No.SM5, 1629-1653.

Duncan J.M. and Seed R.B.(1986) Compaction-induced earth pressures under K_o conditions, Jnl. of Geotech. Eng.,A.S.C.E., 112, No.1, 1-22.

Fang Y-S. and Ishibashi I.(1986) Static earth pressures with various wall movements, Jnl. of Geotech. Eng., A.S.C.E., 112, No.3, 317-333.

Forssblad L.(1965) Investigations of soil compaction by vibration, Acta Polytechnica Scandinavia, Ci 34, 185pp.

Gifford D.G., Wheeler J.R., Kraemer S.R. and McKown A.F. (1987) Spread footings for highway bridges, U.S. Federal Highway Administration, FHWA/RD-86/185, Washington D.C.

Hardin B.O. and Drnevich V.P.(1972) Shear modulus and damping in soils: design equations and curves, Jnl. Soil Mech. and Found. Div., Proc. A.S.C.E., 98, No. SM7, 667-692.

Hansen J. Brinch (1966) Code of Practice for Foundation Engineering (Translation), Bulletin No. 22, Danish Geotechnical Institute, Copenhagen, pp22.

Hansen J. Brinch (1970) A revised and extended formula for bearing capacity, Bulletin No.28, Danish Geotechnical Institute, 5-11.

Henkel D.J.(1956) Discussion of Watson (1956), Proc. I.C.E., Part II, 5, 320-323.

Horne M.R.(1965) The behaviour of an assembly of cohesionless rigid particles I and II, Proc. Roy. Soc., Series A, 286, 62-78.

Horne M.R.(1969) The behaviour of an assembly of cohesionless rigid particles III, Proc. Roy. Soc., Series A, 310, 21-34.

Ingold T.S.(1979) The effects of compaction on retaining walls, Geotechnique, 29, No.3, 265-283.

Iwasaki T., Tatsuoka F. and Takagi Y.(1978) Shear moduli of sands under cyclic torsional shear loading, Soils and Foundations, Japanese Soc. Soil Mech. and

Found. Eng.,18, 39-56.

Jardine R.J., Symes M.J. and Burland J.B. (1984) The measurement of soil stiffness in the triaxial apparatus, Geotechnique, 34, No.3, 323-340.

Jardine R.J., Potts D.M., Fourie A.B. and Burland J.B. (1986) Studies of the influence of non-linear stress-strain characteristics in soil- structure interaction, Geotechnique, 36, No. 3, 377-396.

Ladanyi B.(1960) Etude des relations entre les contraintes et les deformations lors du cisaillement des sols pulverulants, Annales de Travaux Publics de Belgique, No.3, 1-30.

Lau C.K.(1988) Scale effects on footings, Ph.D. Thesis, Cambridge University.

Matteotti G.(1970) Some results of quay wall model tests on earth pressure, Proc. Inst. Civ. Engrs., 47, 185-204.

Meyerhof G.G. (1950) The bearing capacity of sand, Ph.D. Thesis, University of London.

Moulton L.K., GangaRao H.V.S. and Halvorsen G.T. (1985) Tolerable movement criteria for highway bridges, U.S. Federal Highway Administration, FHWA/RD-85/107, Washington D.C.

Norris G.M. (1977) The drained shear strength of uniform quartz sand as related to particle size and natural variation in particle shape and surface roughness, Ph.D. Thesis, University of California, Berkeley.

Poulos H.E. and Davis E.H. (1974) Elastic solutions for soil and rock mechanics, Wiley, New York.

Rehnman S.E. and Broms B.B.(1971) Lateral pressures on basement wall: results from full-scale tests, Proc. 5th Eur. Conf. Soil Mech. and Found. Eng., Madrid, I, 189-197.

Rowe P.W.(1962) The stress-dilatancy relation for static equilibrium of an assembly of particles in contact, Proc. Royal Society of London, Series A, 269, 500-527.

Schmidt B.(1966) Discussion: Earth pressures at rest related to stress history, Canadian Geotechnical Jnl., 3, No.4, 239-242.

Schmertmann J.H. (1970) Static cone to compute static settlement over sand, Jnl. Soil Mech.and Found.Div., Proc. A.S.C.E., 96, SM3, 1011-1043.

Skempton A.W. (1951) The bearing capacity of clays, Building Research Congress, London, 1, 180-189. (In: Selected Papers on Soil Mechanics by A.W. Skempton F.R.S., Thomas Telford Ltd., 1984)

Skempton A.W. (1977) Slope stability of cuttings in brown London clay, 9th Int.Conf.Soil Mech. and Found.Eng., Tokyo, 3, 261-270.

Skempton A.W. (1961) A landslide in boulder clay at Selset Yorkshire, Geotechnique, 11, 280-293

Skempton A.W. and Bjerrum L.(1957) A contribution to the settlement analysis of foundations on clay, Geotechnique, 7, No.2, 168-178.

Sokolovski V.V.(1960) Statics of soil media, Butterworths, London.

Symes M.J. and Burland J.B. (1984) The determination of local displacements on soil samples, ASTM Geotech. Test Jnl.

Terzaghi K.(1934) Large retaining wall tests : 1) Pressure of dry sands, Engineering News-Record, 112, 136-140.

Watson J.D. (1956) Earth movement affecting LTE Railway in deep cutting east of Uxbridge, Proc. I.C.E., Part II, 5, March, 302-316.

Wroth C.P.(1972) General theories of earth pressures and deformations, Proc. 5th Eur. Conf. Soil Mech. and Found. Eng., Madrid, II, 33-52.

Youd T.L.(1972) Compaction of sands by repeated shear straining, Jnl. Soil Mech. and Found. Div., Proc. A.S.C.E., 98, No. SM7, 709-725.

Table 1 Geometry of stress discontinuities

ϑ	φ	30°	32°	35°	40°	45°
30°	R	1.7676	1.8499	1.9870	2.2620	2.6180
	α	47.2	46.3	45.1	43.1	41.1
	β	17.2	16.3	15.1	13.1	11.1
	δ	25.7	27.3	29.8	33.8	37.8
15°	R	1.3468	1.3800	1.4340	1.5388	1.6687
	α	38.1	37.1	35.7	33.3	31.0
	β	23.1	22.1	20.7	18.3	16.0
	δ	28.9	30.8	33.6	38.4	43.1
$7\frac{1}{2}$°	R	1.1625	1.1770	1.2003	1.2444	1.2973
	α	33.9	32.9	31.4	29.0	26.5
	β	26.4	25.4	23.9	21.5	19.0
	δ	29.7	31.7	34.7	39.6	44.5

Table 2 K_n for normal component of pressure on vertical walls

δ/φ \ φ	30	32	35	40	45
0	0.333	0.307	0.271	0.217	0.172
1/3	0.305	0.281	0.247	0.197	0.156
2/3	0.285	0.262	0.229	0.182	0.143
1	0.273	0.250	0.218	0.172	0.134

Table 3 Non-dimensional soil stiffness λ

	I_D	0.2	0.6	1.0
	e	0.79	0.67	0.55
	γ kN/m^3	14.5	15.6	16.8
Z m	K			
1.0	0.4	7580	9014	10863
	0.8	8594	10221	12318
	1.6	10329	12284	14804
	3.2	13128	15612	18815
2.0	0.4	5360	6374	7681
	0.8	6077	7227	8710
	1.6	7304	8686	10468
	3.2	9283	11039	13304
4.0	0.4	3790	4507	5431
	0.8	4297	5110	6159
	1.6	5164	6142	7402
	3.2	6564	7806	9407
8.0	0.4	2680	3187	3840
	0.8	3038	3613	4355
	1.6	3652	4343	5234
	3.2	4641	5519	6652

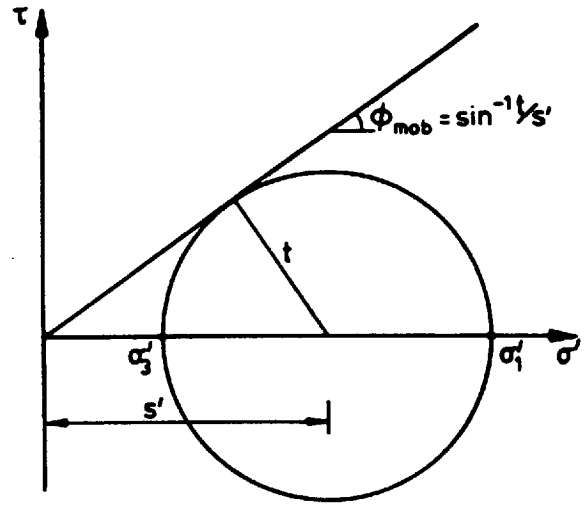

Figure 1.1 Mobilized angle of shearing φ_{mob}

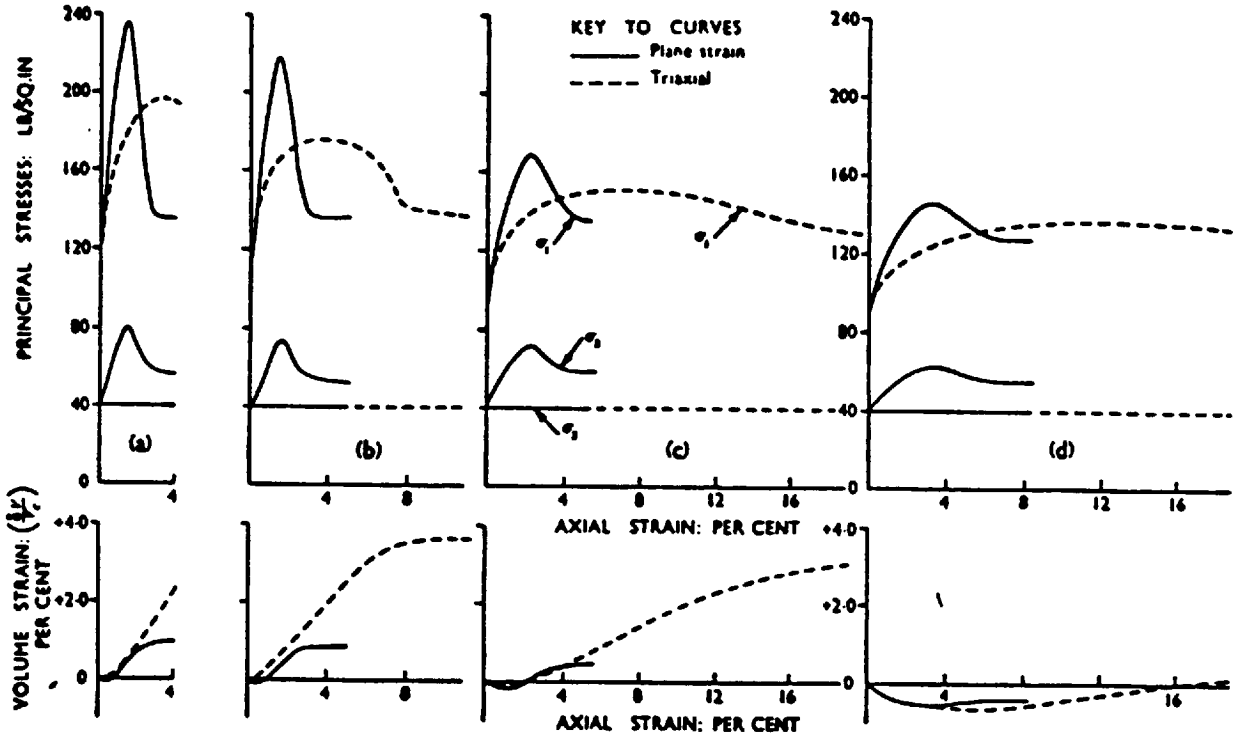

Fig. 17. Comparison of plane strain and triaxial compression tests at different sand densities: (a) Dense. Relative porosity 80%; (b) Medium—Dense. Relative porosity 65%; (c) Loose—Medium. Relative porosity 40%; (d) Loose. Relative porosity 15%

Taken from Cornforth D.H. (1973)

Figure 1.2 Triaxial and plane compression tests on sand

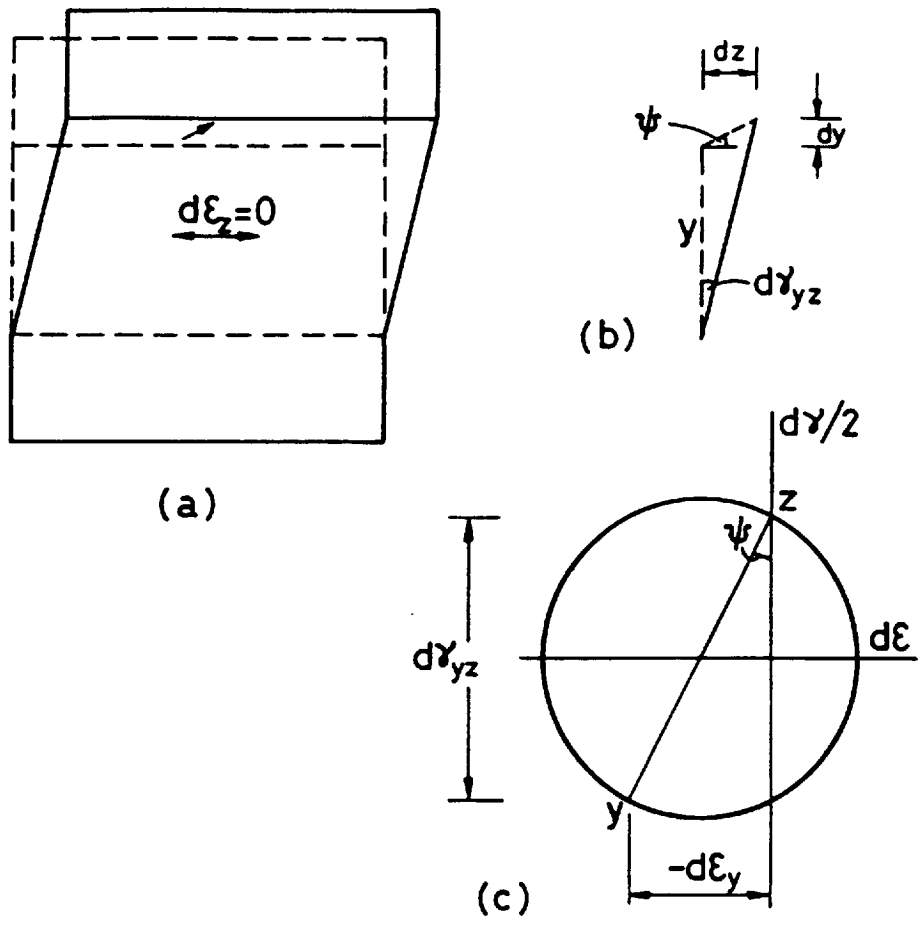

Figure 1.3 Angle of dilatancy ψ

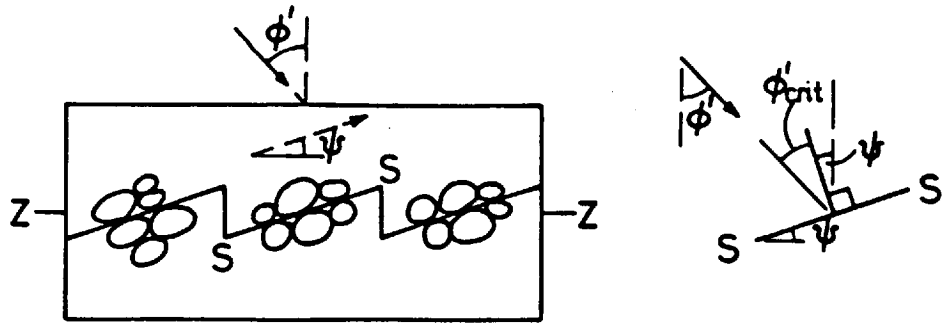

Figure 1.4 Saw-blades model of stress-dilatancy

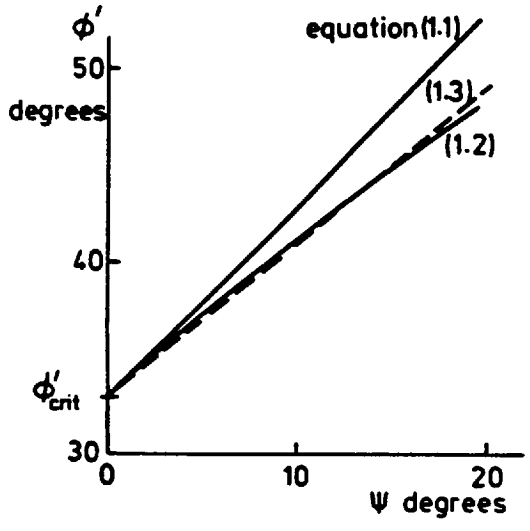

Figure 1.5 Stress dilatancy relations

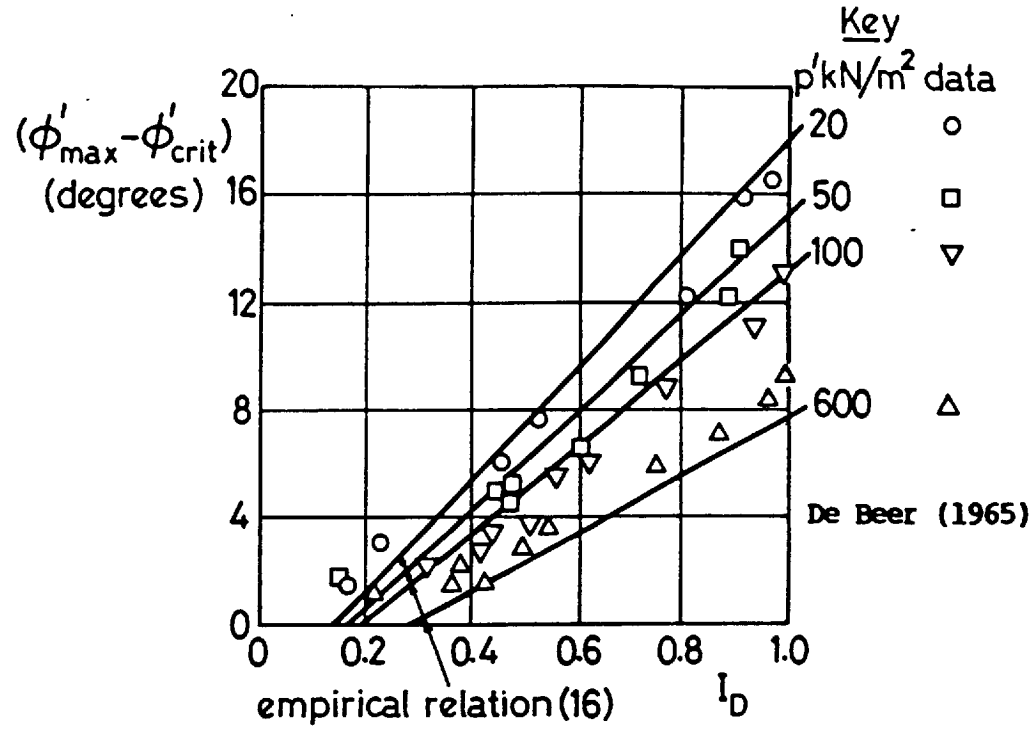

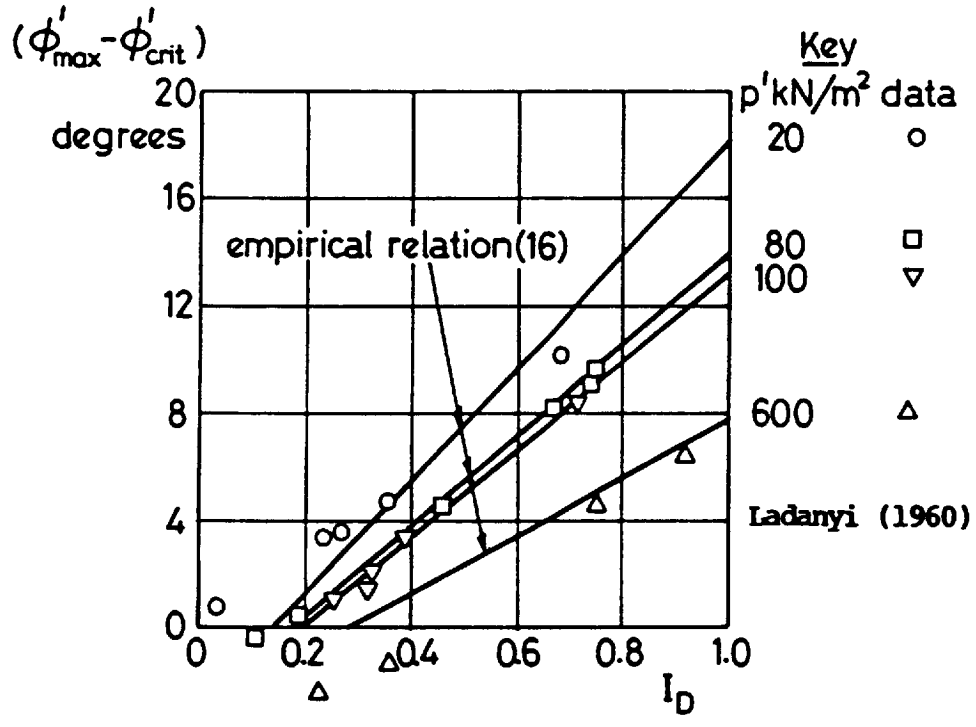

Figure 1.6 Correlations for φ_{max} versus I_D and p'

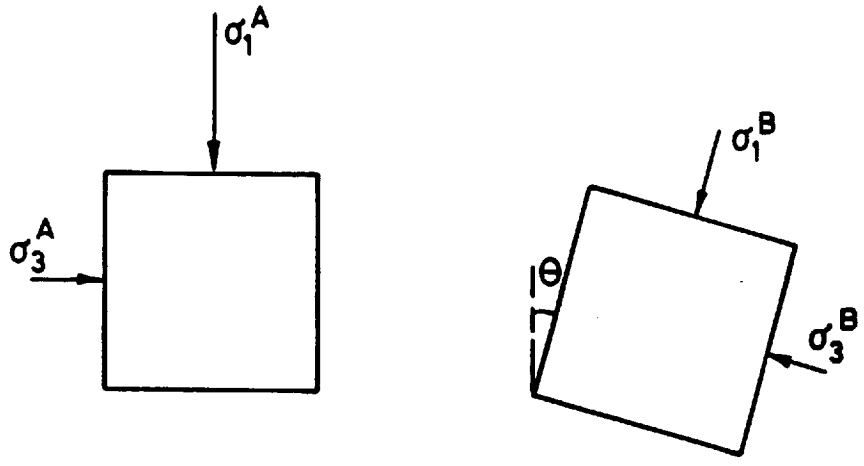

Figure 1.7 Superposition of independent stress states A and B

(a) when $\theta = 0$

(b) when $\theta = 30°$

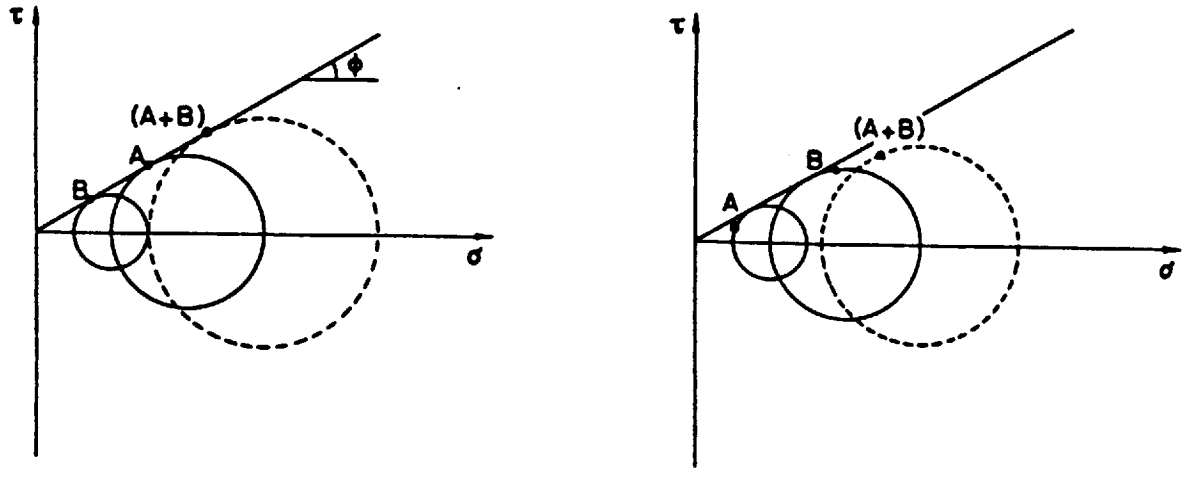

Figure 1.8 Superposition of "safe" stresses

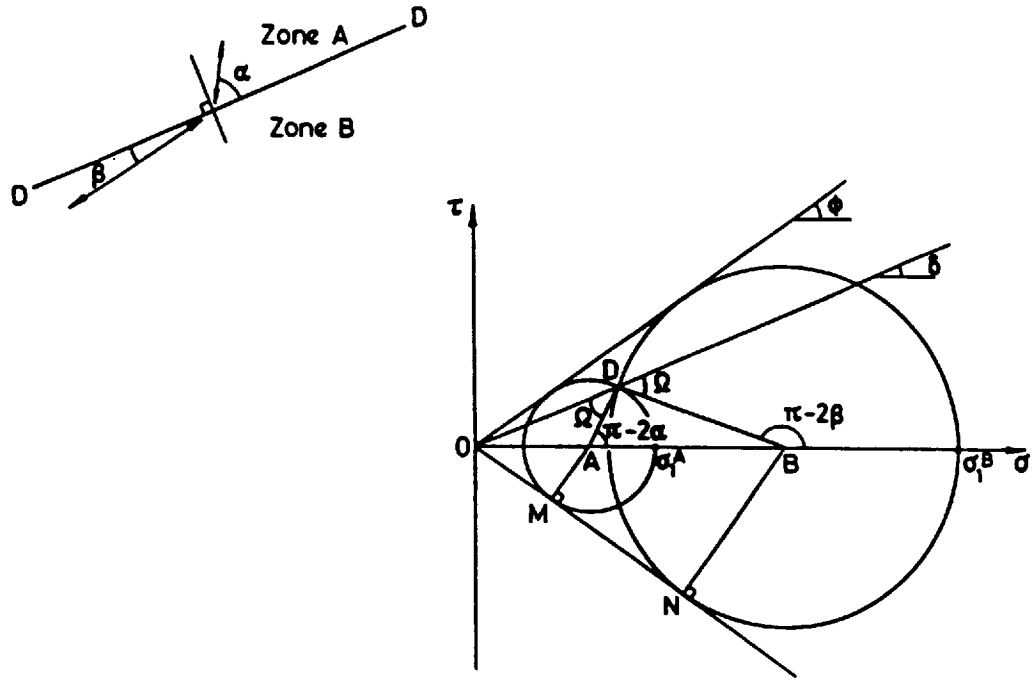

Figure 1.9 A plastic stress discontinuity

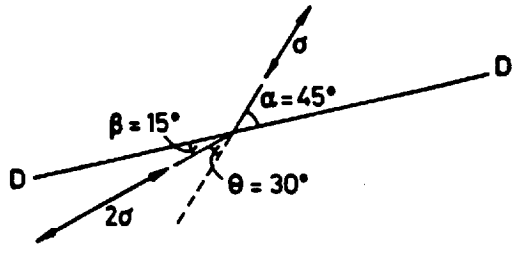

Figure 1.10 A 30° stress jump: $\varphi = 35.3°$, $\delta = 30°$

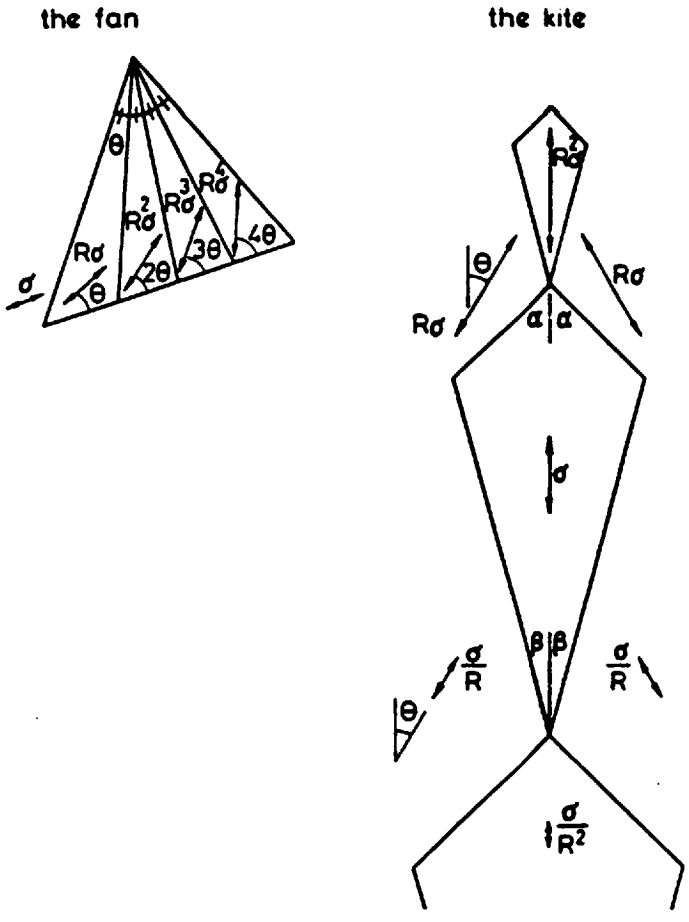

Figure 1.11 Patterns of stress discontinuities

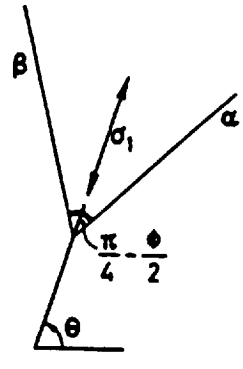

Figure 1.12 Plastic stress characteristics

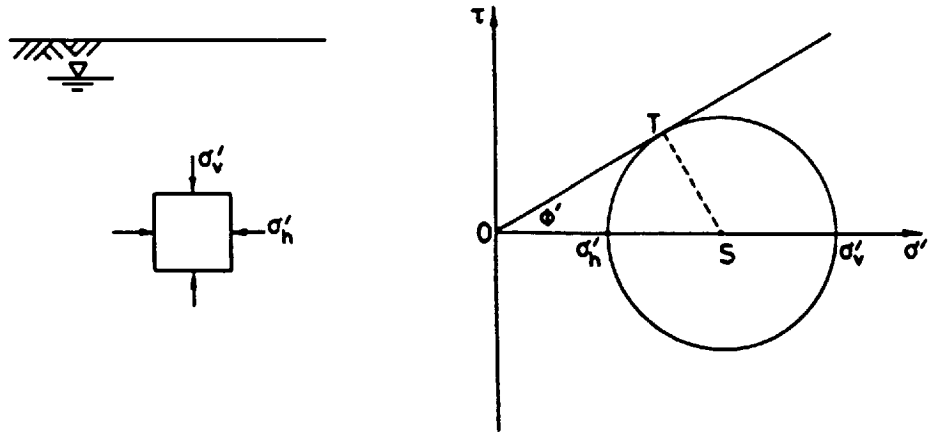

Figure 2.1 Limiting Mohr circle of stress

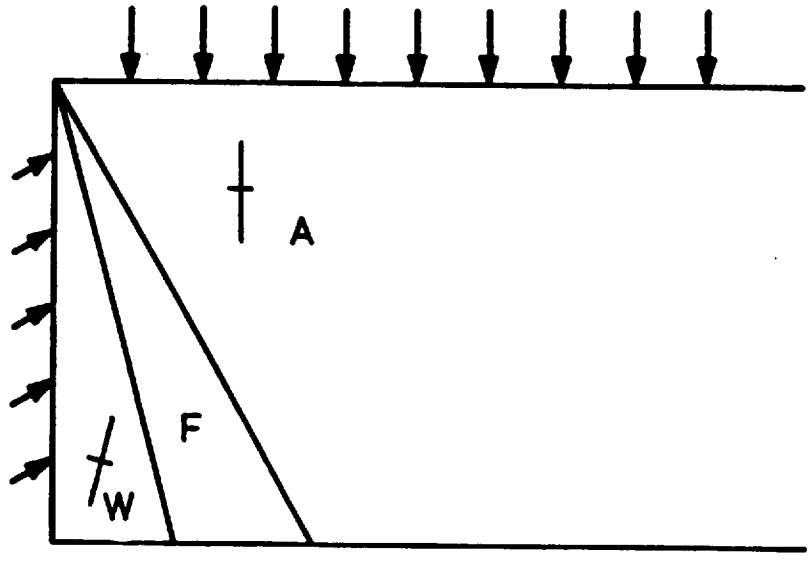

Figure 2.2 "Active" wall problem: weightless soil

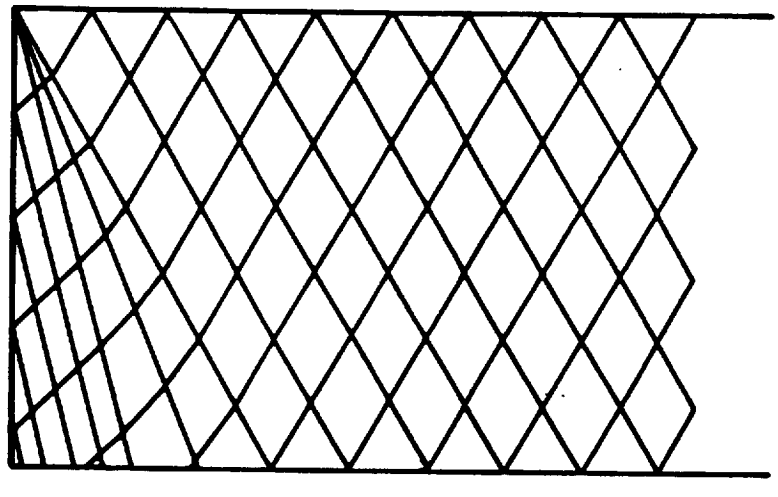

Figure 2.3 Stress characteristics for rough wall and "active" soil

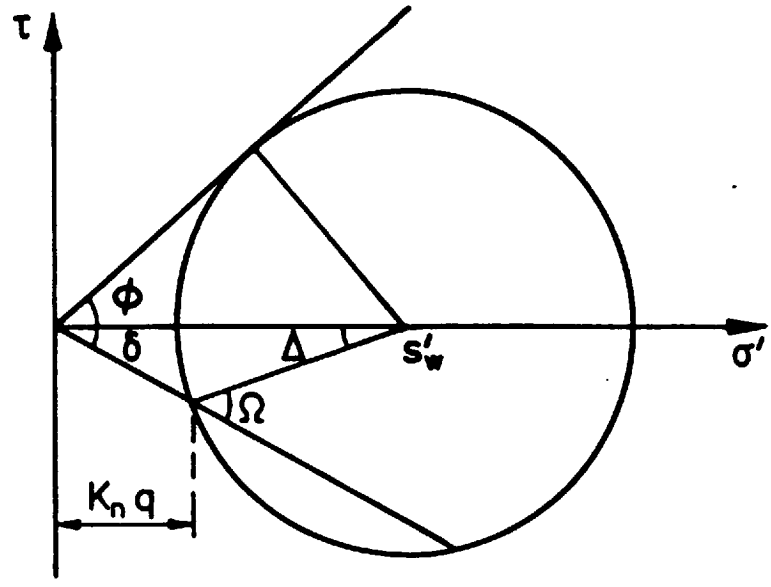

Figure 2.4 Stress analysis for rough wall and "active" soil

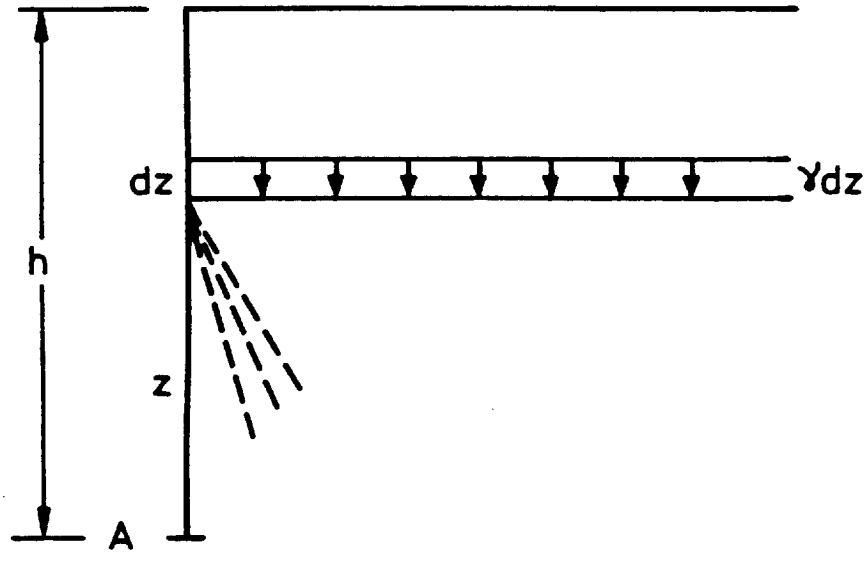

Figure 2.5 Superposition to solve for self-weight

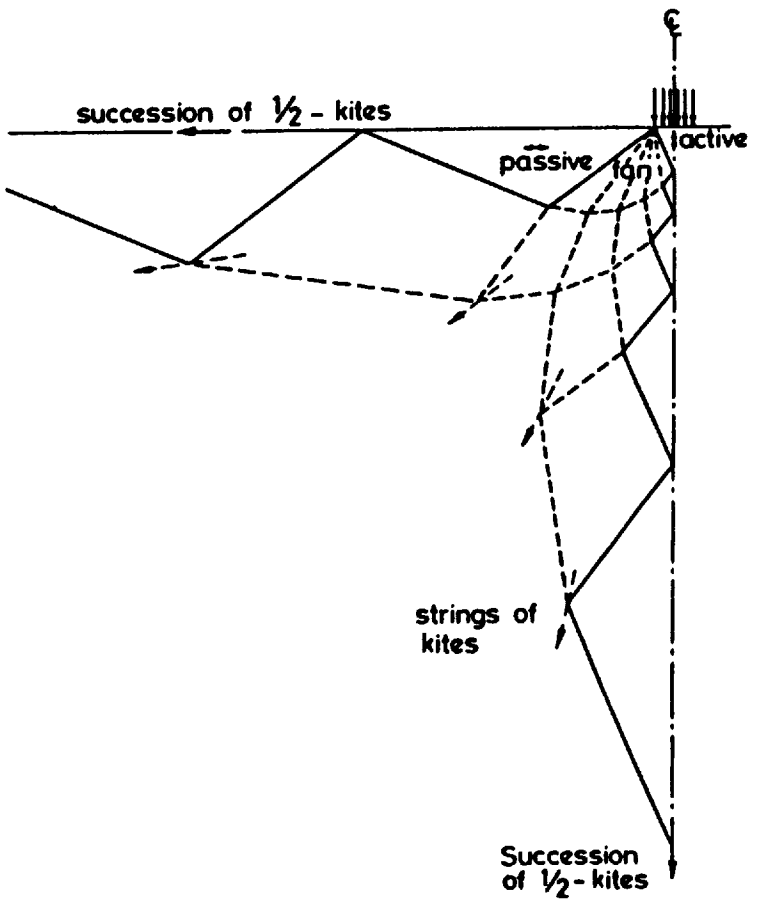

Figure 2.6 Extended stress field beneath strip load on weightless soil

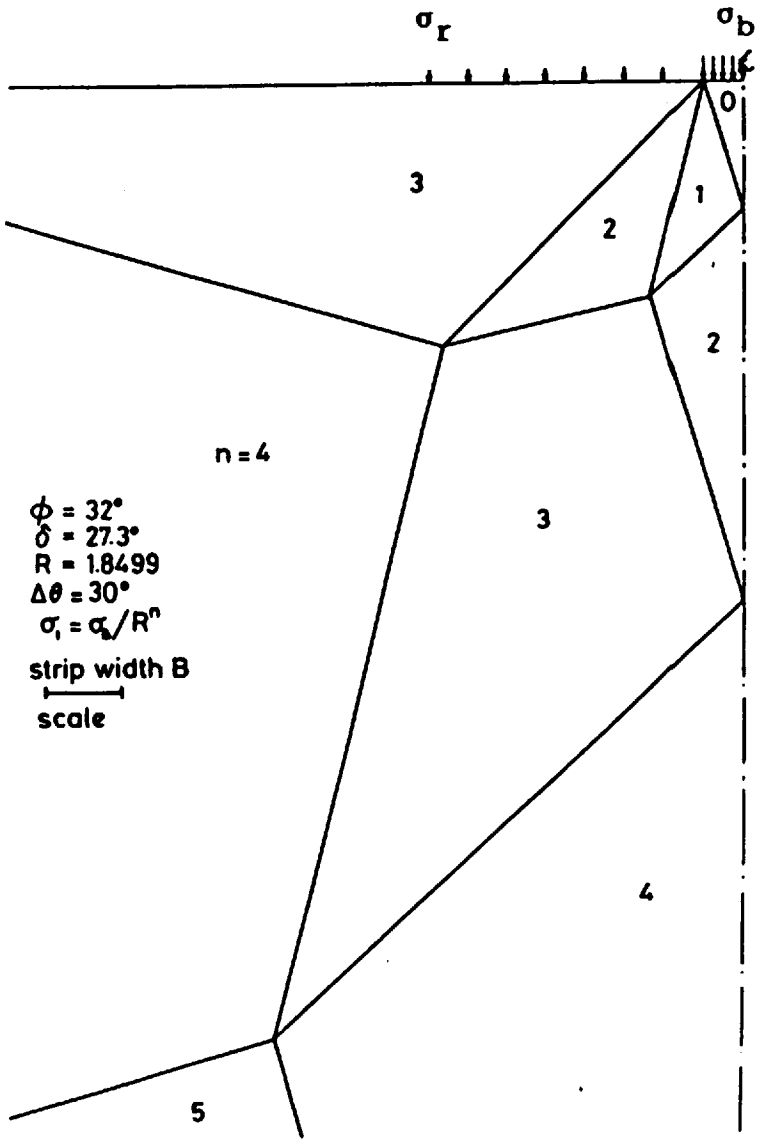

Figure 2.7 Stress field: φ = 32°, Δϑ = 30°

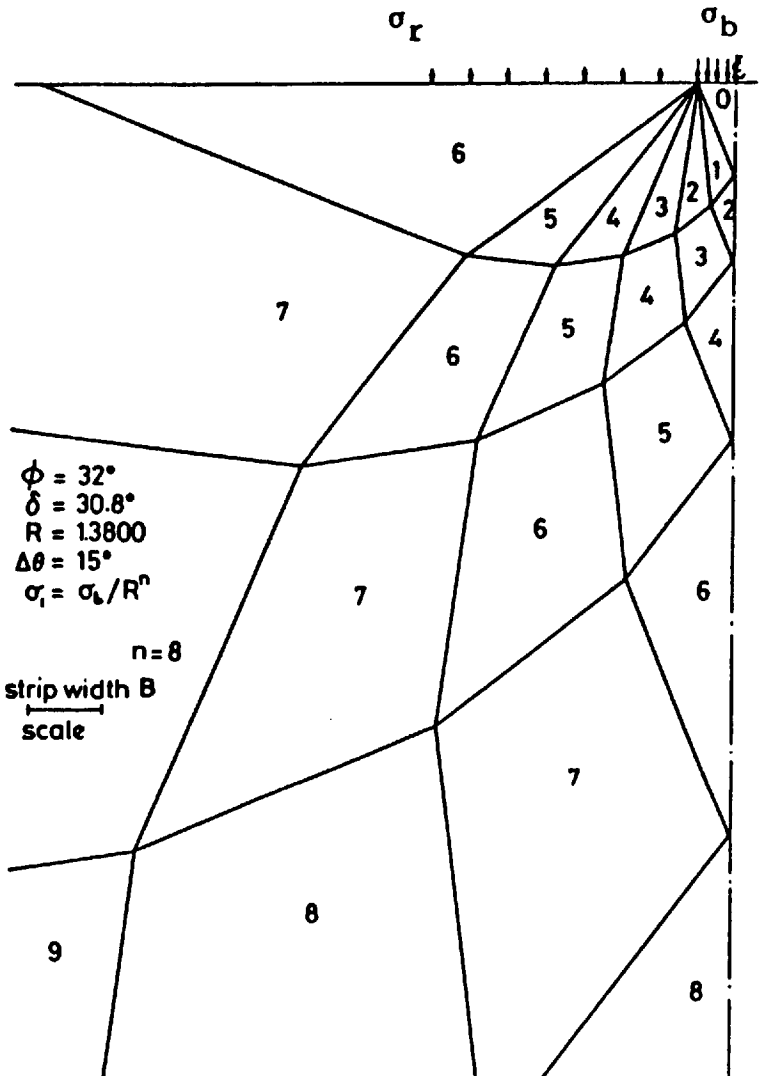

Figure 2.8 Stress field: φ = 32°, Δϑ = 15°

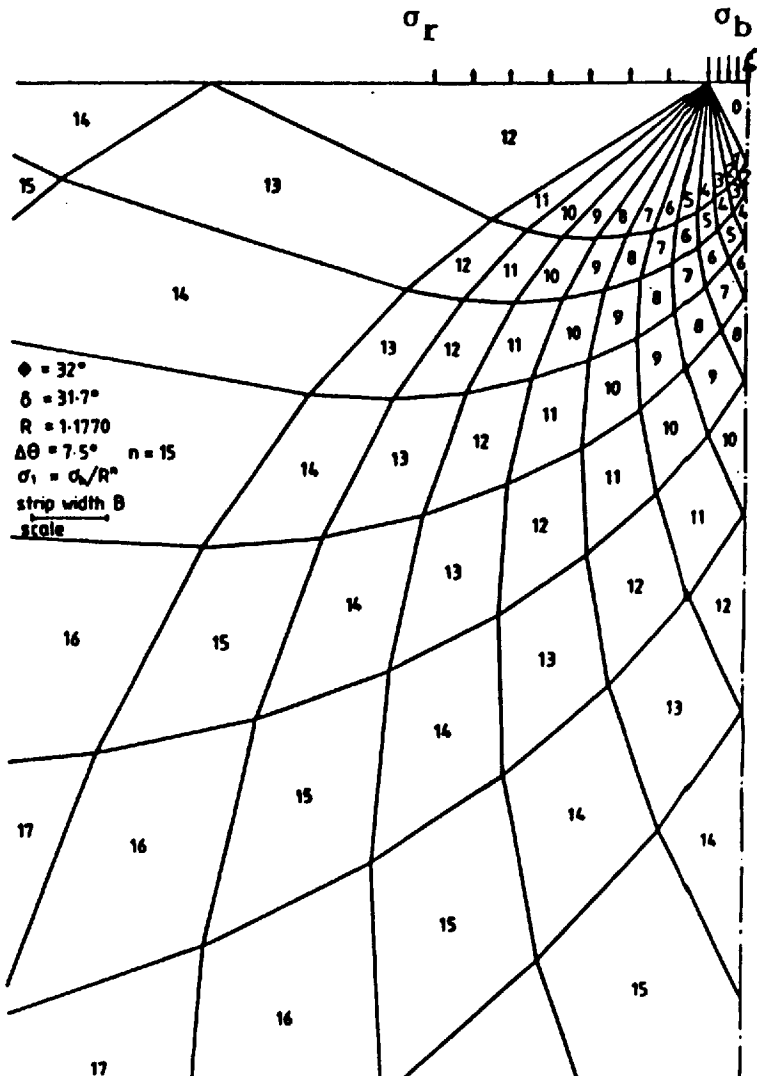

Figure 2.9 Stress field: φ = 32°, Δϑ = 7.5°

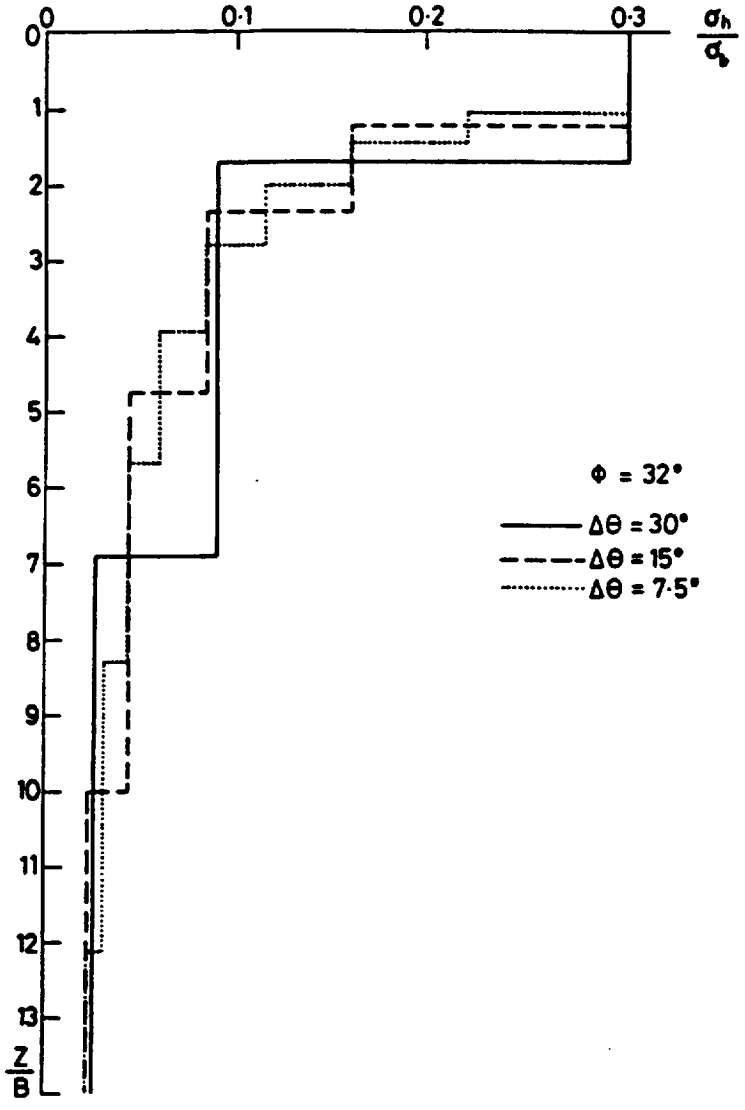

Figure 2.10 Profile of horizontal stress beneath centre of strip load

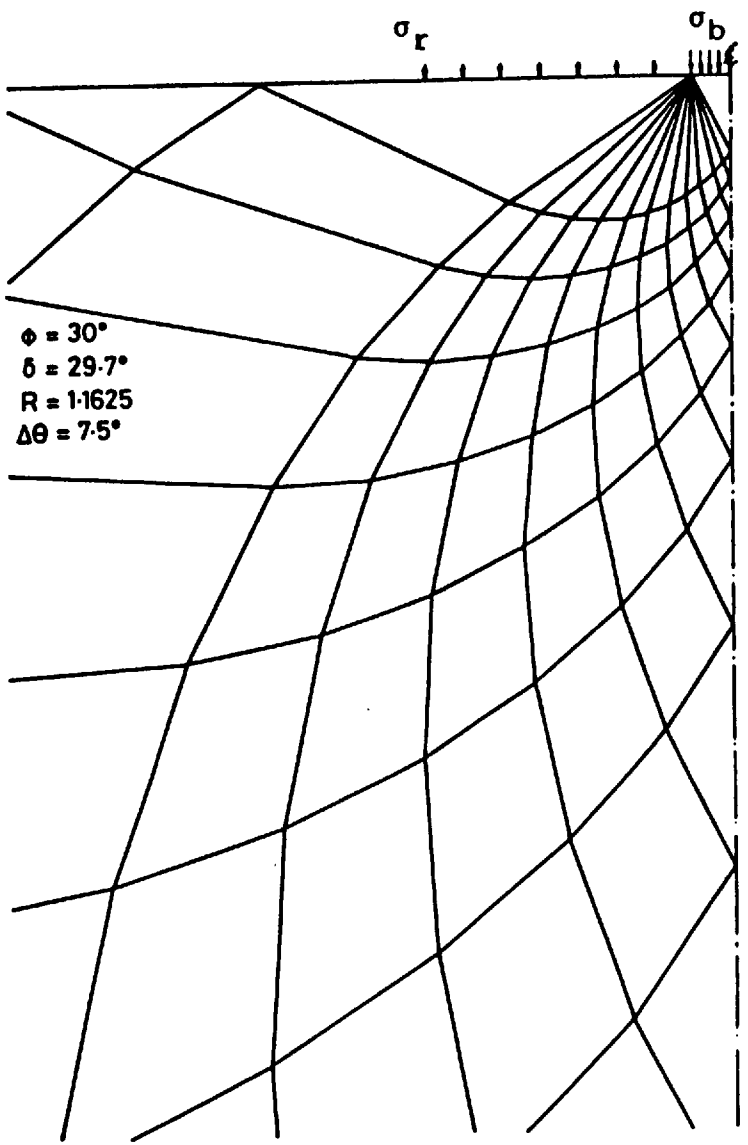

Figure 2.11 Stress field: $\varphi = 30°$, $\Delta\theta = 7.5°$

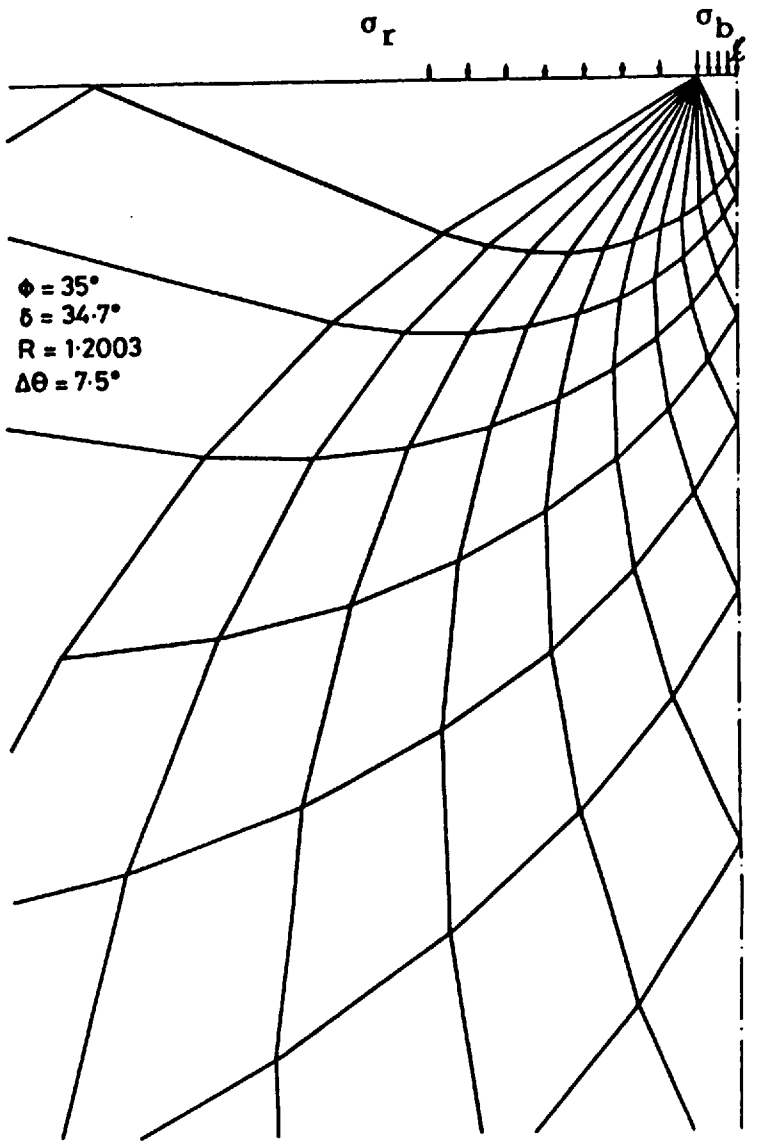

Figure 2.12 Stress field: $\varphi = 35°$, $\Delta\theta = 7.5°$

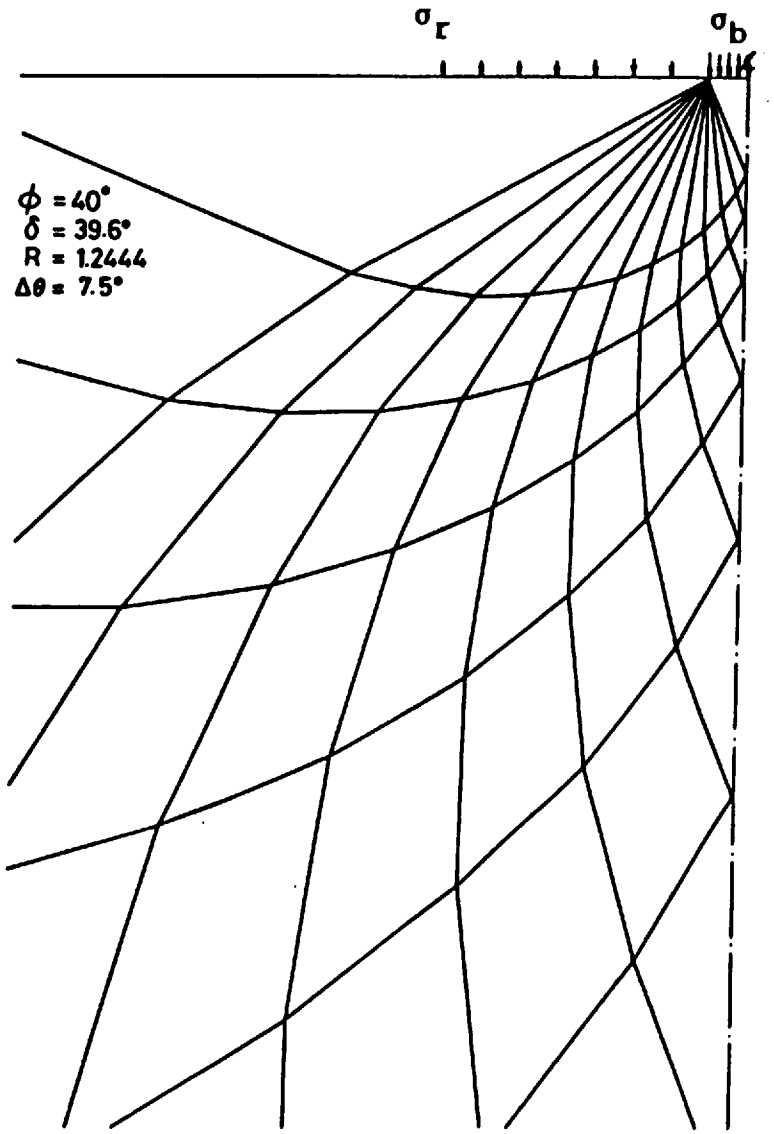

Figure 2.13 Stress field: φ = 40°, $\Delta\theta$ = 7.5°

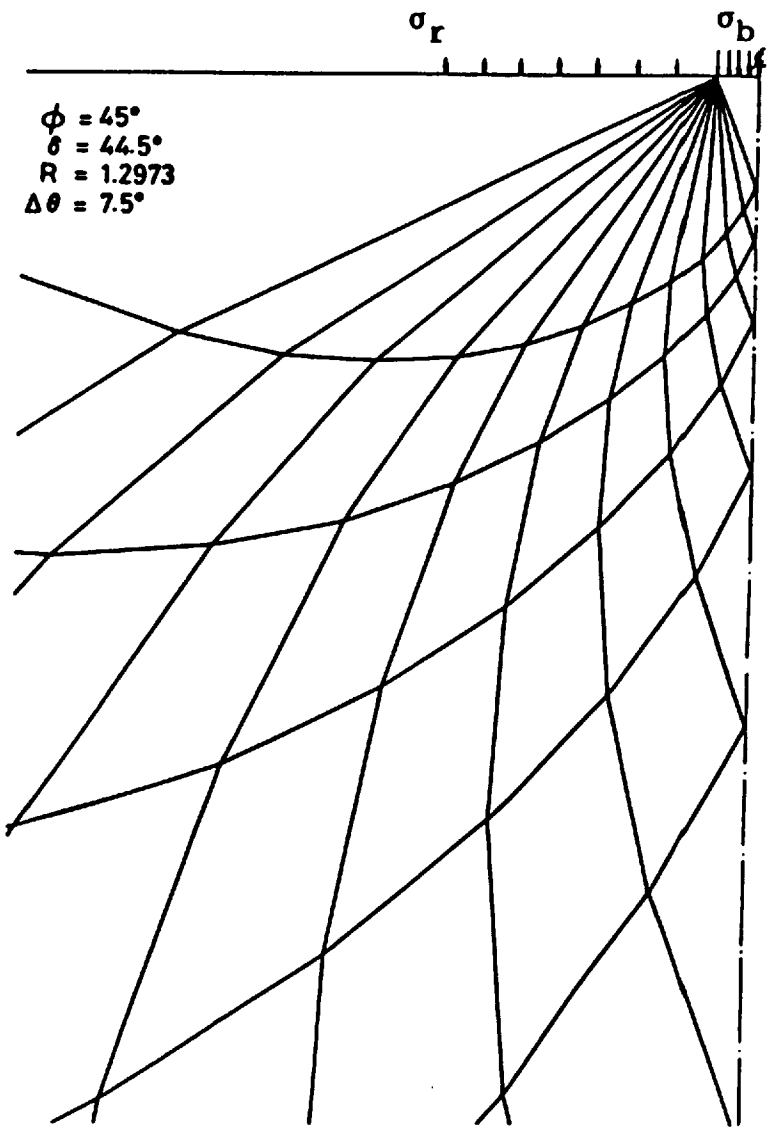

Figure 2.14 Stress field: φ = 45°, $\Delta\theta$ = 7.5°

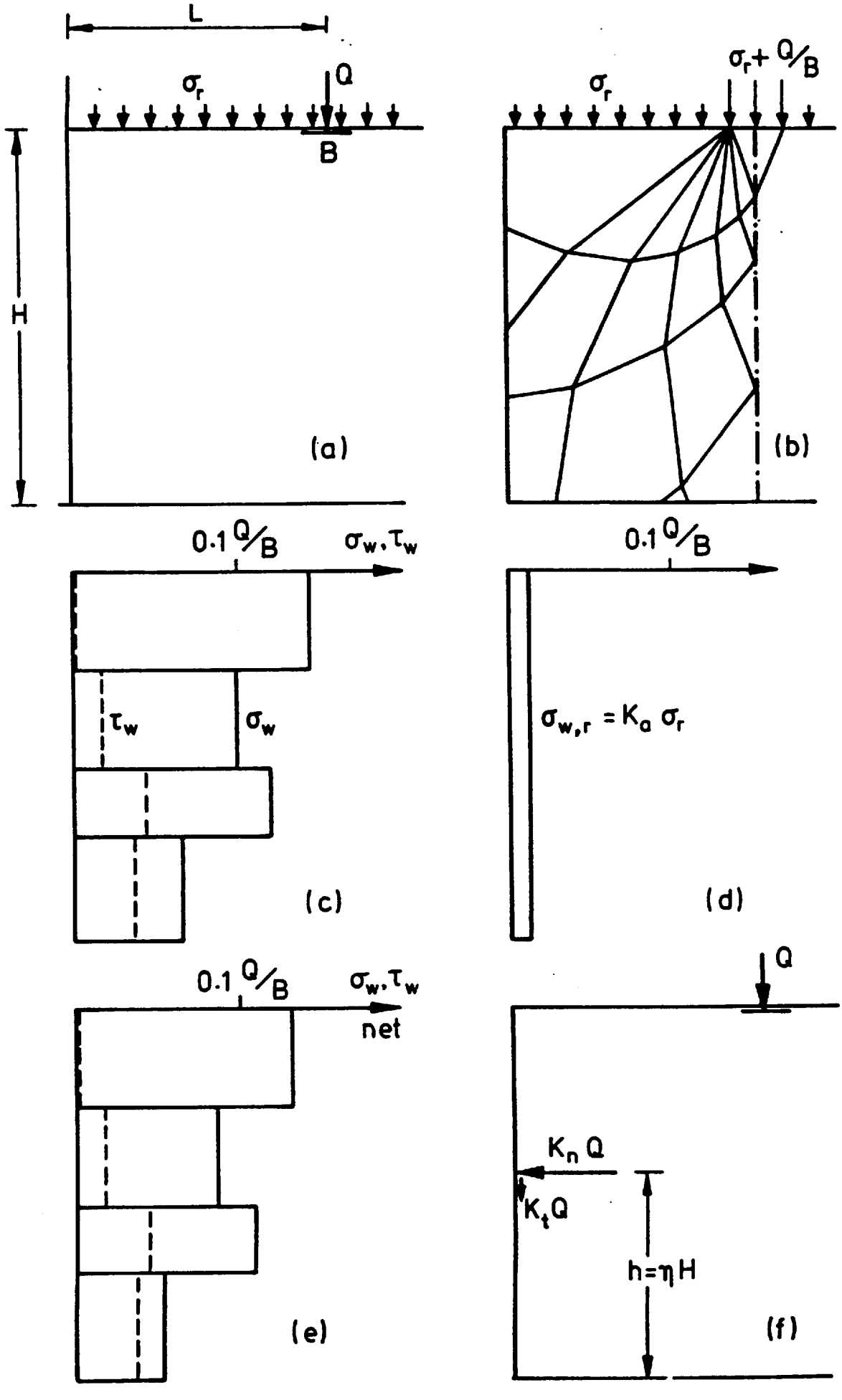

Figure 2.15 Integrated thrust coefficients K_n, K_t, η

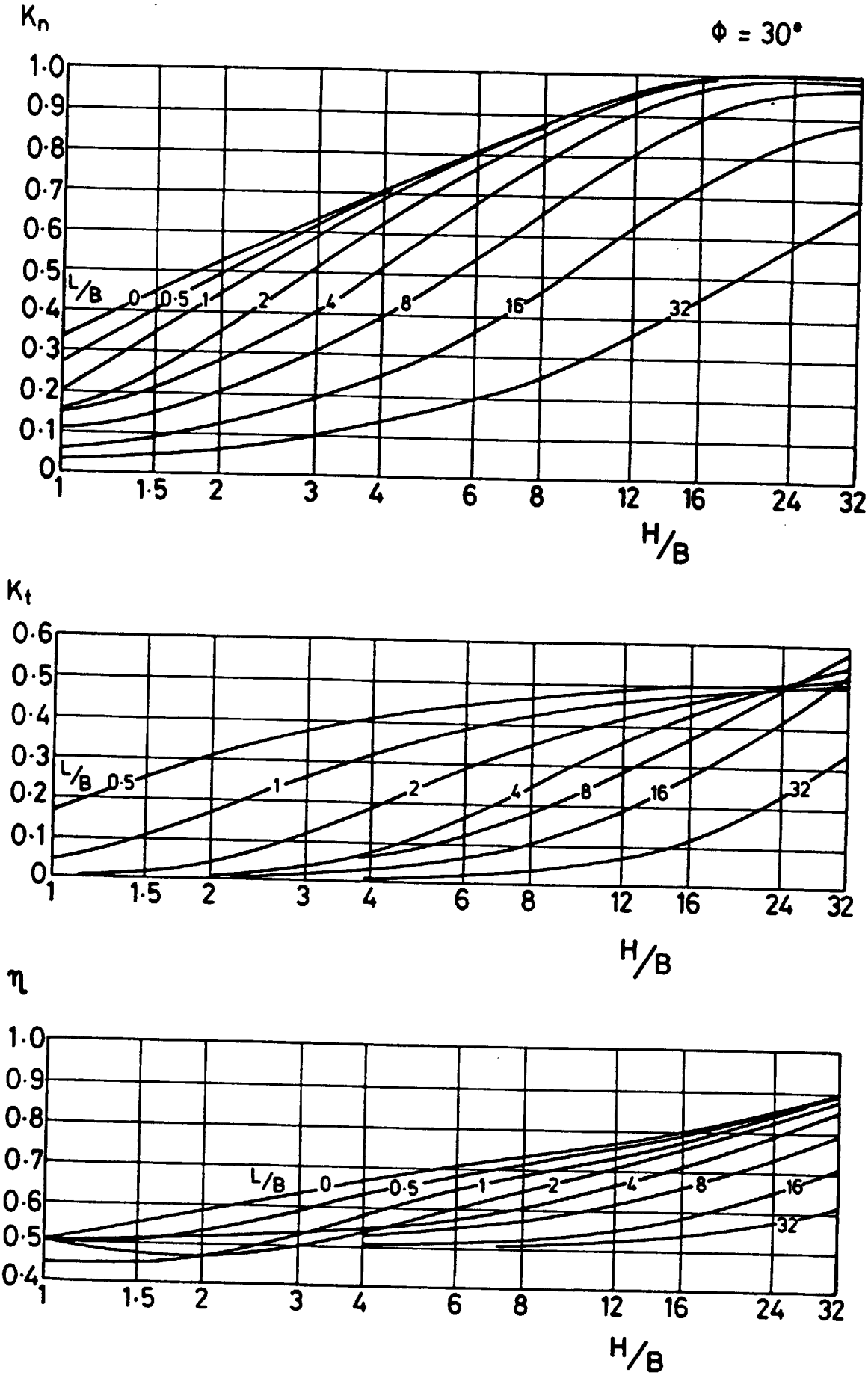

Figure 2.16 Thrust coefficients for strip loads: $\varphi = 30°$

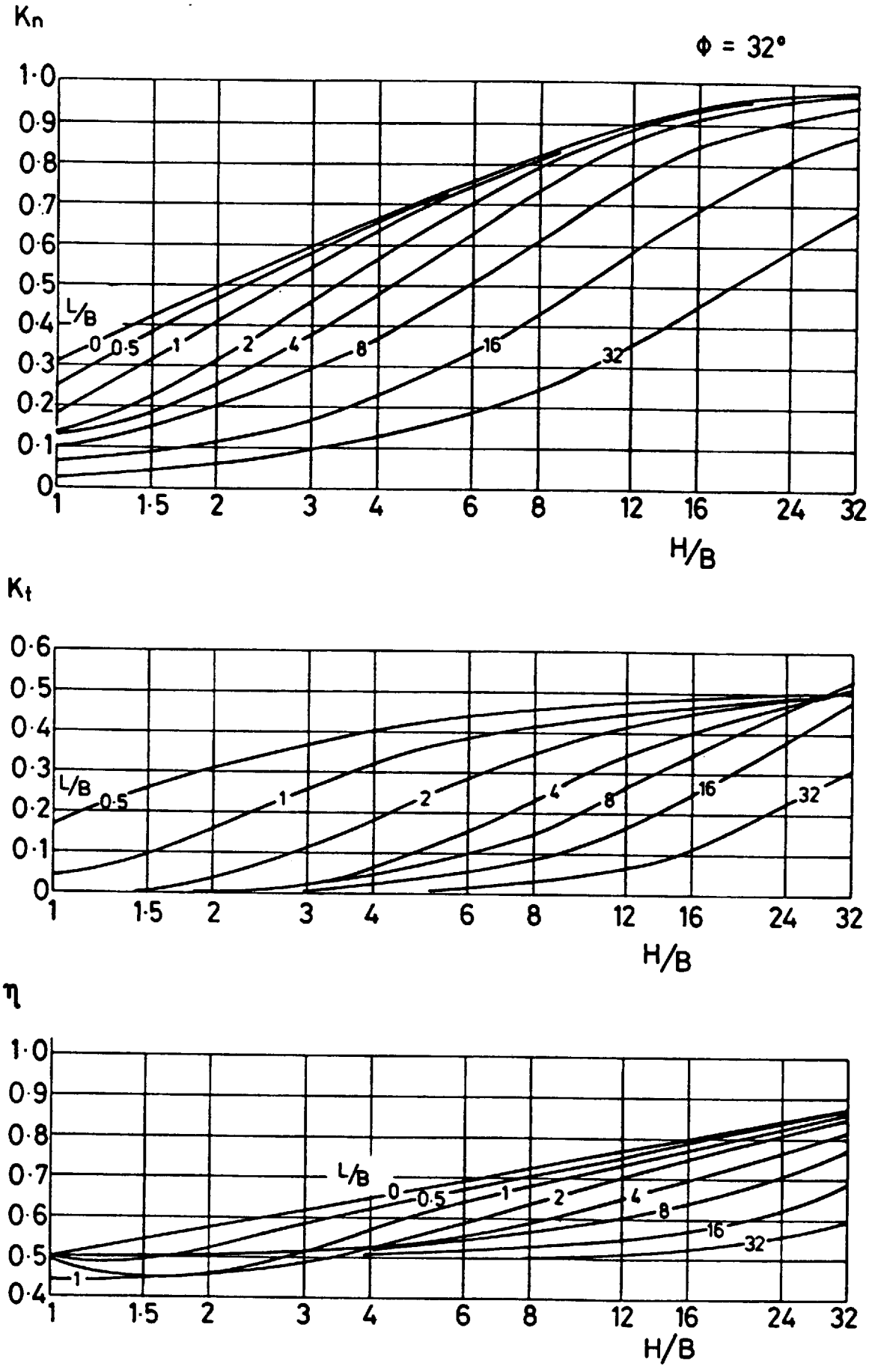

Figure 2.17 Thrust coefficients for strip loads: $\varphi = 32°$

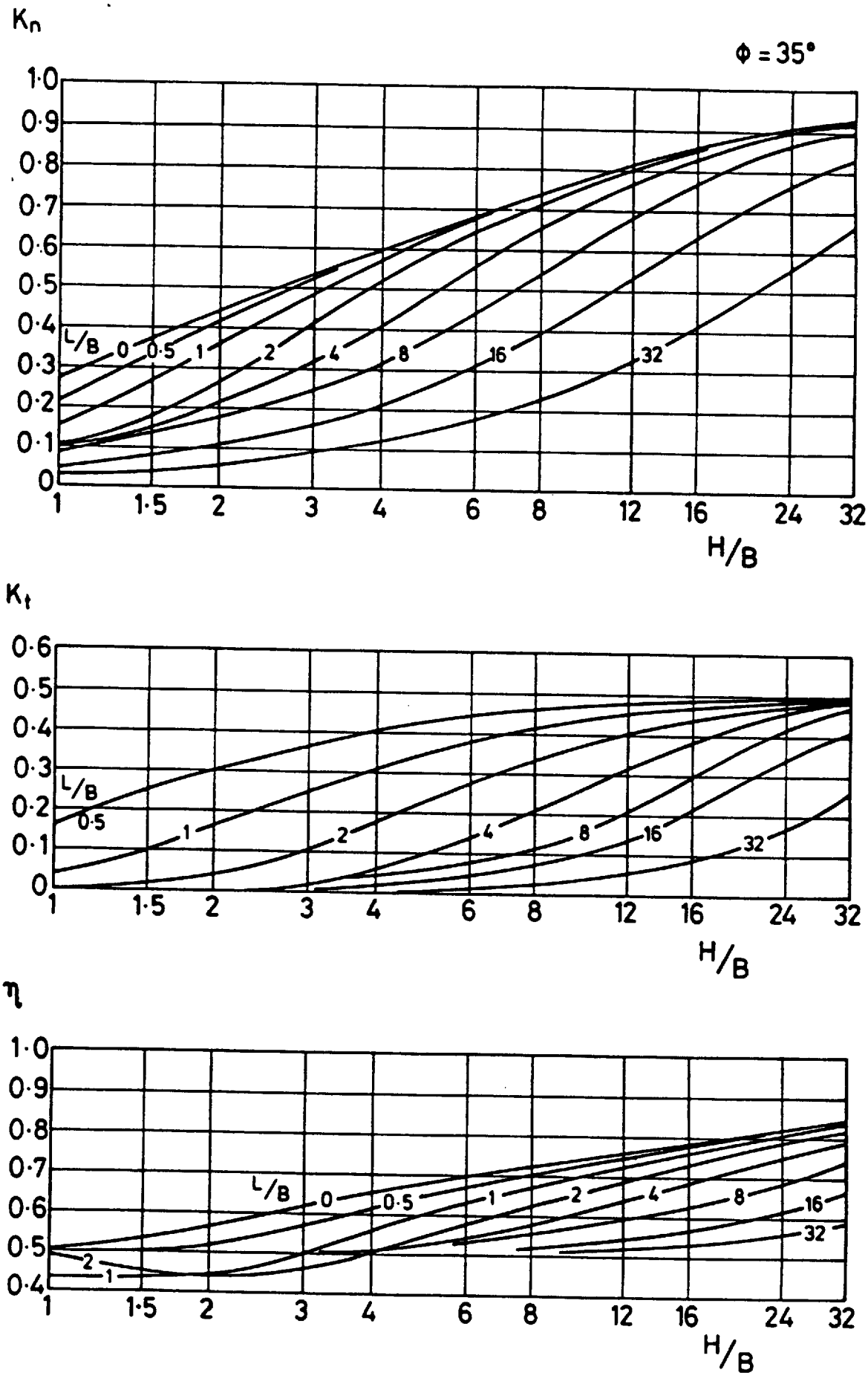

Figure 2.18 Thrust coefficients for strip loads: $\varphi = 35°$

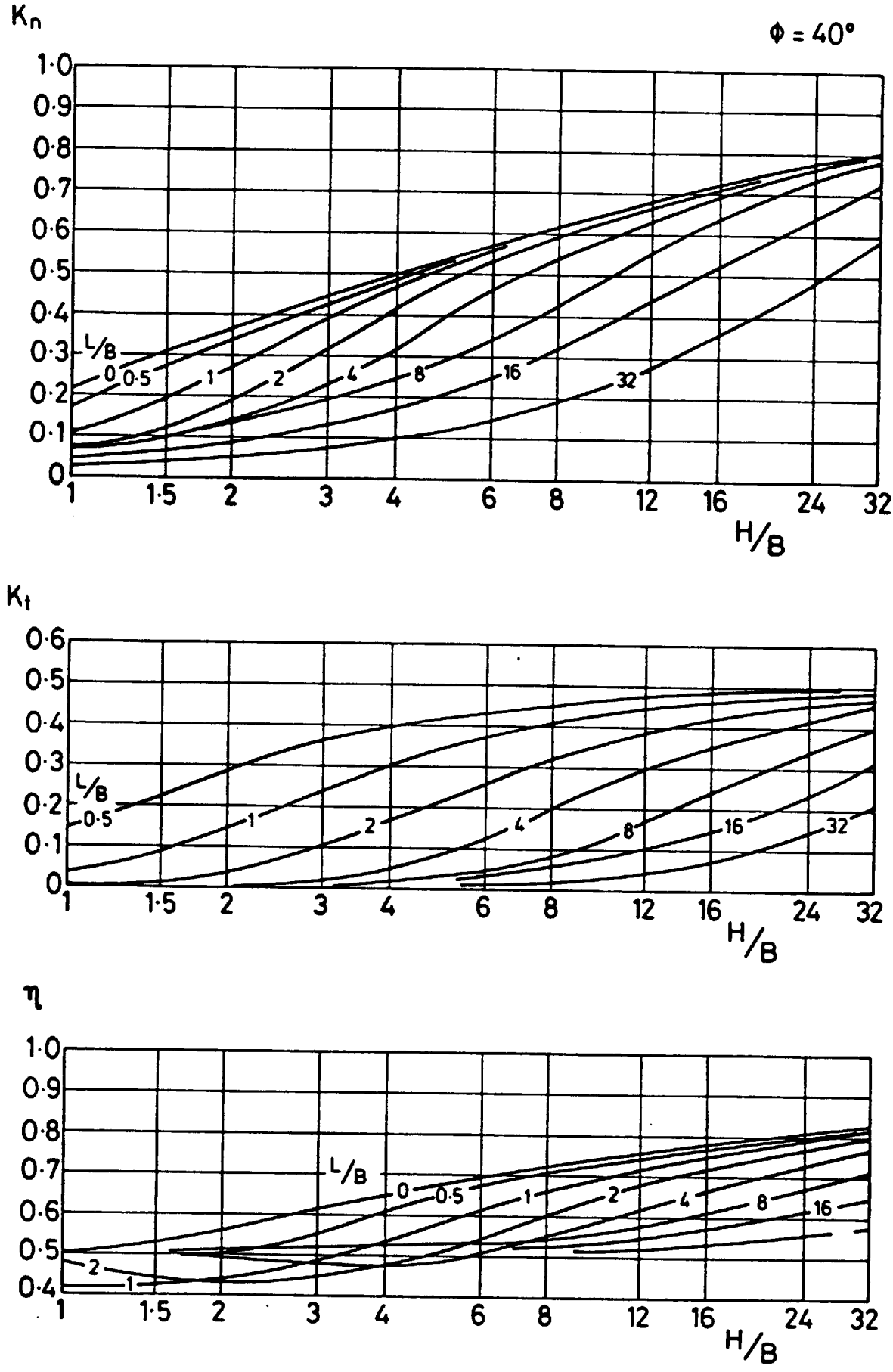

Figure 2.19 Thrust coefficients for strip loads: $\varphi = 40°$

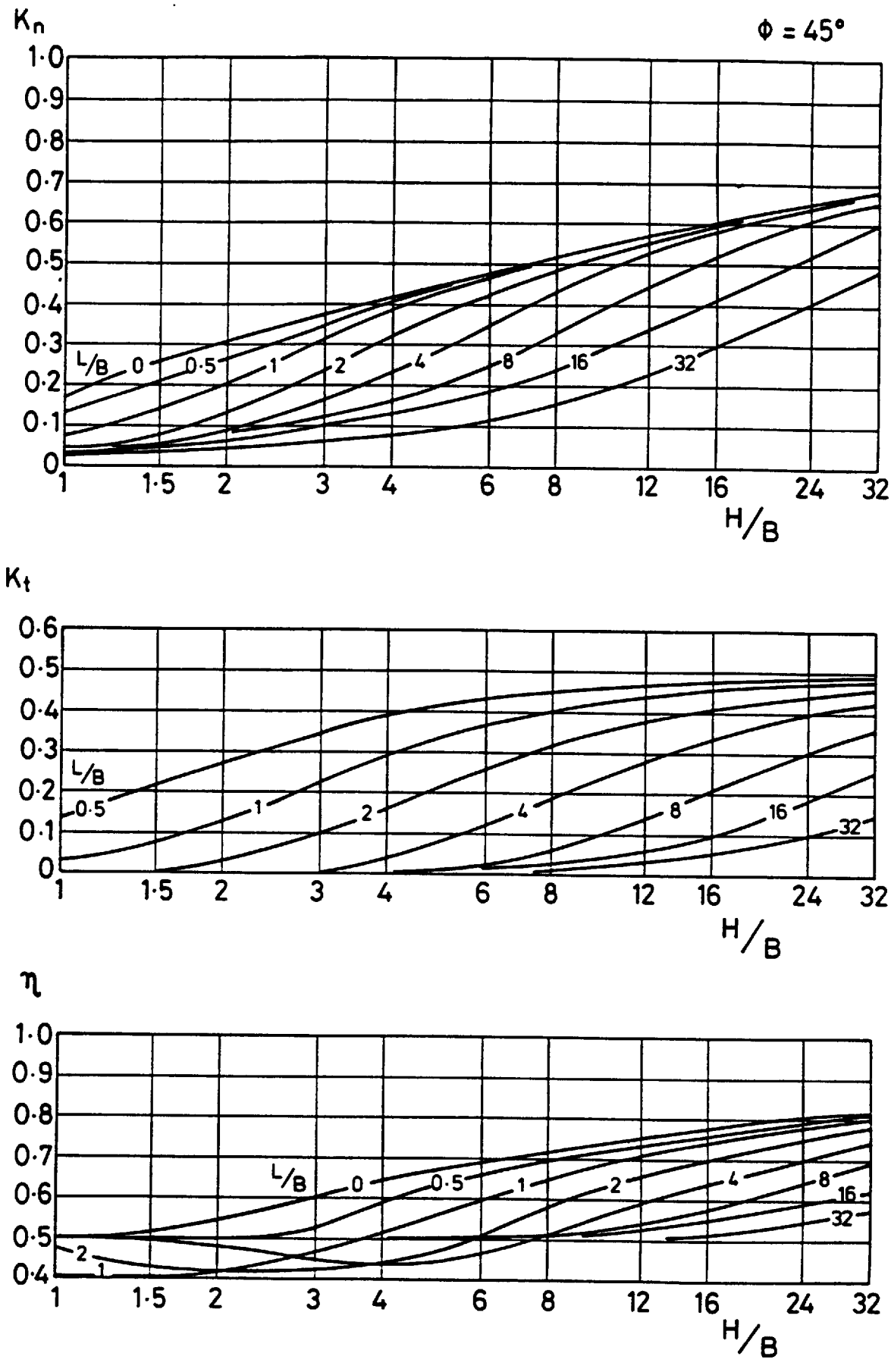

Figure 2.20 Thrust coefficients for strip loads: $\varphi = 45°$

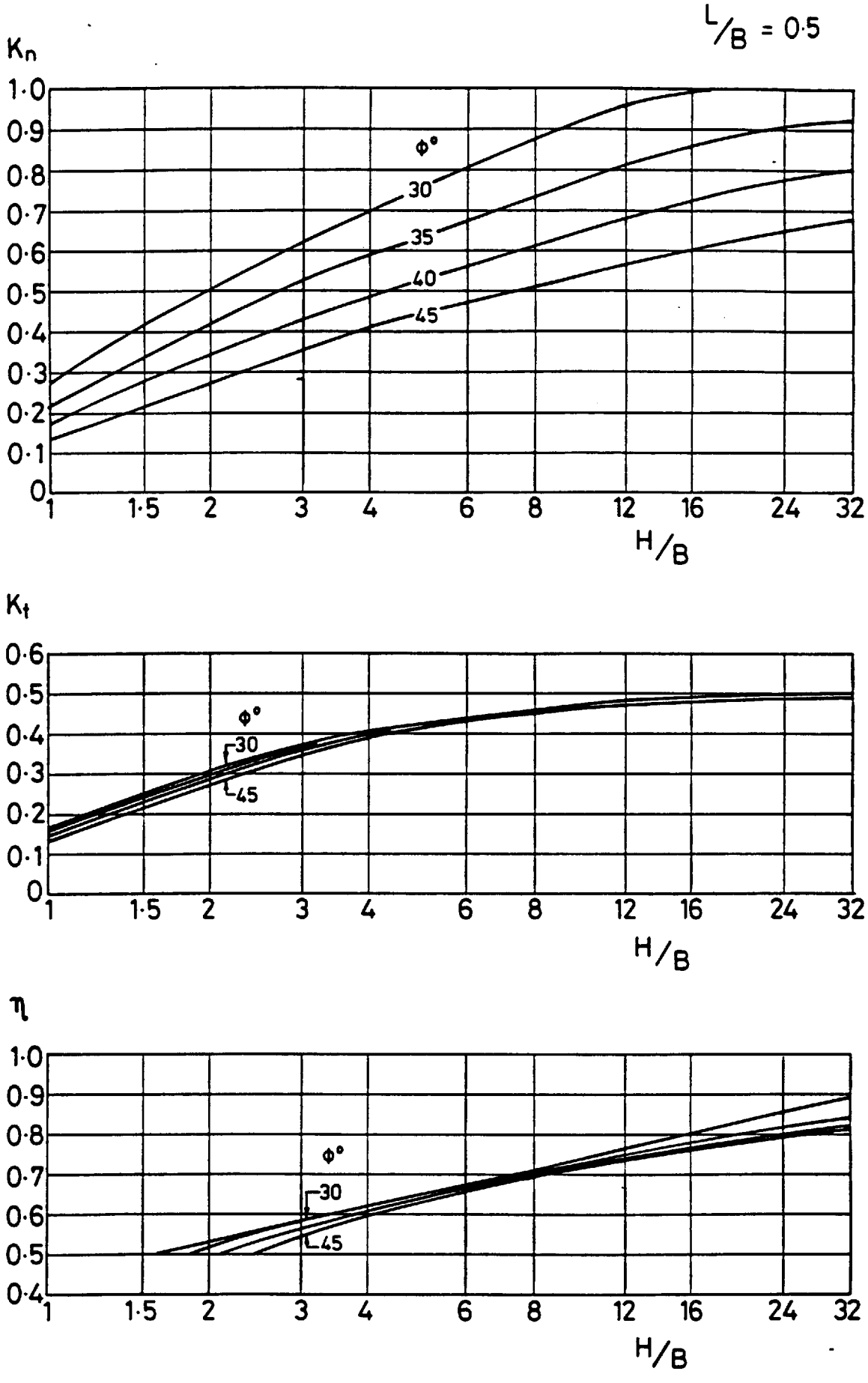

Figure 2.21 Thrust coefficients for strip adjacent to wall: L/B = 0.5

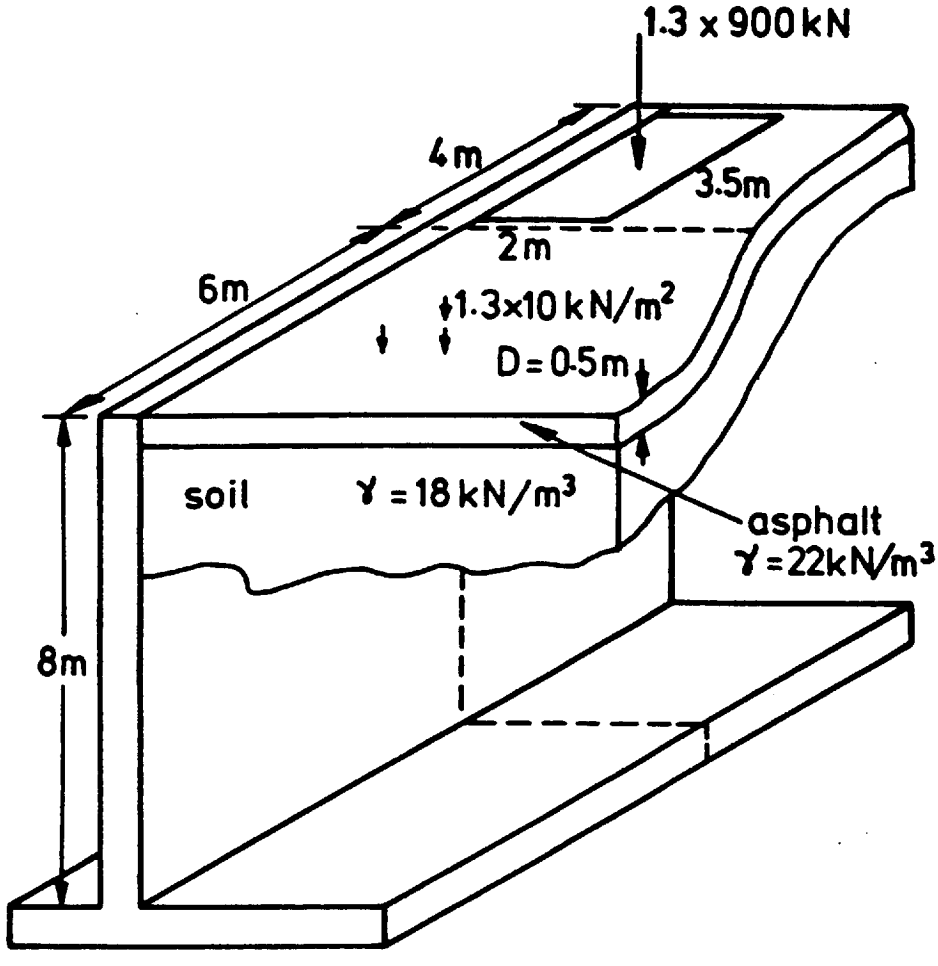

Figure 2.22 Superposing load and self-weight effects

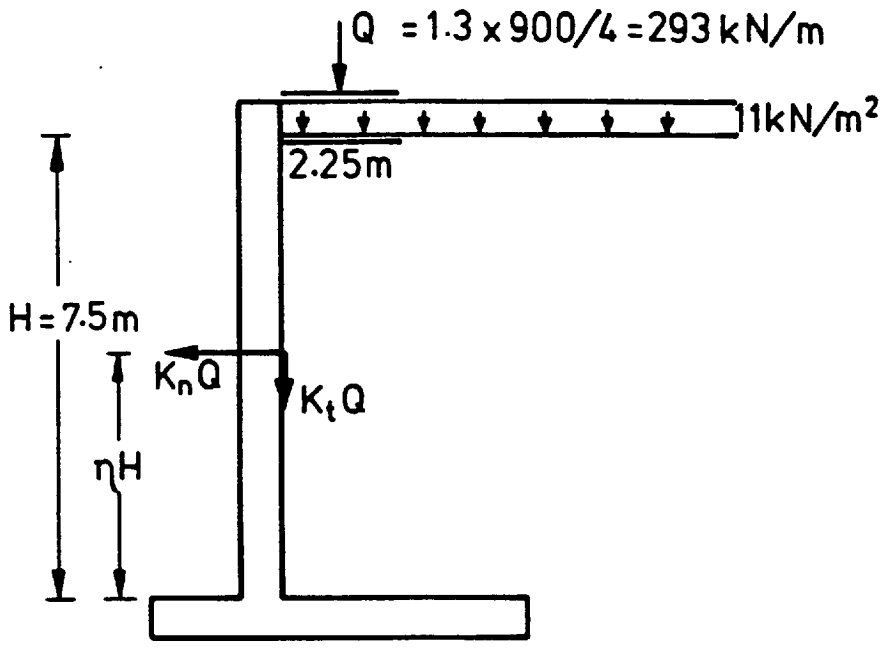

a) 4m section under HB load

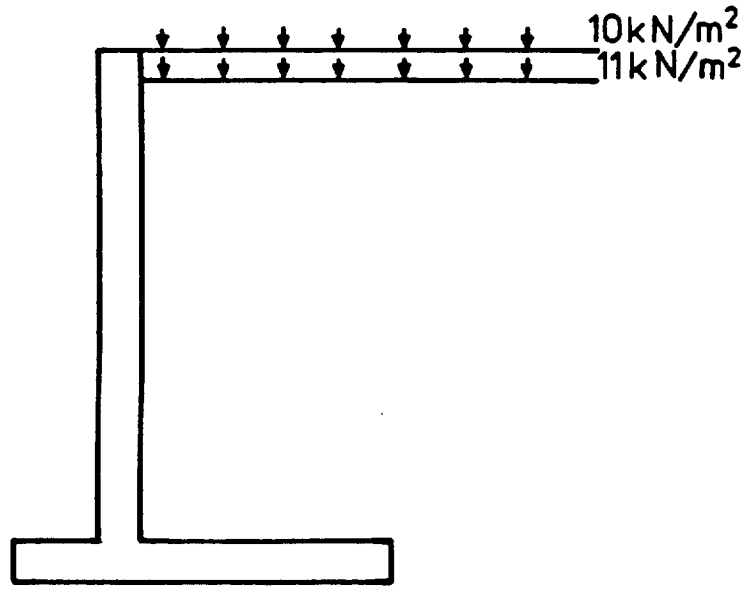

b) 6m section under HA load

Figure 2.23 Two-dimensional idealization of superposition

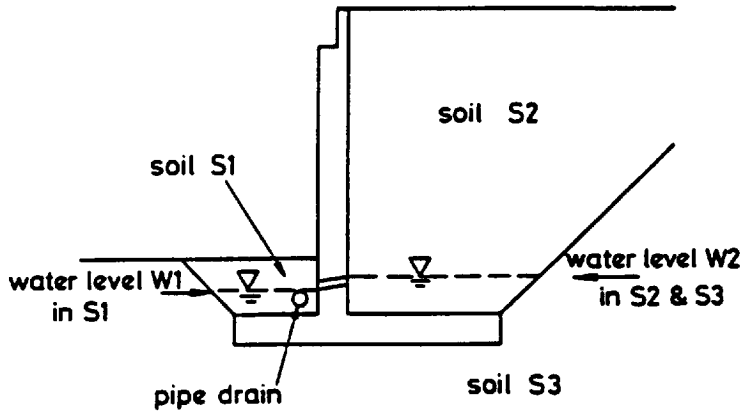

Figure 2.24 Typical water levels ($k_1 \geq k_2 \geq k_3$)

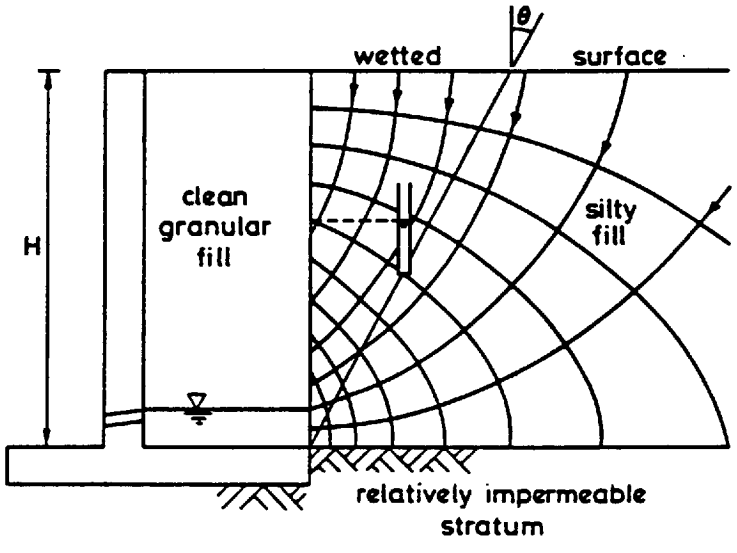

Figure 2.25 Example of vertically drained flow

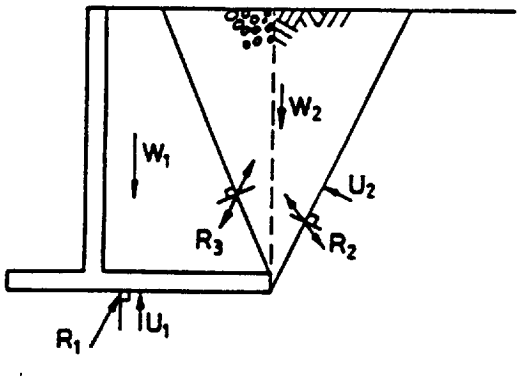

Figure 2.26 Double block sliding mechanism

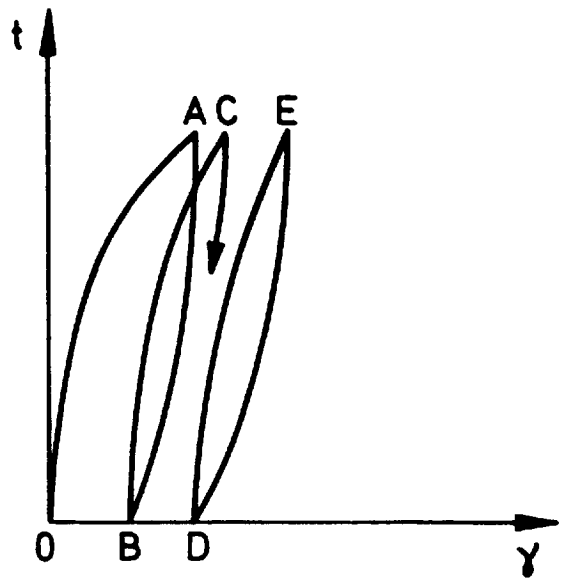

Figure 3.1 Cyclic stress-strain curve

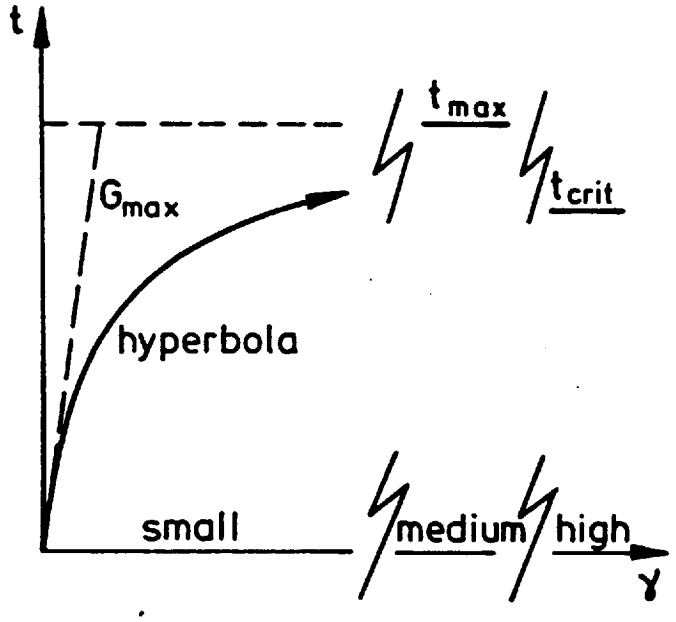

Figure 3.2 Hyperbolic approximation

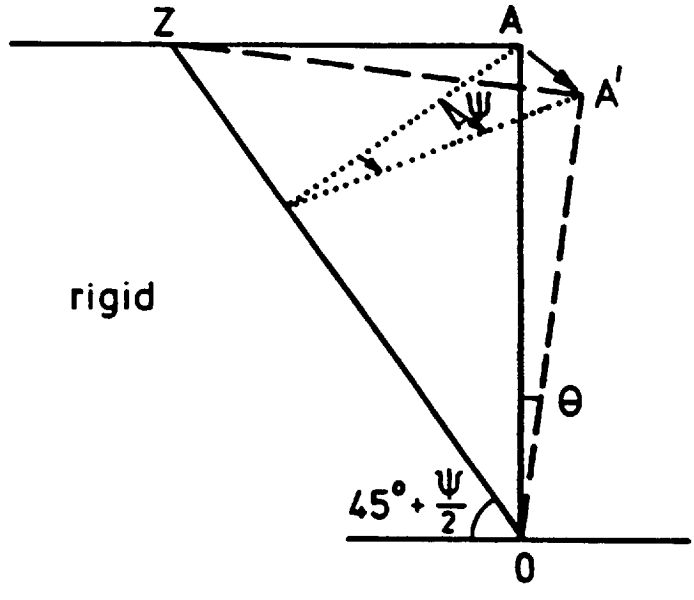

Figure 3.3 Simple displacement field: Bransby and Milligan (1975)

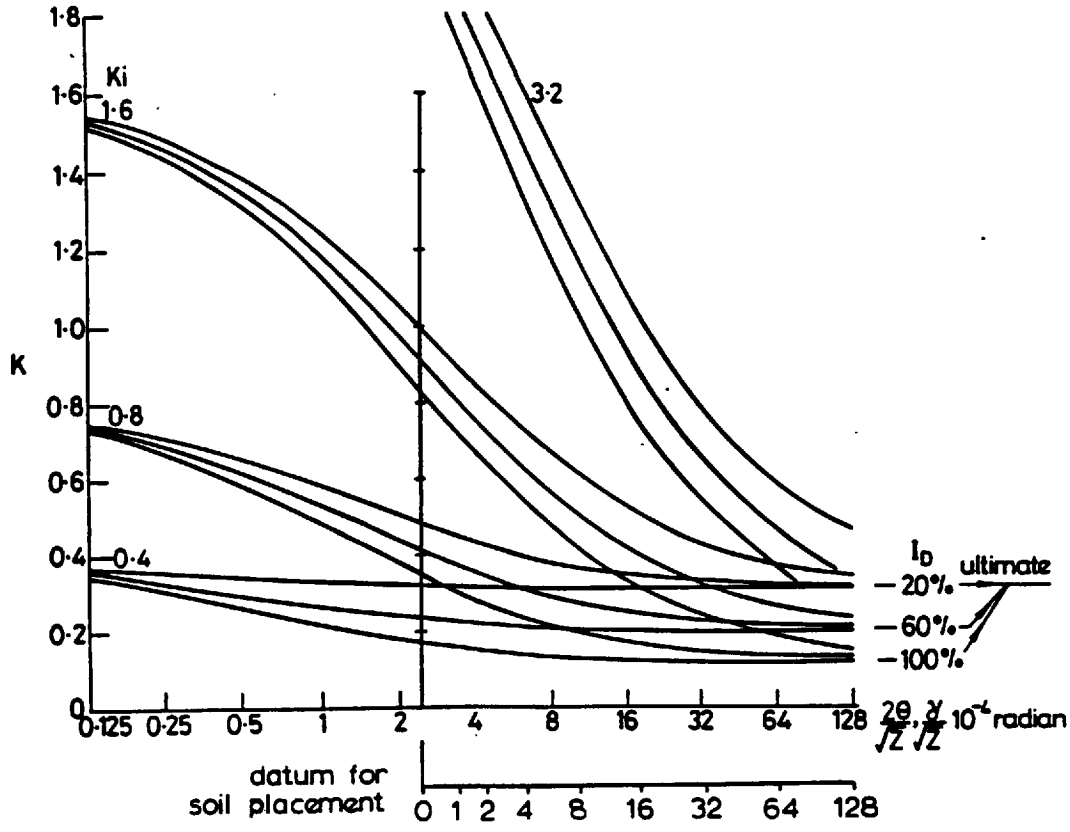

a) Outward

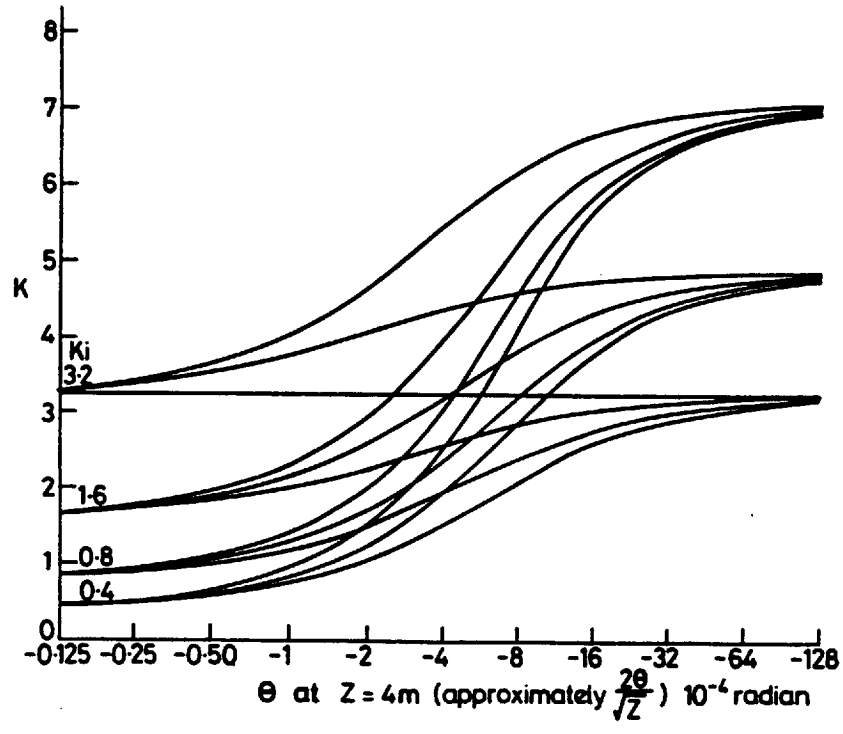

b) Inward

Figure 3.4 Earth pressure coefficient versus wall rotation

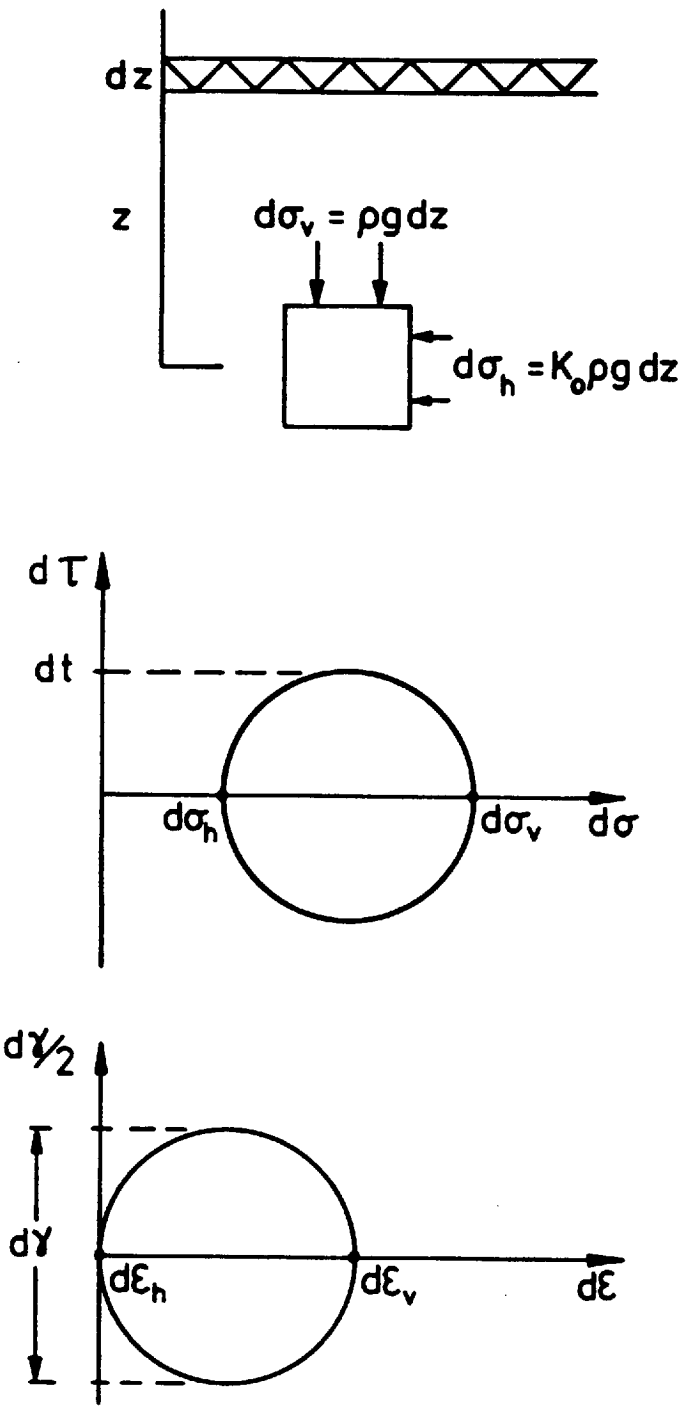

Figure 3.5 Stress and strain under K_o construction conditions

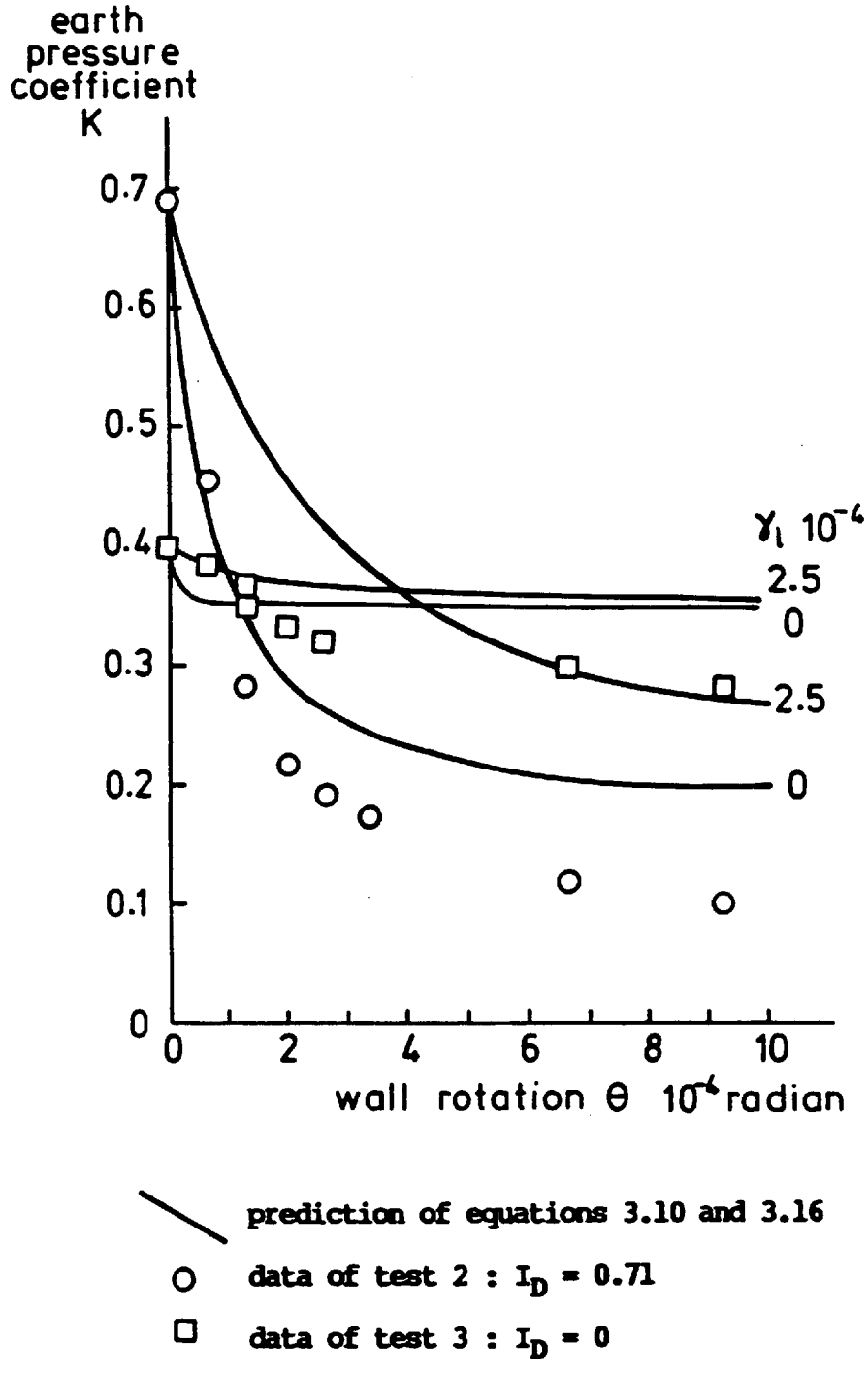

Figure 3.6 Terzaghi (1934) model wall tests

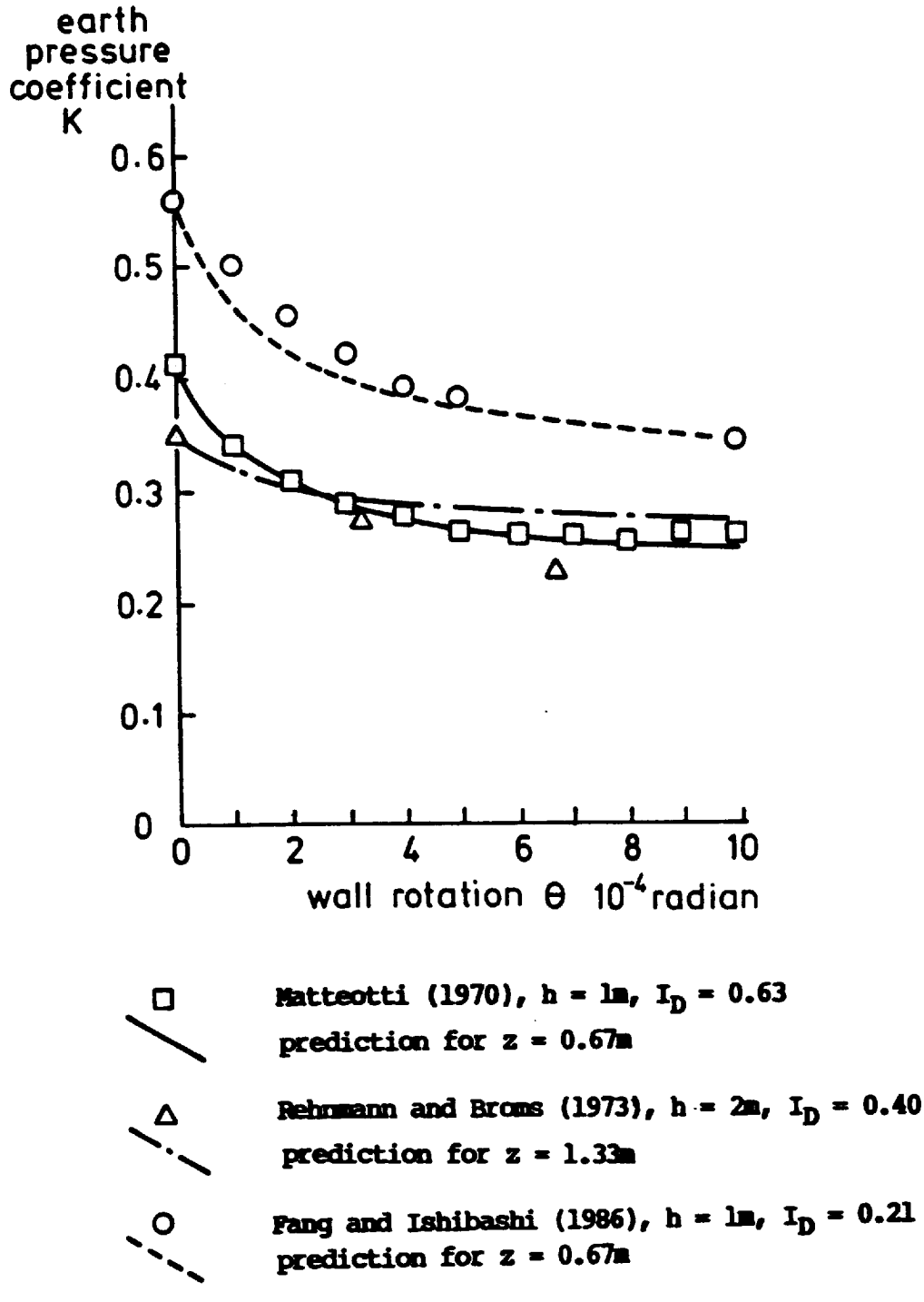

Figure 3.7 Data of model walls retaining uncompacted sand:
Predictions based on initial strain $\gamma_i = 2.5/z\ 10^{-4}$

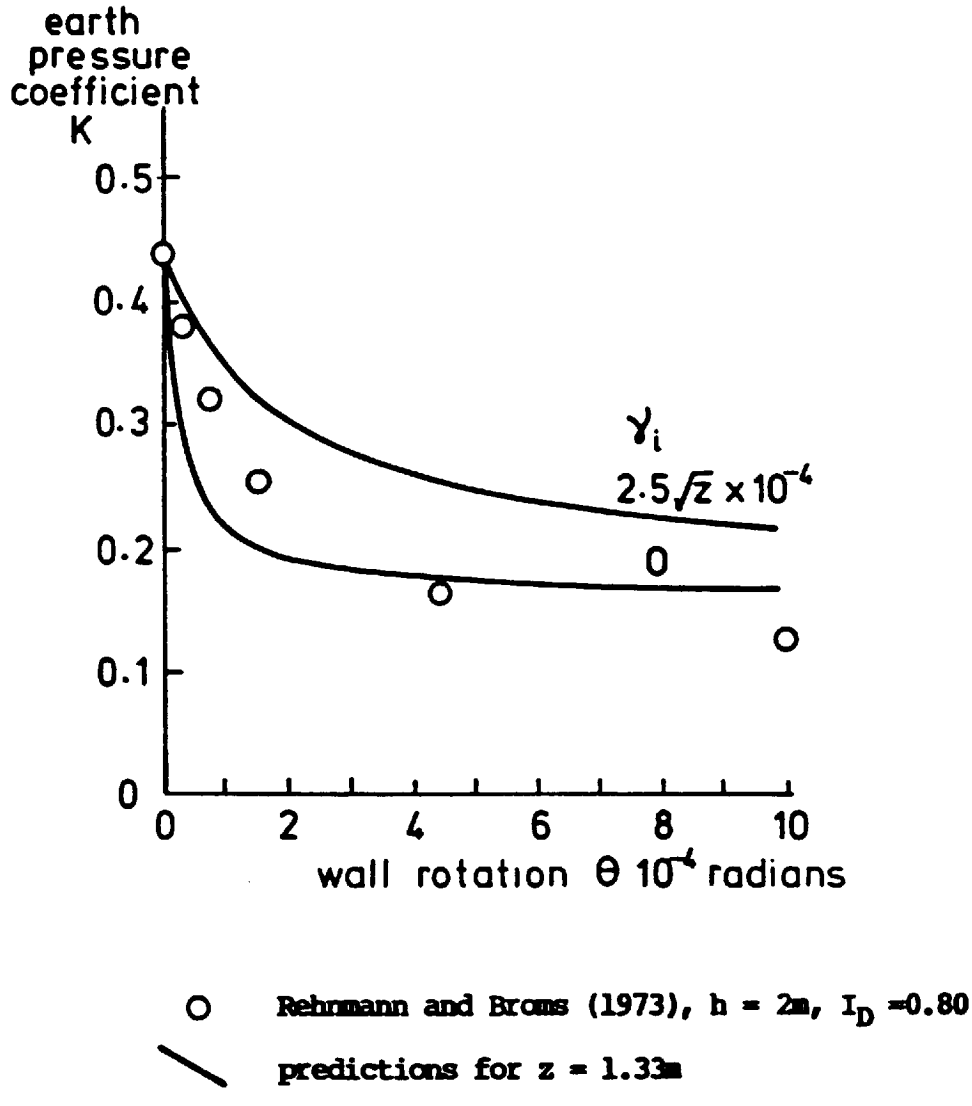

Figure 3.8 Data of model wall retaining compacted sand

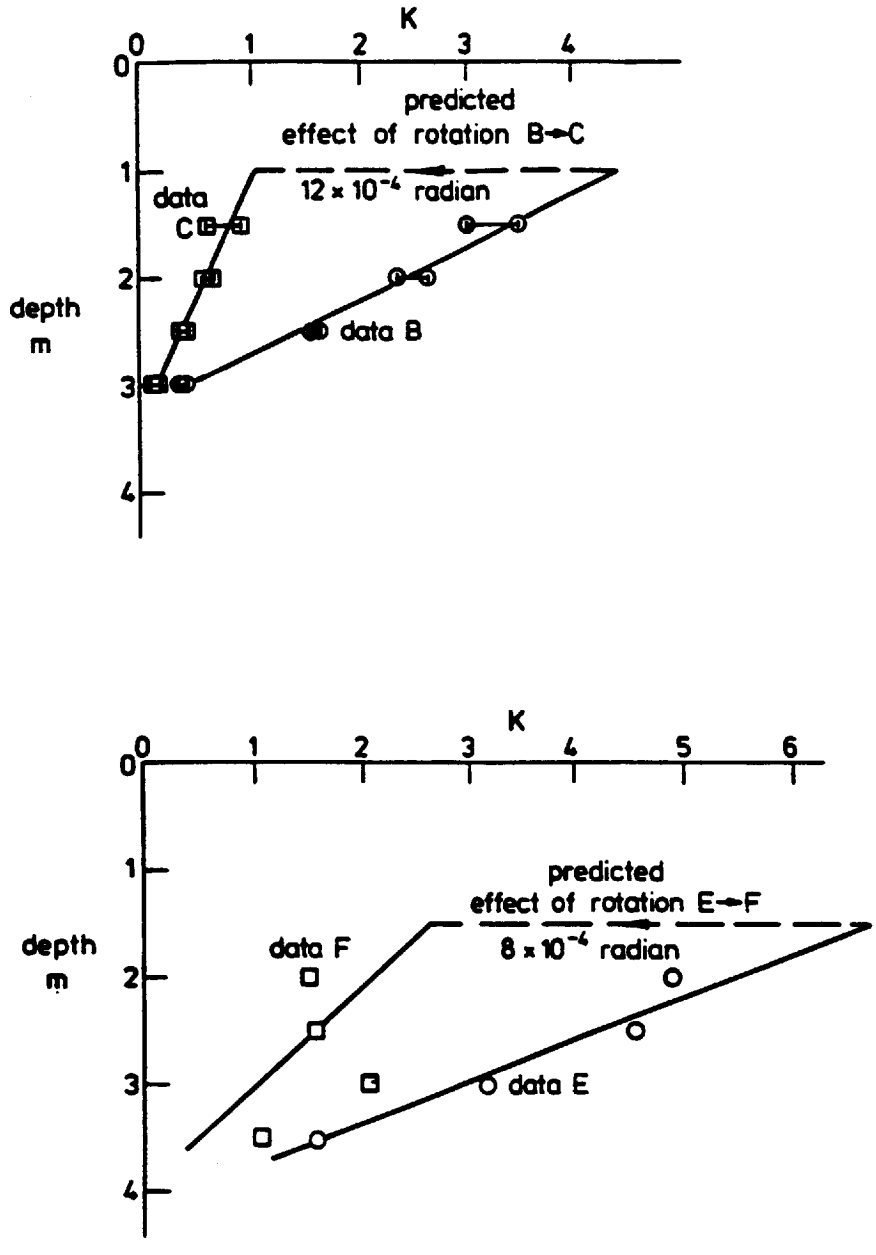

a) Outward rotation

Figure 3.9 Data of earth pressure changes behind abutment wall

Broms and Ingleson (1971)

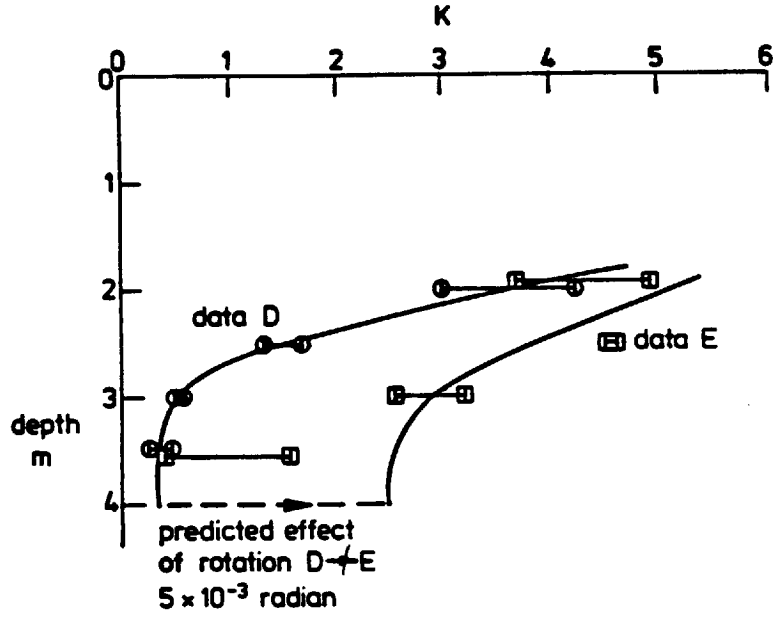

b) Inward rotation

Figure 3.9 Data of earth pressure changes behind abutment wall

Broms and Ingleson (1971)

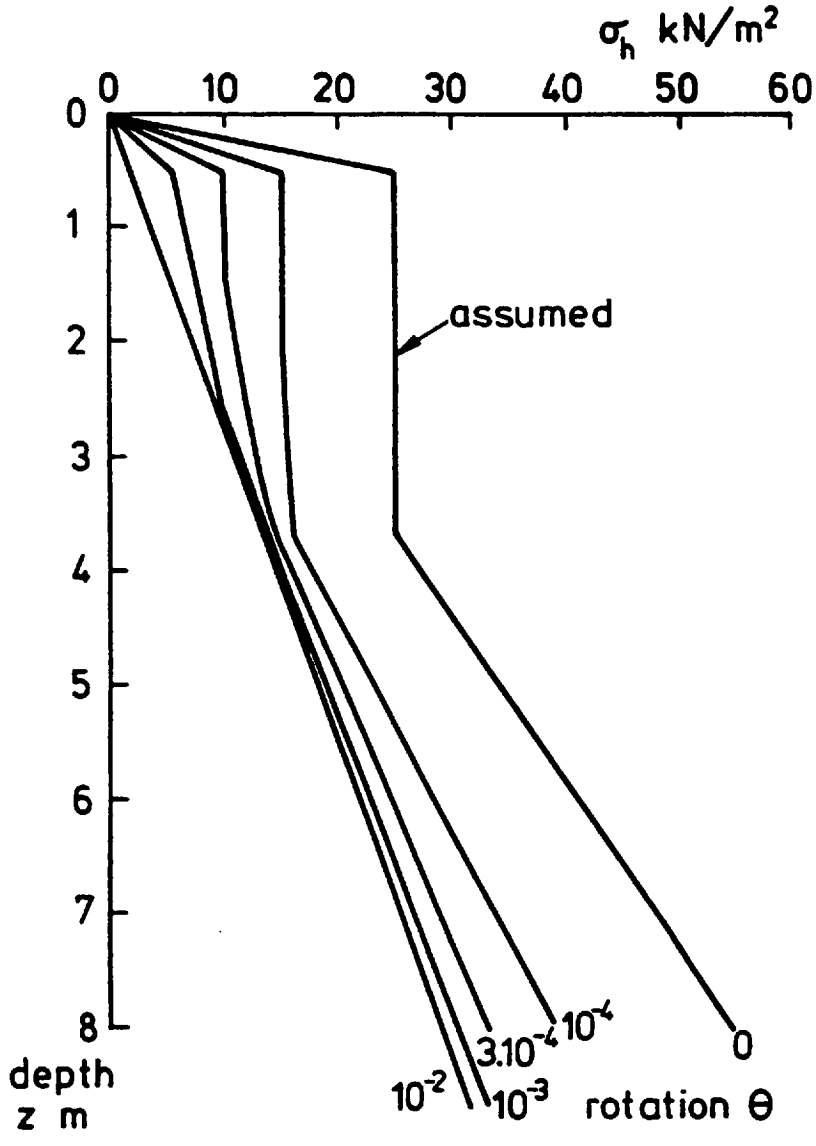

a) $\gamma_i = 0$

Figure 3.10 Typical earth pressures variations on outward rotation

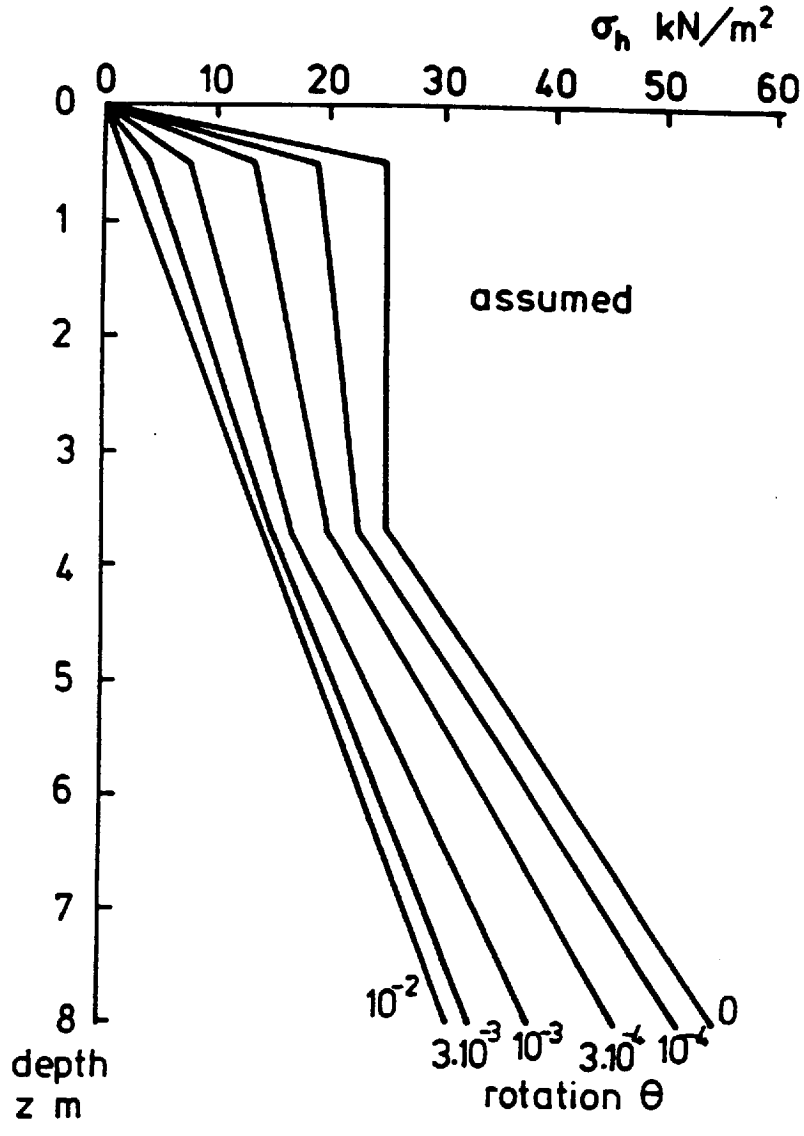

b) $\gamma_i = 2.5/z\ 10^{-4}$

Figure 3.10 Typical earth pressures variations on outward rotation

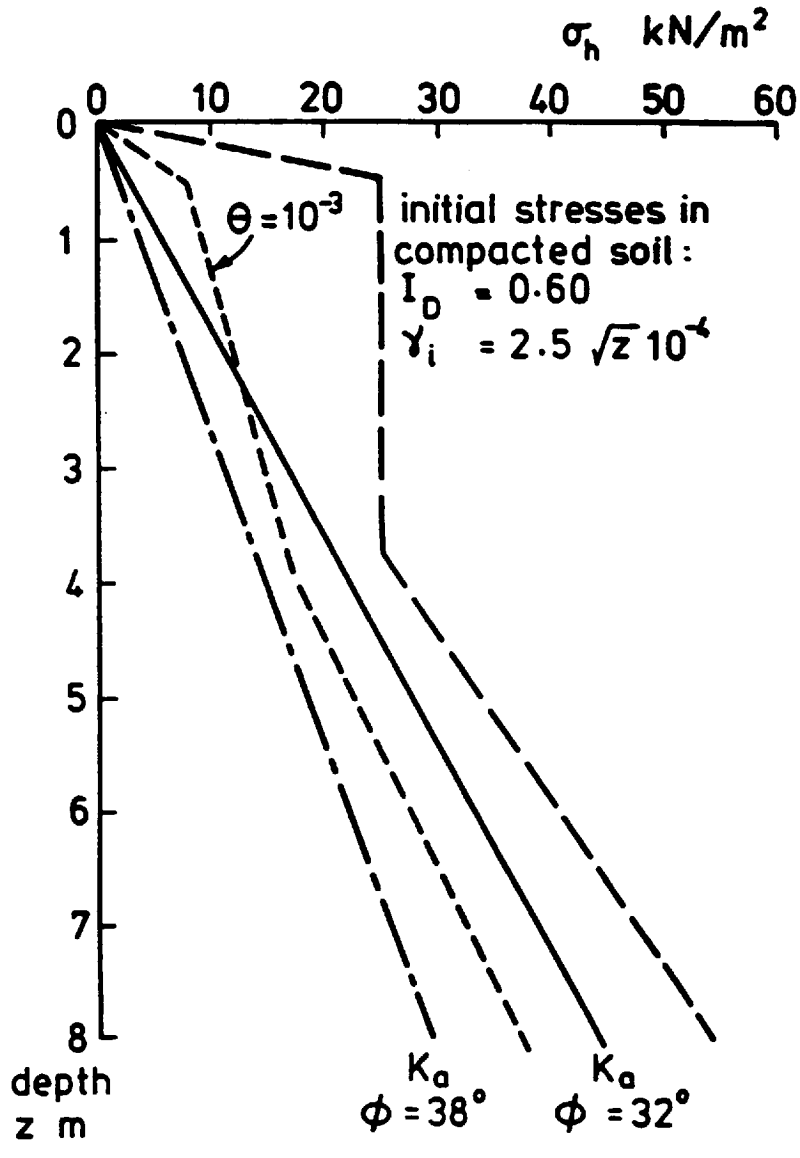

Figure 4.1 Comparitive effects of outward wall rotation

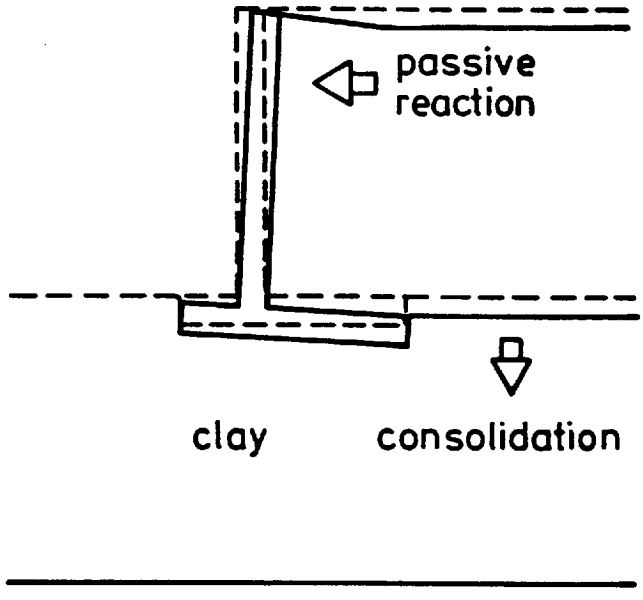

Figure 4.2 Inward wall rotation due to consolidation

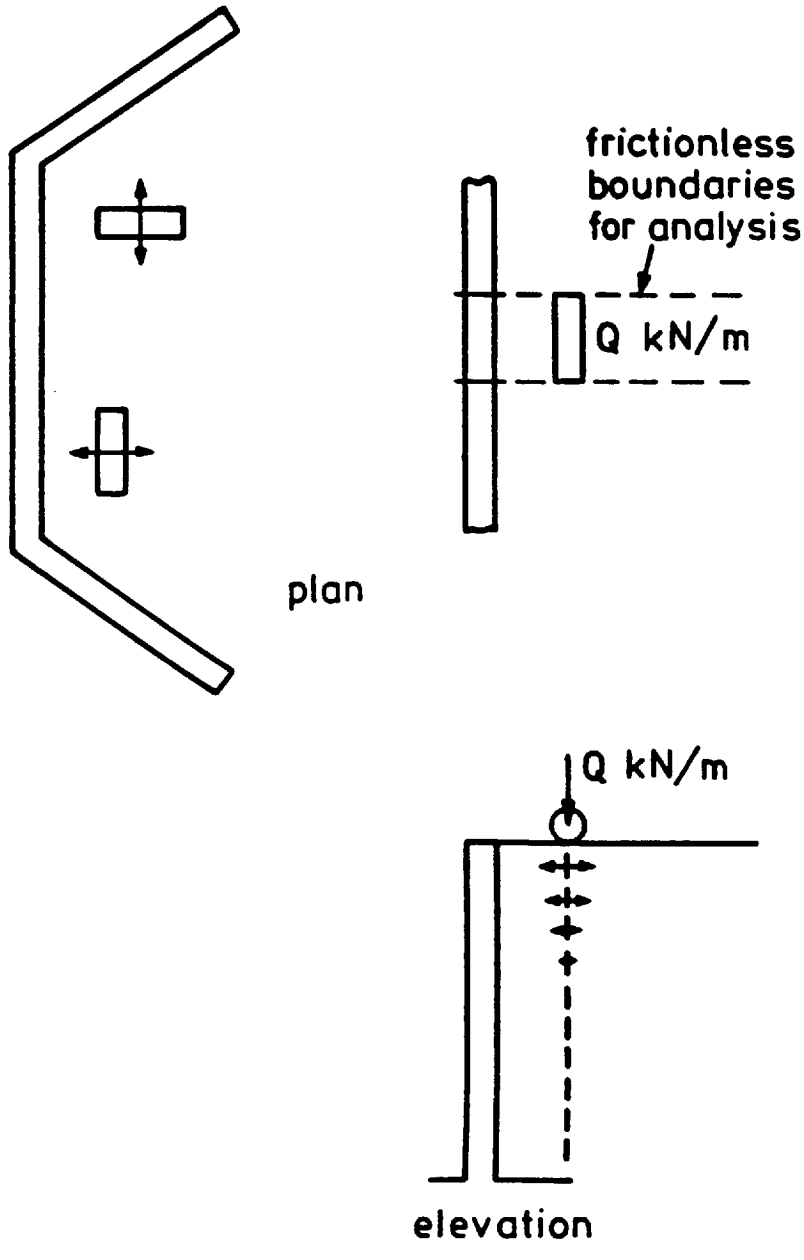

Figure 4.3 Idealisation for stress effects beneath roller

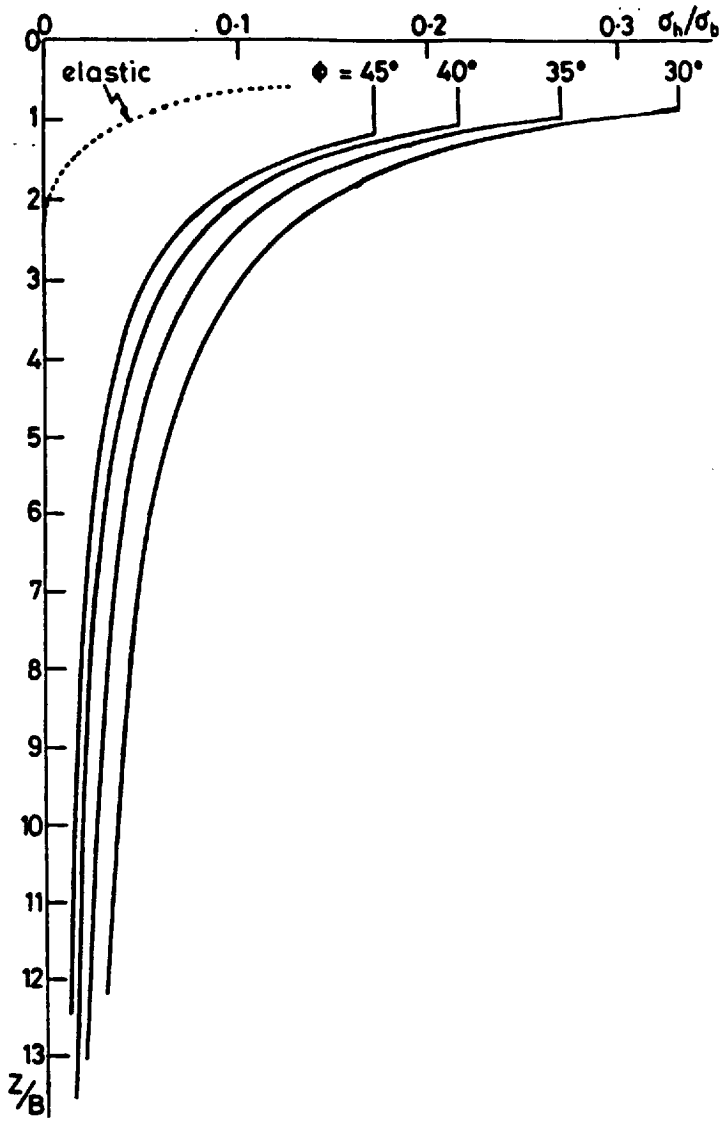

Figure 4.4 Lateral stress increments due to surface load

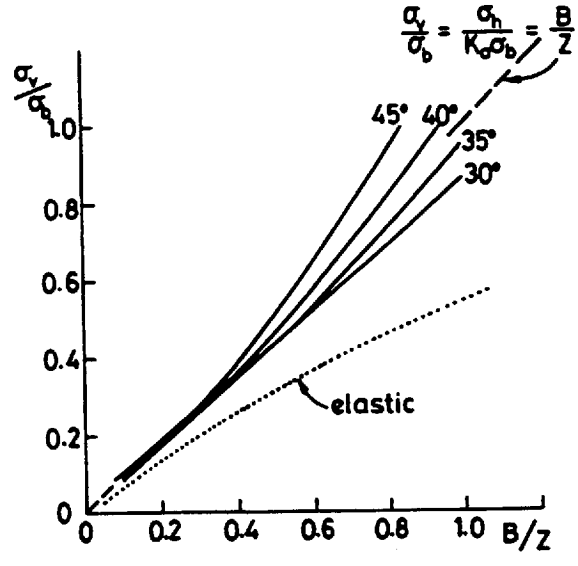

Figure 4.5 Vertical stress increments due to surface load

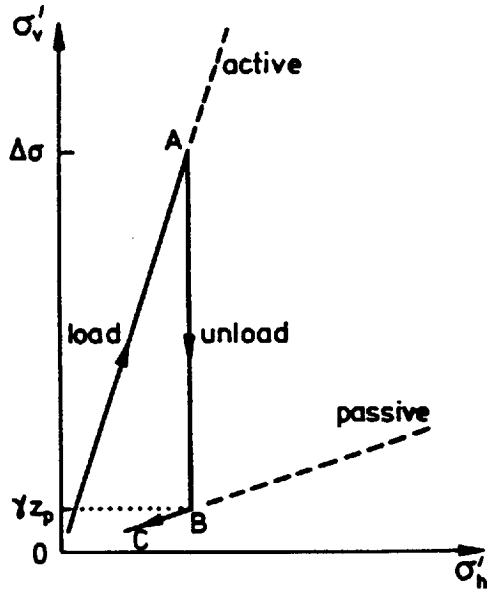

Figure 4.6 Broms' compaction stress approach

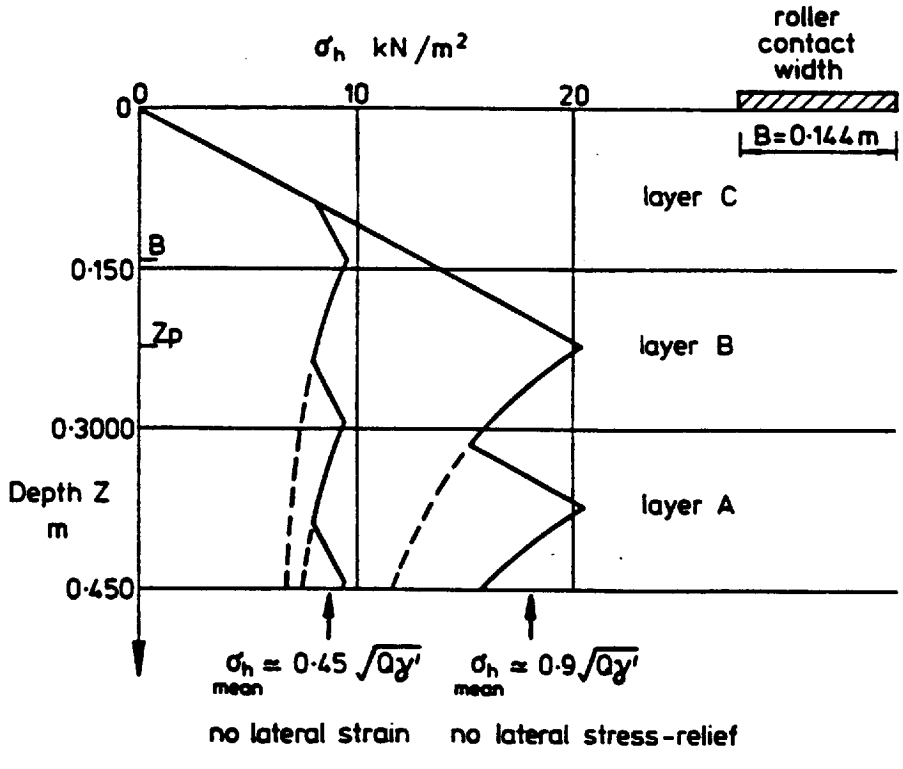

Figure 4.7 Stress variation through three compacted layers

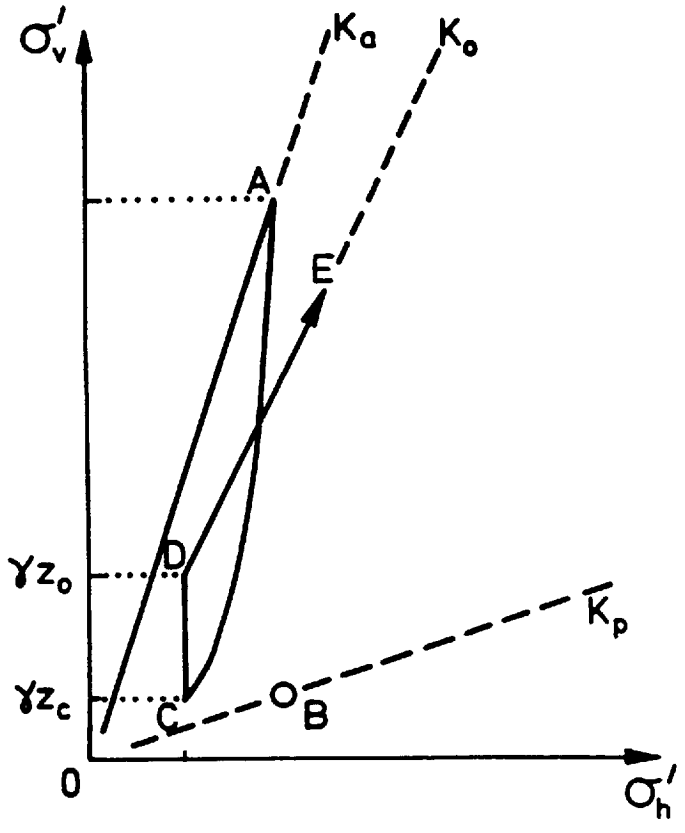

O soil dumped

A under compactor

B Broms' critical point

C possible rebound point

D burial sufficient to mobilize K_o

E additional K_o compression

Figure 4.8 Unload/reload stress path for a compacted soil layer

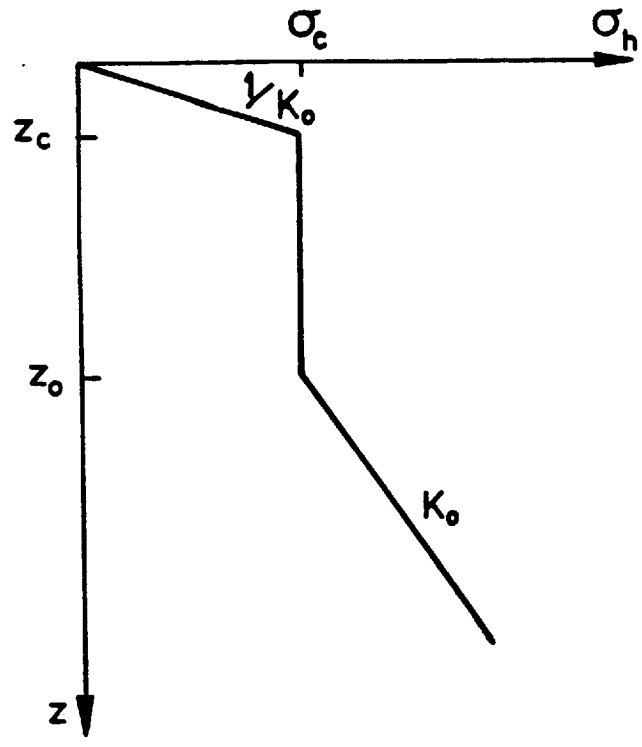

Figure 4.9 Broms' lateral stress distribution

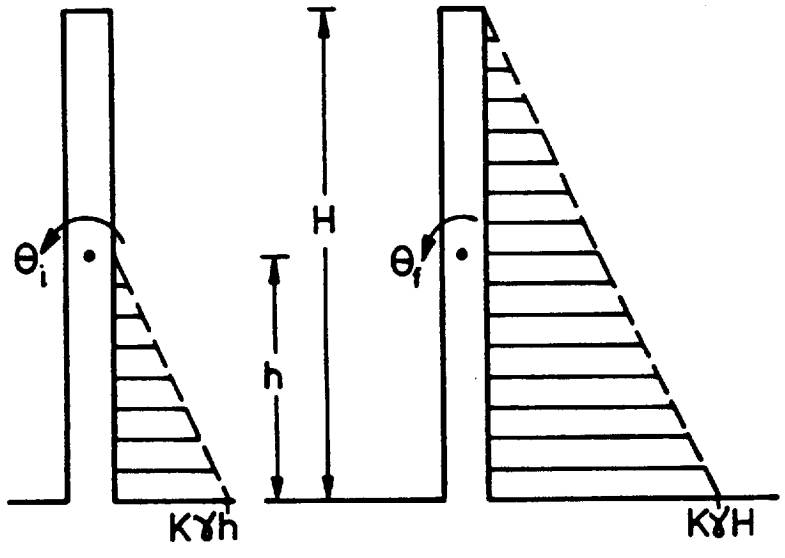

Figure 4.10 Flexural analysis of cantilever wall

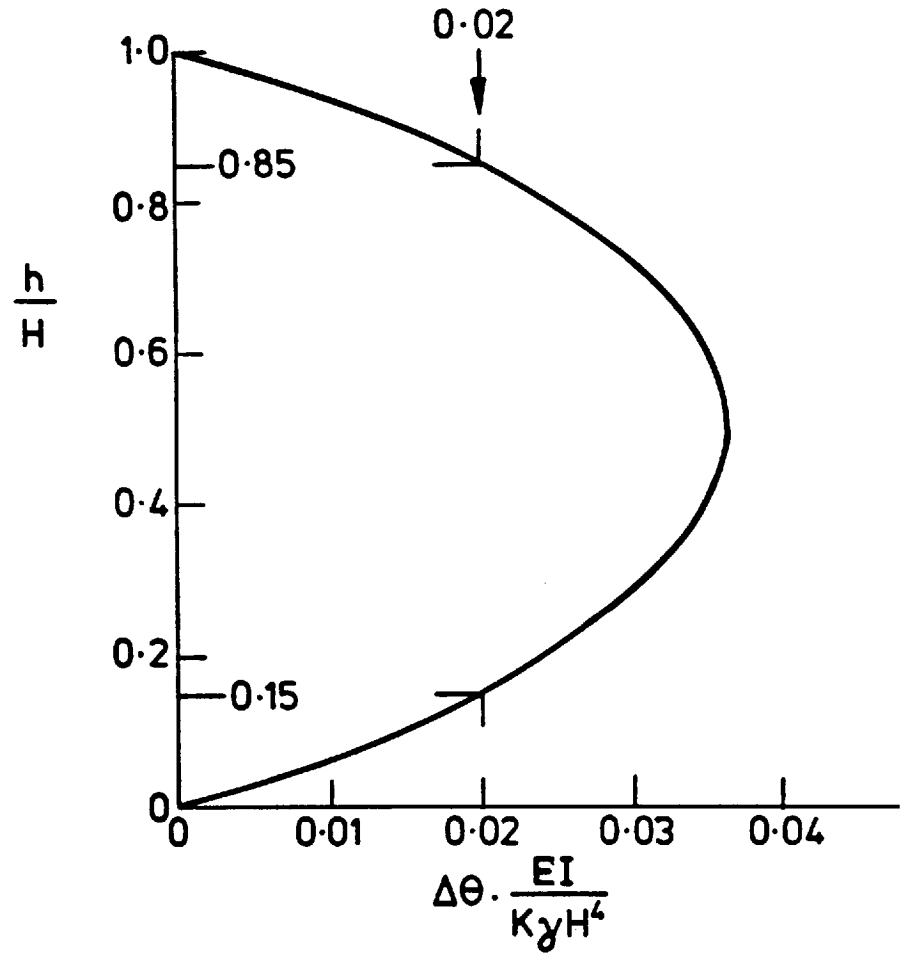

Figure 4.11 Wall rotations following placement of soil

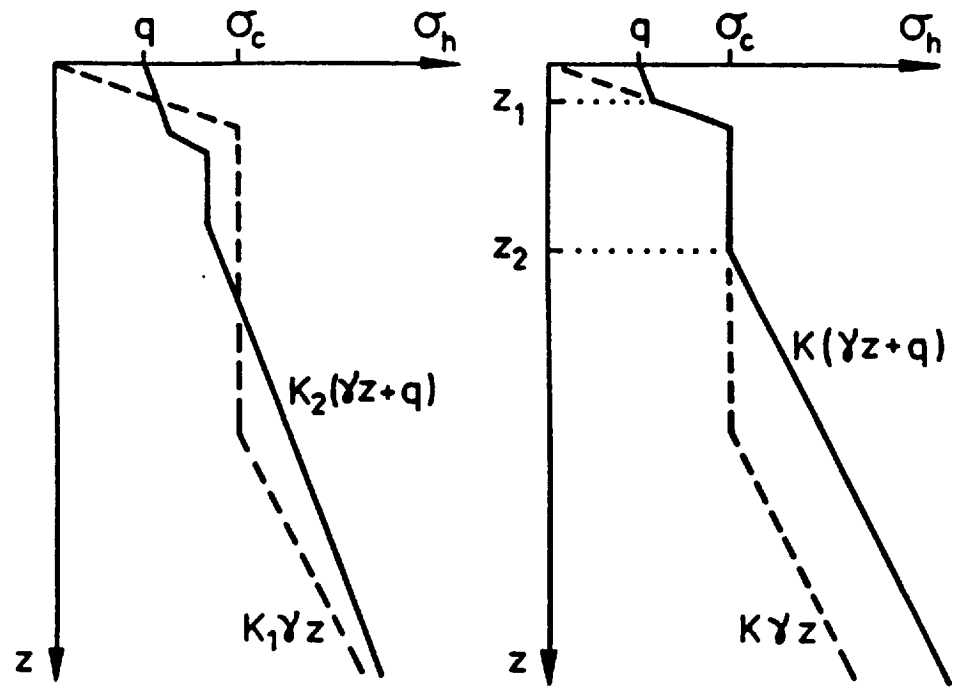

a) Actual b) Idealised

Figure 4.12 Superposition of uniform surcharge on precompressed fill

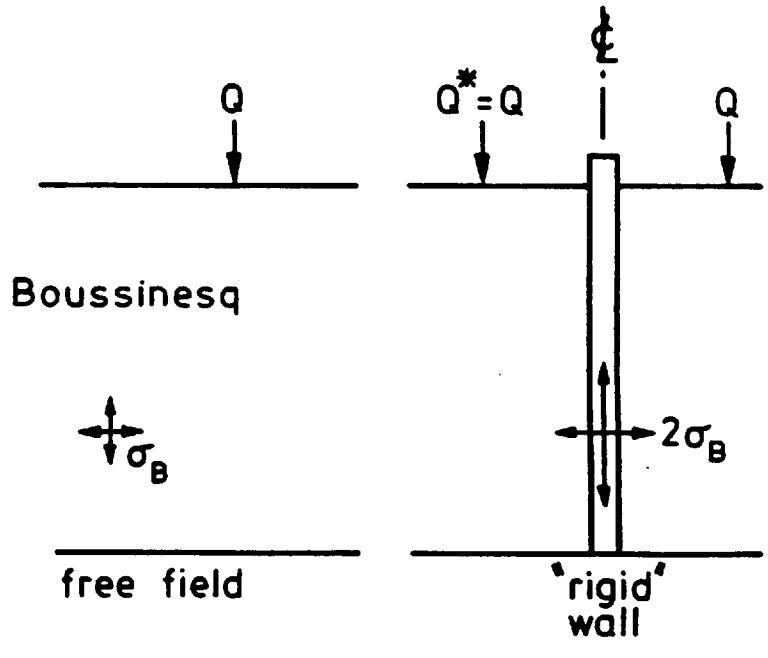

Figure 4.13 Elasticity: "image" load to create immobile plane of symmetry

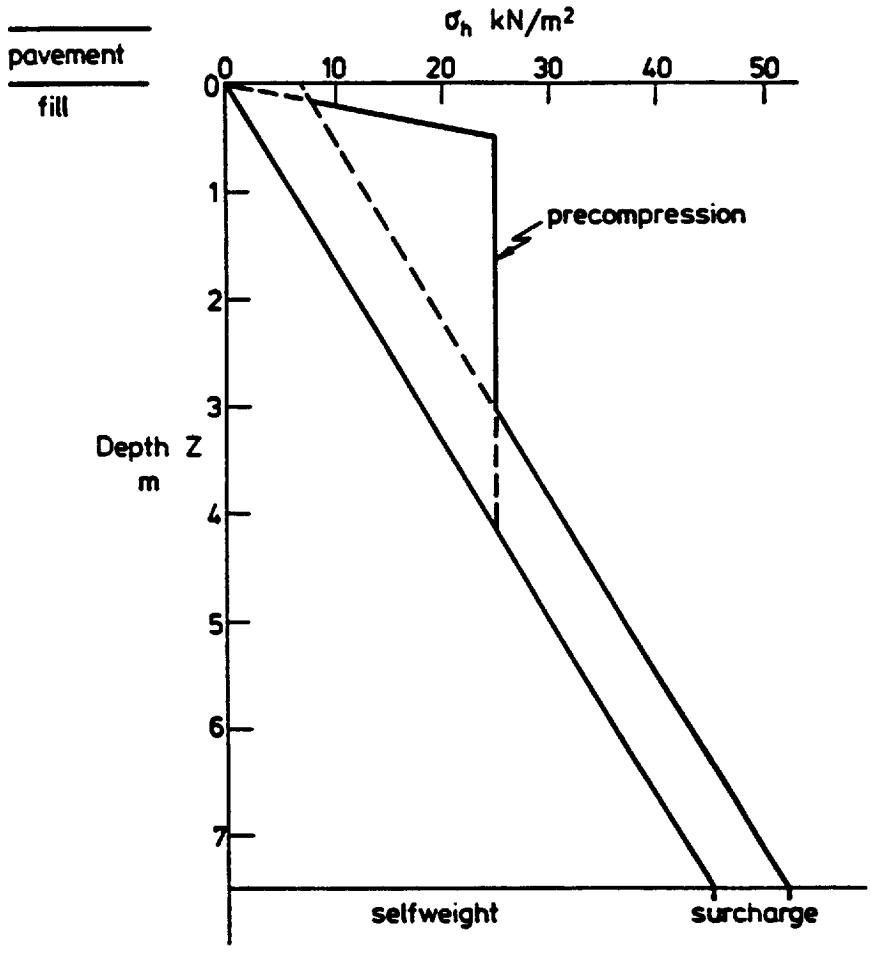

Figure 4.14 Superposition example

Section (b) : HA loaded

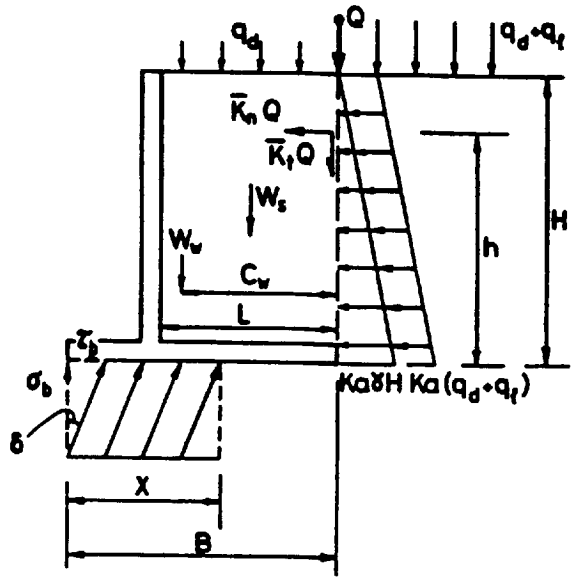

Figure 5.1 Free body diagram for L-wall with dry granular backfill

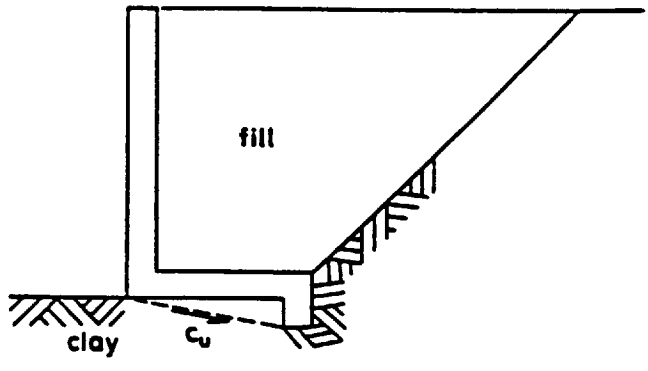

Figure 5.2 Shear key for L-wall on clay

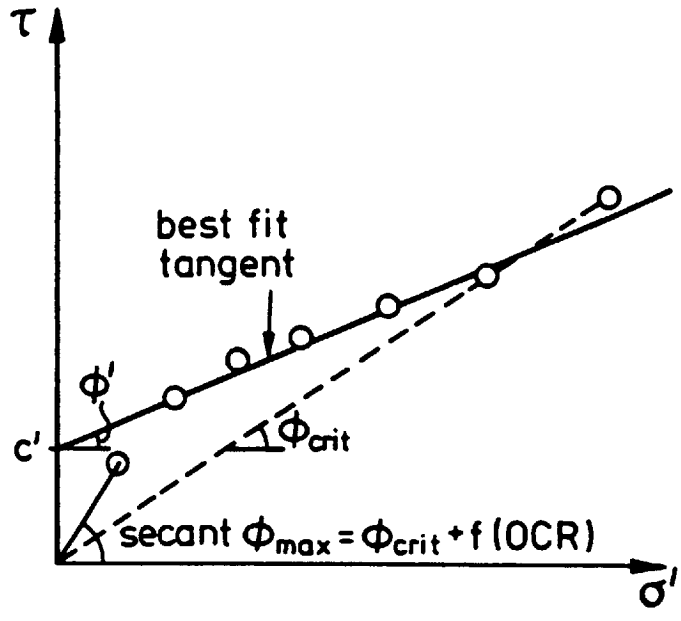

Figure 5.3 Secant and tangent strength parameters

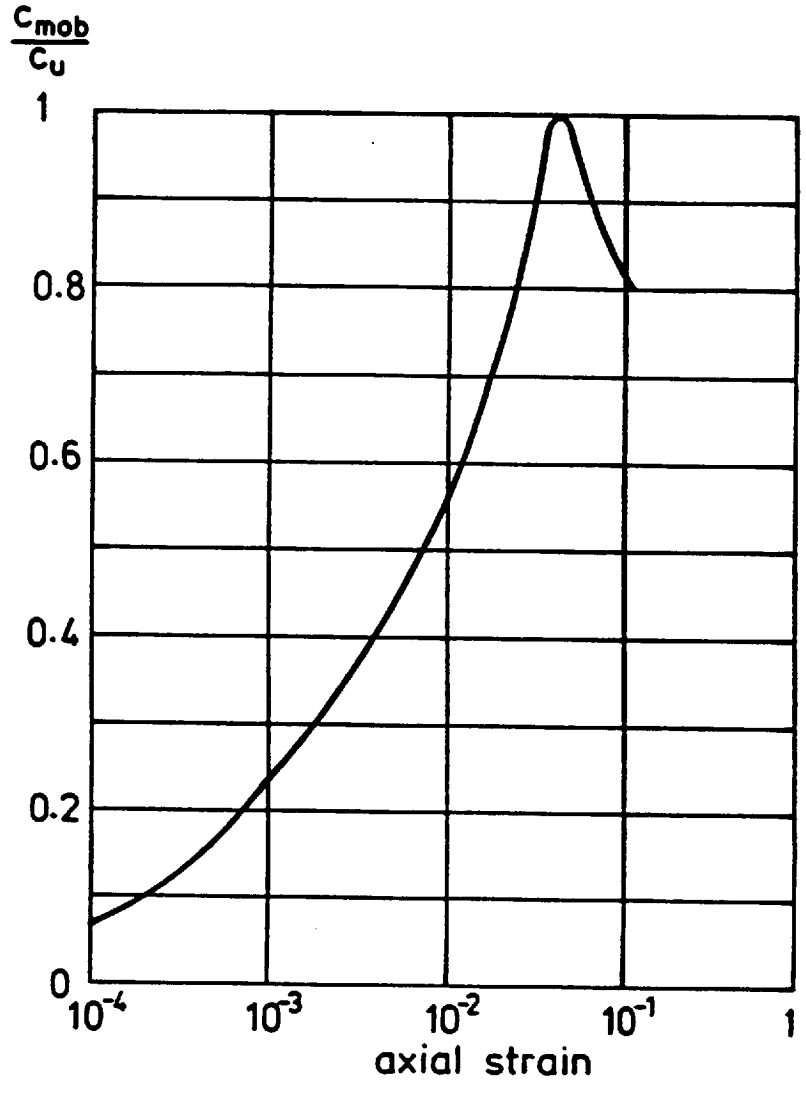

Figure 6.1 Undrained strength mobilisation of London clay sample: Jardine et al (1984)

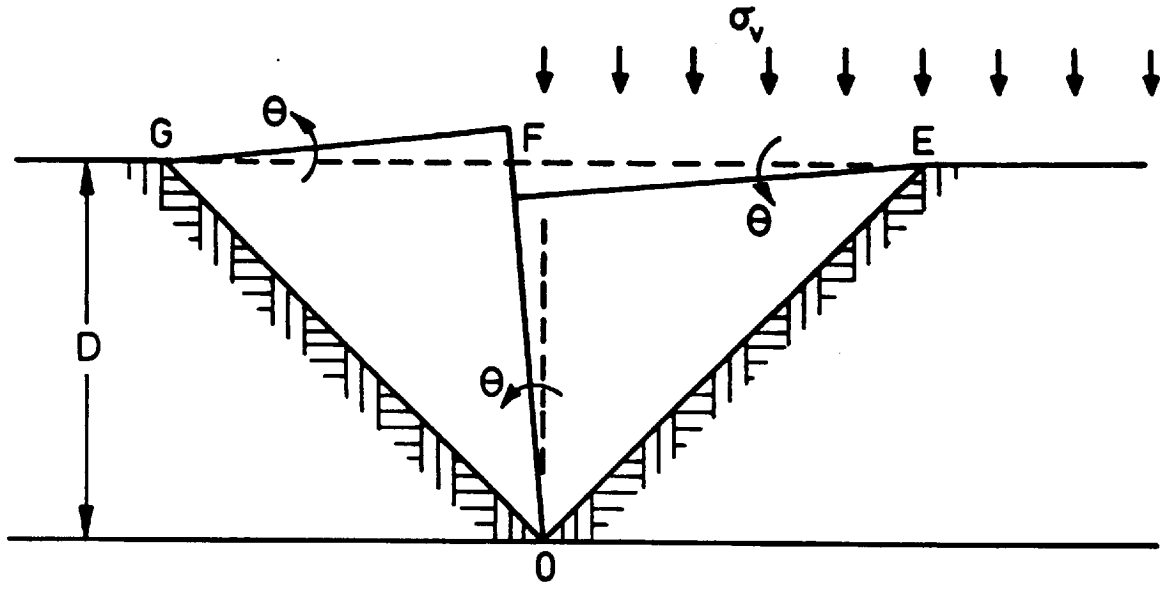

Figure 6.2 Surcharge on clay: simplified undrained shear mechanism

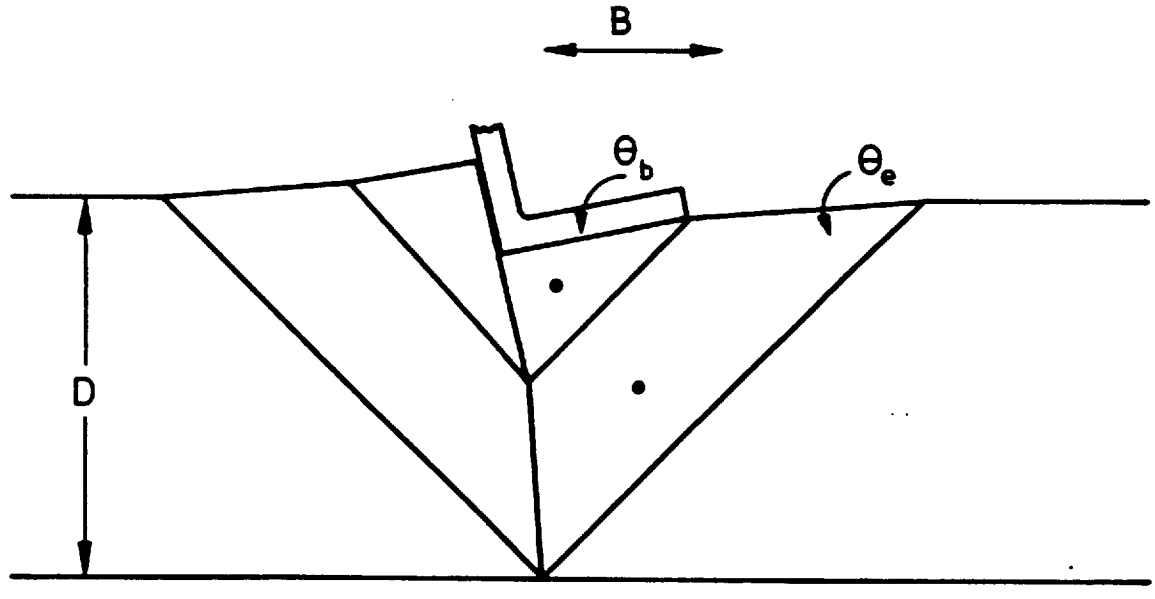

Figure 6.3 Approximate treatment of stiffness variation

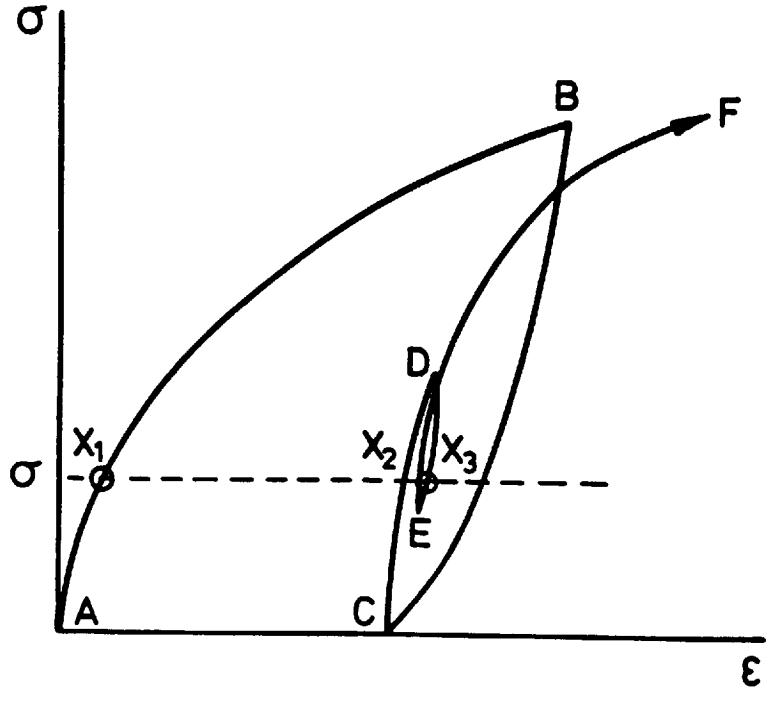

Figure 6.4 Typical soil hysteresis

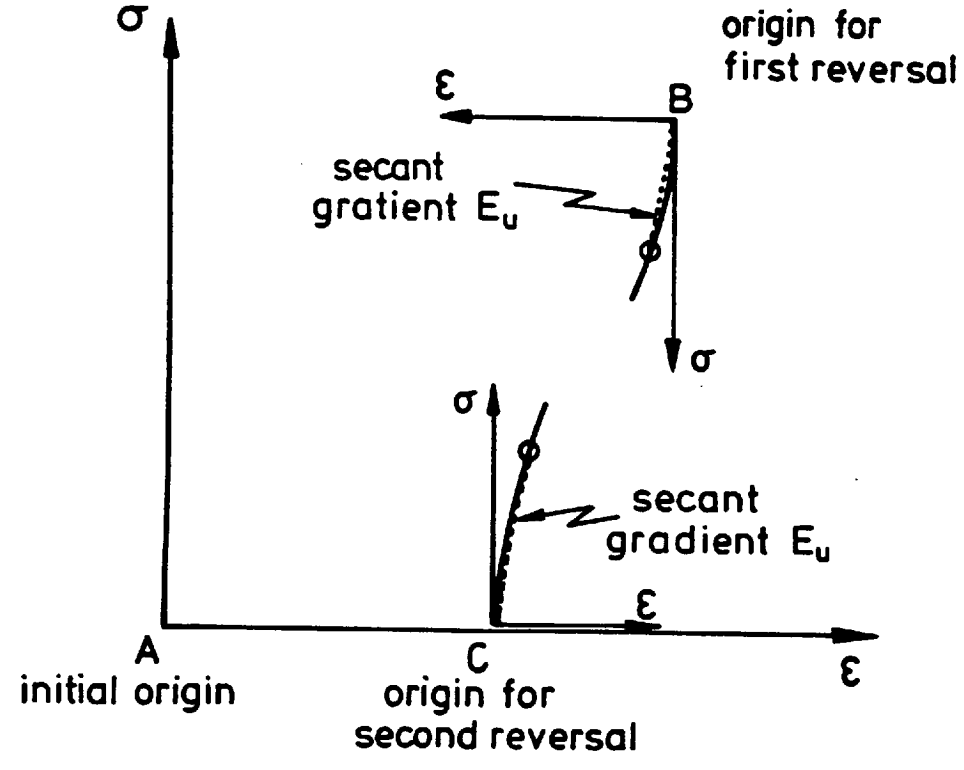

Figure 6.5 Definition of strain origin and secant modulus

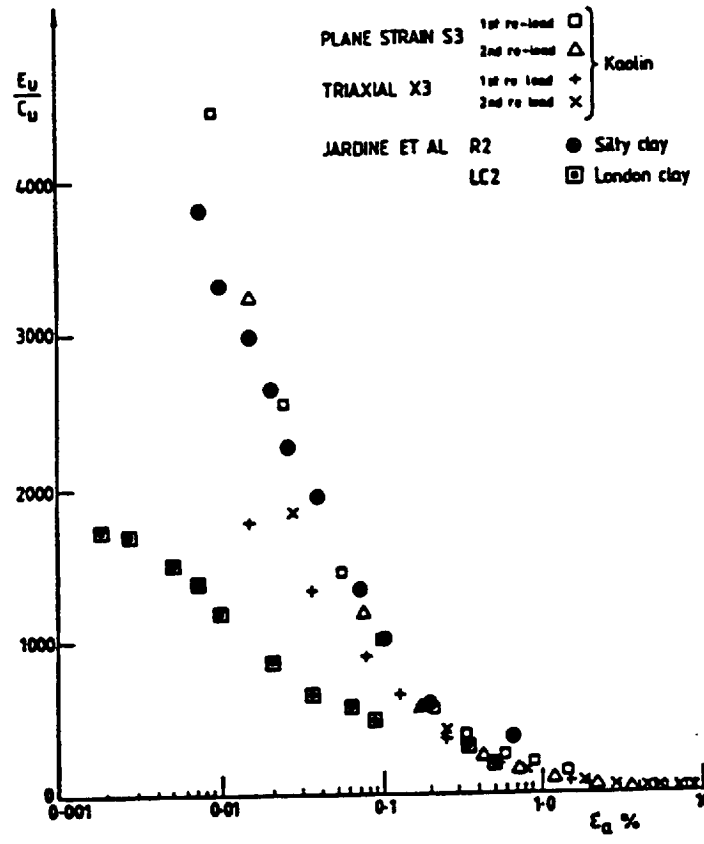

Figure 6.6 E_u/c_u versus log axial strain for three clays

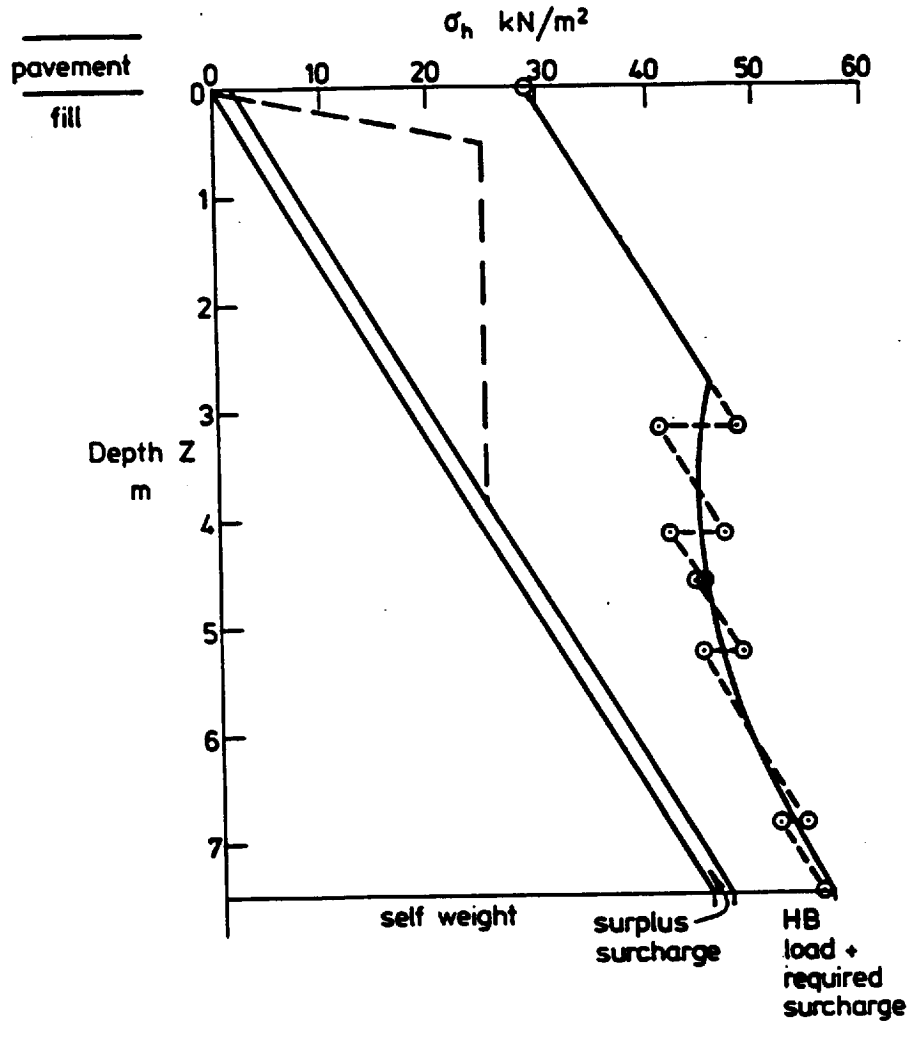

Figure 4.14 Superposition example

Section (a) : HB loaded